GREEN SYNTHESIS, CHARACTERIZATION AND ELECTROCHEMICAL BIOSENSOR APPLICATION OF Fe_3O_4-Au CORE-SHELL NANOPARTICLES

ELISA RASOULI

INSTITUTE FOR ADVANCED STUDIES
UNIVERSITY OF MALAYA
KUALA LUMPUR

2021

GREEN SYNTHESIS, CHARACTERIZATION AND ELECTROCHEMICAL BIOSENSOR APPLICATION OF Fe_3O_4-Au CORE-SHELL NANOPARTICLES

ELISA RASOULI

INSTITUTE FOR ADVANCED STUDIES
UNIVERSITY OF MALAYA
KUALA LUMPUR

2021

UNIVERSITY OF MALAYA

ORIGINAL LITERARY WORK DECLARATION

Name of Candidate: **Elisa Rasouli**

Matric No: **17057544/1**

Name of Degree: Doctor of philosophy

Title of Thesis ("this Work"):

Green synthesis, characterization and electrochemical biosensor application of Fe_3O_4-Au core-shell nanoparticles

Field of Study: **Chemistry (Nanotechnology)**

I do solemnly and sincerely declare that:

(1) I am the sole author/writer of this Work;
(2) This Work is original;
(3) Any use of any work in which copyright exists was done by way of fair dealing and for permitted purposes and any excerpt or extract from, or reference to or reproduction of any copyrighted work has been disclosed expressly and sufficiently and the title of the Work and its authorship have been acknowledged in this Work;
(4) I do not have any actual knowledge nor do I ought reasonably to know that the making of this work constitutes an infringement of any copyrighted work;
(5) I hereby assign all and every right in the copyright to this Work to the University of Malaya ("UM"), who henceforth shall be the owner of the copyright in this Work and that any reproduction or use in any form or by any means whatsoever is prohibited without the written consent of UM having been first had and obtained;
(6) I am fully aware that if in the course of making this Work I have infringed any copyright whether intentionally or otherwise, I may be subject to legal action or any other action as may be determined by UM.

Candidate's Signature Date:

Subscribed and solemnly declared before,

Witness's Signature Date:

Name:

Designation:

GREEN SYNTHESIS, CHARACTERIZATION AND ELECTROCHEMICAL BIOSENSOR APPLICATION OF Fe_3O_4-Au CORE-SHELL NANOPARTICLES.

ABSTRACT

In this study, Fe_3O_4 nanoparticle (NP) and core-shell Fe_3O_4-Au NP have been synthesized using natural honey as a green synthesis method. It was found that honey is an effective reducing agent and stabilizer in producing NPs. The particle size of the synthesized material can be controlled by varying the concentration of honey. The particle size could be controlled below 10 nm. The NPs were characterized by field emission scanning electron microscopy (FE-SEM), energy dispersive x-ray (EDX) analysis, transmission electron microscopy (TEM), selected area electron diffraction (SAED) analysis, X-Ray diffraction (XRD) analysis, ultraviolet-visible spectrophotometer (UV-Vis) analysis, Fourier transformed infrared spectroscopy (FTIR) analysis, vibrating sample magnetometry (VSM) analysis and cytotoxicity test analysis to investigate the surface morphology, chemical composition, functional group, magnetic properties and toxicity. The TEM image of Fe_3O_4 NPs showed that particle size decreased from 3.21 nm to 2.22 nm with increasing honey content from 0.5% to 3.0% (w / v) respectively, and increased from 3.21 nm to 4.11 nm in Fe_3O_4 NPs and Fe_3O_4 -Au NP (by ratio molar 1: 1), after being coated with a gold shell. VSM results revealed the superparamagnetic behavior of both Fe_3O_4 NPs and Fe_3O_4-Au NPs, with a decrease in the saturated magnetization from 23.78 emu g^{-1} for Fe_3O_4 NPs to 16.98 emu g^{-1} for NP Fe_3O_4-Au (with a ratio of 1: 1), which is assigned to the formation of gold shells. The FESEM analysis shows that the synthesized NPs possesses a spherical structure, which increases the surface area and provides an ideal environment for sensor applications. The presence of gold from the EDX analysis, SAED analysis and UV-Vis analysis demonstrated the successful gold shell formation on the surface of Fe_3O_4 - NPs.

The glassy carbon electrode (GCE) and screen-printed carbon electrode (SPCE) were modified with the core-shell Fe_3O_4-Au NPs for the electrochemical detection of dopamine and human papillomavirus (HPV). In the first stage, the two electrodes are modified through a chemical modification process, i.e. the Fe_3O_4-AuNPs-GCE and Fe_3O_4-AuNPs-SPCE. Cyclic voltammetry (CV) analysis confirmed that both Fe_3O_4-Au-GCE and Fe_3O_4-AuNPs-SPCE showed good electron transfer properties. In fact, modification of the bare electrode with the core-shell Fe_3O_4-Au NPs enhances the electron transfer properties and conductivity compared to the bare electrodes. The enhanced electrocatalytic performance of the modified Fe_3O_4-AuNPs-GCE electrodes is due to the large surface area and high conductivity, in addition to the rapid electron transfer provided by Fe_3O_4-AuNPs, confirming the important role of the NPs. These modified electrodes are stable in the potential window and has good sensitivity and selectivity towards dopamine detection.

A 14-base thiolated DNA probe was assembled onto the surface of Fe_3O_4-AuNPs-SPCE and was allowed to be hybridizedf with a complementary 14-base DNA target (synthetic oligonucleotide). The electrochemical detection of hybridization events between the immobilized DNA probes and complementary HPV sequences is monitored by CV and different pulse voltammetry (DPV) using the $[Fe(CN)_6]^{3-/4-}$ as indicator redox. The electrodes showed varying redox current signals $[Fe(CN)_6]^{3-/4-}$ in the absence and presence of the complementary DNA targets. The optimal performance of Fe_3O_4-AuNPs-SPCE for the HPV electrochemical detection was obtained with different DNA probe concentrations (1 μM and 10 μM). Thus the sensitivity and selectivity of the sensor were studied under the optimized DNA probe concentration.

SINTESIS HIJAU, PENCIRIAN DAN APLIKASI BIO-PENDERIA ELEKTROKIMIA BAGI CENGKERANG-KERAS NANOZARAH Fe_3O_4-Au.

ABSTRAK

Dalam kajian ini, bahan nanozarah (NZ) Fe_3O_4 dan teras-tempurung nanozarah Fe_3O_4-Au telah berjaya disintesis menggunakan madu asli dengan kaedah sintesis hijau. Juga didapati bahawa madu berfungsi sebagai agen penurunan dan penstabil dalam menghasilkan bahan NZ tersebut. Saiz zarah dari bahan yang disintesis dapat dikawal dengan perubahan kepekatan madu asli. Saiz zarah dapat dikawal kurang dari 10 nm. Bahan NZ tersebut dicirikan oleh mikroskopi FE-SEM, analisis EDX, mikroskopi TEM, analisis SAED, analisis XRD, analisis UV-Vis, analisis FTIR, analisis VSM, dan analisis ujian sito-toksisitas untuk memahami morfologi permukaan, komposisi kimia, kumpulan berfungsi, sifat magnetik dan sifat keracunan NP. Imej TEM Fe_3O_4 NP menunjukkan bahawa ukuran zarah menurun dari 3.21 nm hingga 2.22 nm dengan peningkatan kandungan madu masing-masing dari 0.5% hingga 3.0% (w / v) dan meningkat dari 3.21 nm hingga 4.11 nm di Fe_3O_4 NZ dan Fe_3O_4 -Au NZ (dengan nisbah molar 1: 1), setelah dilapisi dengan tempurung emas. Hasil VSM mendedahkan tingkah laku superparamagnetik oleh kedua-dua NZ Fe_3O_4 dan NP Fe_3O_4-Au, dengan penurunan magnetisasi tepu dari 23,78 emu g^{-1} untuk NP Fe_3O_4 kepada 16,98 emu g^{-1} untuk NP Fe_3O_4-Au NP (dengan nisbah 1: 1), yang ditugaskan untuk pembentukan cengkerang emas. Analisis FESEM menunjukkan bahawa morfologi permukaan NZ tersebut mempunyai struktur sfera, yang menunjukkkan peningkatan luas permukaan dan menyediakan persekitaran yang ideal untuk aplikasi sensor. Kehadiran emas daripada analisis EDX, analisis SAED dan analisis UV-Vis membuktikan kejayaan dalam pengagregatan tempurung emas di atas permukaan Fe_3O_4 - NZ.

Bahan teras-tempurung Fe_3O_4-Au NZ dimodifikasikan dengan elektrod GCE dan SPCE untuk pengesanan secara elektrokimia ke atas bahan dopamin dan papillomavirus manusia (HPV). Pada peringkat pertama, kedua elektrod diubah melalui proses modifikasi kimia, iaitu Fe_3O_4-AuNPs-GCE dan Fe_3O_4-AuNPs-SPCE. Analisis CV mengesahkan bahawa kedua Fe_3O_4-Au-GCE dan Fe_3O_4-AuNPs-SPCE menunjukkan sifat pemindahan elektron yang baik. Sebenarnya, pengubahsuaian permukaan kedua-dua elektrod tersebut dengan bahan teras-tempurung Fe_3O_4-Au NZ meningkatkan sifat dan kekonduksian pemindahan elektron berbanding dengan elektrod yang tidak dimodifikasikan. Prestasi tinggi elektro-pemangkinan yang dipertingkatkan oleh bahan Fe_3O_4-Au NZ-GCE adalah disebebkan oleh luas permukaan yang besar dan kekonduksian yang tinggi serta pemindahan elektron yang pantas dengan kehadiran bahan Fe_3O_4-Au NZ, yang mengesahkan peranan penting NZ. Elektrod yang dihasilkan tersebut adalah cukup stabil dalam penentuan bahan analit dengan kaedah elektrokimia dan menunjukkan kepekaan dan kepemilihan yang baik terhadap pengesanan dopamin.

Permukaan elektrod Fe_3O_4-AuNPs-SPCE telah dihiasi oleh bahan probe DNA thiolated 14-bes untuk membolehkan penghibridan oleh bahan DNA sasaran 14-bes pelengkap (oligonukleotida sintetikProses hibridisasi di antara probe DNA ter-immobilasasi dengan urutan HPV pelengkap dikesan oleh teknik voltammetri siklik (CV)

dan voltammetri nadi yang berbeza (DPV) dengan menggunakan $[Fe(CN)_6]^{3-/4-}$ sebagai penunjuk redoks. Bahan elektrod tersebut yang mempunyai isyarat arus redoks $[Fe(CN)_6]^{3-/4-}$ mempunyai tindakbalas yang berbeza dengan tanpa kehadiran dan dengan kehadiran bahan sasaran DNA pelengkap. Prestasi optimum Fe_3O_4-Au NZ-SPCE untuk pengesanan elektrokimia HPV diperoleh dengan kepekatan probe DNA yang berbeza (1 μM dan 10 μM). Kemudian kepekaan dan selektiviti elektrod penderia tersebut dikaji di bawah kepekatan probe DNA yang optimum.

ACKNOWLEDGMENTS

In the name of God Allah, the most beneficent and the most merciful. First and foremost, all praise is due to God Allah Almighty *subhanahu wa-ta'ala,* on whom we ultimately depend, for his endless blessing and allowing me to achieve what I have achieved today.

I would like to take this opportunity to express my deepest thankfulness and appreciation to my supervisors Prof. Dr. Wan Jeffrey Basirun and Prof. Dr. Mohd Rafie Bin Johan for giving me the opportunity, confidence, and guidance during my doctorate candidature. I owe incredible gratitude to them as they have been tremendously patient and supportive in all situations we have gone through. I would like to further extend my gratitude to Dr. Majid Rezaei, Dr. Mohammad Reza Mahmudian, Dr.Mehran Sookhakian, Dr. Kamyar Shameli and Dr. Zohreh Shahnavaz for being a great advisor, motivators as well as teachers throughout the period it took to complete this thesis.

Above all, I would sincerely love to take this opportunity to express my endless love and appreciation to my mom who was my first school teacher for her unconditional love, support, and patience during the period of my study, by which without her I would not be what I am today. Her existence is the best thing in my life.

I would love to deeply express my special gratitude to my family, especially my siblings for their unconditional love, encouragement, guidance, and support in all aspects of my life.

Special thanks and gratefulness go to my friend and brother Mohammed Ahmed Gharawi for his support and guidance during the whole study of my doctorate. His advice, encouragement, and patience were endless, and I owe him remarkable gratitude. He has been with me through thick and thin, and I have seen "A friend in need is a friend indeed" in him.

Thanks and appreciations go to the members in the D227 Lab, Dr. Ladan, Sofia, Shalauddin, and Shamima.

Last but not least, I would like to acknowledge the University of Malaya for Postgraduate Research Grant (PPP Grant PG126-2015B) and Equitable Society Research Cluster (ESRC) research grants GC001C-14SBS and GC001D-14AET.

TABLE OF CONTENTS

LIST OF FIGURES

LIST OF TABLES

LIST OF SYMBOLS AND ABBREVIATIONS

NP	**Nanoparticle**
NPs	**Nanoparticles**
XRD	**X-Ray Diffraction**
UV-VIS	**Ultraviolet-visible spectrophotometer**
TEM	**Transmission electron microscopy**
FESEM	**Field emission scanning electron microscopy**
EDX	**Energy dispersive x-ray**
FTIR	**Fourier Transformed Infrared Spectroscopy**
VSM	**Vibrating Sample Magnetometry**
SAED	**Selected area electron diffraction**
CV	**Cyclic voltammetry**
DPV	**Different pulse voltammetry**
GCE	**Glassy carbon electrode**
SPCE	**Screen-printed carbon electrode**
Au-Fe_3O_4	**Gold-coated iron oxide**
ssDNA	**single-stranded DNA**
DA	**Dopamine**
HPV	**Human papillomavirus**
MNPs	**Metallic nanoparticles**
Qds	**Quantum dots**
HC2	**Hybrid capture HPV DNA Test 2**
PCR	**Polymerase chain reaction**
HPV-16	**Human papillomavirus DNA type 16**
rGO	**Reduced graphene oxide**

SPIONs	**Superparamagnetic iron oxide nanoparticles**
NMPO	**1-methyl-2- pyrrolidinone**
bcc	**Body-centered cubic**
fcc	**Face-centered cubic**
TB	**Blocking temperature**
TEOS	**Tetraethylorthosilicate**
MGNCs	**Magnetic gold nanocomposites**
MRI	**Magnetic resonance imaging**
MNCs	**Magnetic nanocrystals**
MKs	**Magnetic kernels**
MSNPs	**Magnetic silica nanoparticles**
BSA	**Bovine serum albumin**
PPI	**Poly(propyleneimine)**
PEI	**Polyetherimide**
CTAB	**Hexadecyltrimethylammonium bromide**
PEG	**Polyethylene glycol**
PAA	**Polyacrylic acid**
TOPO	**Trioctyl-phosphine oxide**
TOP	**Tri-n-octylphosphine**
OA	**Oleic acid**
ODA	**Octadecylamine**
OAm	**Oleyl amine**
DDA	**Dodecylamine**
PAMAM	**Poly(amidoamine)**
EG	**Ethylene glycol**
ODE	**1-octadecene**

RCA	**Rolling circle amplification**
WE	**Working electrodes**
SCE	**Saturated calomel electrode**
EIS	**Electrochemical impedance spectroscopy**
MO NPs	**Metal oxide nanoparticles**
CNT	**Carbon nanotubes**
GO	**Graphene oxide**
AA	**Ascorbic acid**
UA	**Uric acid**
SPGE	**Screen-printed gold electrodes**
SWV	**Square wave voltammetry**
αOVA	**Anti-ovalbumin**
αHPV	**Alpha-papillomavirus**
PANi–MWCNT	**Polyaniline-multiwalled carbon nanotube film**
IDA	**Interdigitated platinum electrode arrays**
LOD	**Limit of detection**
SWCNTs	**Single-walled carbon nanotubes**
G/Au NR/PT	**Graphene/Au nanorod/ polythionine**
MB	**Methylene blue**
PGE	**Pencil graphite electrode**
HCV	**Hepatitis C virus**
AQ-PNA	**Anthraquinone-labeled pyrrolidinyl peptide nucleic acid**
LOQ	**Limit of quantification**
CNOs	**Carbon nano-onion**
PAA	**Phenylacetic acid**
PM	**Phenyl maleimide**

G-PANI	**Graphene-polyaniline**
ePAD	**Electrochemical paper-based analytical devices**
POC	**Point-of-care**
DI	**Deionized**
EDTA	**Ethylenediaminetetraacetic acid**
PBS	**Phosphate buffer solution**
Tris	**Tris-(hydroxymethyl) aminomethane**
GPES	**General-purpose electrochemical system**
RE	**Reference electrode**
CE	**Counter electrode**
OFAT	**One-factor-at-a-time**
Ms	**Saturation magnetization**
DAQ	**Dopamine quinone**

CHAPTER 1: INTRODUCTION

1.1 Background of study

The interest in novel material with unique characteristics or properties in the discipline of science and technology has increased (Lugani, Sooch, Singh, & Kumar, 2021). Lately, the advancement, successes, and availability of scientific data in the field of nanotechnology permit the development of nanoparticles (NPs) with the desired physical, material, and chemical properties (S. Chaturvedi & Dave, 2014). Besides, controlling the composition of nanocomposite may lead to the establishment of new methods and technologies in various fields including physics, chemistry, and material science. Due to the universal compositions and structures, the focus of research interest is growing in the area of core-shell nanostructures (Gawande et al., 2015). In such nanostructures, the interaction between the core and the shell may lead to the development of new properties and functions (Zhihua Wang, Fu, Tian, Han, & Gu, 2016). Figure 1.1 represents the schematic structure of the core-shell NPs (X. Wang, Cui, Yu, Zeng, & Yang, 2016) (Z. Wang et al., 2016). The precursors used in the construction of core-shell nanostructures and the physical properties of the ingredients may lead to the establishment of a new group of nanoparticles. This new development is useful in a wide range of applications such as nano-optics, magnetic devices, nanomedicine, biotechnology, and others. To achieve a variety of physical properties and effects, various combinations of organic and inorganic compounds could be used in the nanostructure fabrication. This study mainly uses two types of materials that have been widely explored such as magnetic NPs and Au-NPs. Magnetic NPs, exclusively iron oxide nanoparticles (Fe_3O_4-NPs) has been studied in biomedical applications such as biosensors, drug delivery, treatment of hyperthermia for malignant cells, resonance imaging agent,

magnetic separation and cell sorting due to their unique magnetic properties and their biocompatibility (N. Zhu et al., 2018).

Gold nanoparticles (Au-NPs) contain chemical and optical properties that are especially useful for biomedical applications; for example, gene and drug delivery, highly sensitive diagnosis assaying, as well as RNA and DNA detection (H. Liu, Hou, Zhang, & Wu, 2010). Presently, there are considerable efforts to consolidate therapeutic functions and diagnostic in a single nanoscale system for a more effective application against cancer. The NPs have great potential to achieve such dual functions, particularly if more than one type of nanostructure can be consolidated in the nano assembly which is referred as core-shell. An example of these novel NPs is the core-shell NPs which are widely used in advanced nanotechnology such as drug targeting and RNA/DNA detection.

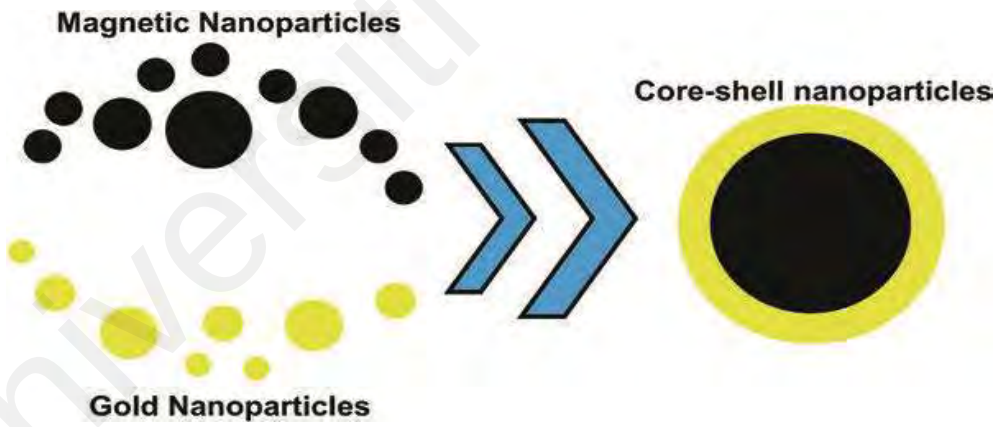

Figure 1.1: Schematic structure of core-shell Fe_3O_4-Au NPs reproduced with permission from the publisher (Manisekaran, 2018).

Metallic nanoparticles (MNPs) can play an important role in modifying the electrode surface through increasing the surface area, high catalytic effectiveness, and increasing mass transport (Shi & Ma, 2010). In the recent decade, magnetic nanoparticles have demonstrated their singularity by having the ability to increase faster electron transfer kinetics between the

electrodes, large surface-to-volume ratio and provide the active site for the biomolecules (Hayat, Catanante, & Marty, 2014; Lata, Batra, Karwasra, & Pundir, 2012; Teymourian, Salimi, & Khezrian, 2013).

Metallic nanoparticles (MNPs) is a potential candidate material and plays an important role in an extensive range of applications such as optoelectronics, bio-labeling, catalysis, electronics and sensing due to their exclusive characteristics (Das et al., 2017; Jeevanandam, Barhoum, Chan, Dufresne, & Danquah, 2018; Razzaque, Hussain, Hussain, & Tan, 2016). Gold nanoparticles (AuNPs) have been widely used in the construction of various types of electrochemical sensors, in compare to other types of MNPs, attributable to their ease of functionalization, outstanding biocompatibility and excellent catalytic activity (I.-H. Cho, Kim, & Park, 2020; Pan et al., 2020).

The iron oxide NPs or noble metal NPs modified working electrodes have shown considerable enhancements in antifouling and electrocatalytic properties, although the challenge of detecting 10^{-6} – 10^{-9} molar levels of DA in human blood serum remains (Atta & El-Kady, 2010; Eddin & Fen, 2020; Fernandes et al., 2014; Yunpeng Huang, Miao, Ji, Tjiu, & Liu, 2014; Ratnam, Manjunatha, Janardan, Naidu, & Ramesh, 2020). Magnetic core-shell Fe_3O_4-Au nanoparticles (NPs) have been broadly used in the construction of bio interfaces for non-enzymatic electrochemical biosensors. For instance, Zhao *et al*. utilized Fe_3O_4-Au NPs to construct a highly specific and ultrasensitive electrochemical aptasensor for thrombin sensing (J. Zhao et al., 2011).

Similarly, Li *et al*. studied the voltammetry response of Fe_3O_4-Au NPs/ Gold-labelled antigen towards *Bacillus thuringiensis* Cry1Ac, which exhibited wide linearity with high sensitivity and selectivity (Jianping Li, Xu, Wei, & Hao, 2013). The outstanding conductivity

and biocompatibility of Fe_3O_4-Au NPs improved the performance through chemical modification, consequently provide the way for its excellent anti-fouling properties (Baldrich, Gómez, Gabriel, & Muñoz, 2011).

The use of nucleic acid (DNA/RNA) biosensor based on DNA hybridization procedures has developed a promising diagnostic device for nucleic acid detection because of its ability to shorten the assay time, high specificity and allowing detection in real-time (Abu-Salah et al., 2015; Rashid & Yusof, 2017; Samson, Navale, & Dharne, 2020; Wipawakarn, Ju, & Wong, 2012). DNA biosensors are sensing tools consisting of single-stranded DNA probe as biological recognition elements combined with the sensor transducer for converting hybridized DNA into a measurable analytical signal (Taufik, Yusof, Tee, & Ramli, 2011). Numerous transduced hybridization detection have been recorded such as the 2 electrochemical transducers (N.-y. Wu, Gao, He, Chang, & Xu, 2013), optical transducer (Delport et al., 2012; Lai, Tan, & Yang, 2011), piezoelectric transducer (Rodaree et al., 2011) and electrical transducer (Sorgenfrei et al., 2011).

Over the past few years, the application of nucleic acid-based electrochemical sensor has extremely increased in the detection of the microbial pathogen, which offers a quick detection with high sensitivity, cost-effective, portability and ease of miniaturization (Wei, Lillehoj, & Ho, 2010; N.-y. Wu et al., 2013; Q. Wu, Zhang, Yang, Yuan, & Zhang, 2019). Generally, the electrochemical methods are based on the DNA hybridization where a single-stranded DNA (ssDNA) known as DNA probe is immobilized on the electrode surface to capture or hybridize with the specific DNA target (Rosario & Mutharasan, 2014; Q. Wu et al., 2019). This hybridization process is transformed into a suitable signal based on the redox

activities of either direct detection (guanine or adenine bases oxidation) or indirect detection (redox indicator, enzyme, and nanoparticle label).

With the growth of nanotechnology fields, it has been demonstrated that the application of nanomaterials in DNA biosensors enhances the DNA immobilization on the transducer surface and functions as the signal amplifier for the hybridization procedures, consequently improving the electrochemical responses of the DNA biosensor (Bezinge, Suea-Ngam, deMello, & Shih, 2020; Girousi & Kinigopoulou, 2010; R. P. Singh, 2011).

Several kinds of nanomaterials have been discovered in the construction of DNA sensors based nanomaterials such as gold nanoparticles (AuNPs) (F. Gao, Zhu, Lei, Geng, & Ju, 2013; Lv et al., 2020; Niu et al., 2017), nanowires (Chu et al., 2021; Tran, Tran, Dang, Huynh, & Mai, 2020), carbon nanotubes (S. Han, Liu, Zheng, & Wang, 2020; Heydarzadeh, Roshanfekr, Peyman, & Kashanian, 2020), quantum dots (Qds) (Fuku, Baker, & Iwuoha, 2020; X. Gao, Cai, Li, & Jie, 2020; Ngo, Chaibun, Yin, Lertanantawong, & Surareungchai, 2021) and nanoporous substrates (Yuzhen Huang et al., 2021; Yunjiao Wang et al., 2021).

1.2 Problem statements and research motivation

Various methods for synthesis of metal and metal oxide NPs such as physical, chemical, and green methods have been used. Nanostructured metals and metal oxides produced using physical and chemical methods are found to be hazardous and highly toxic towards living cells. This is the main problem that limits the utilization of NPs in the biomedical industry.

Most synthetic methods of nanoparticles involve the use of aggressive chemicals such as hydrazine, dimethylformamide, and sodium borohydride which may pose hazards to the environment. Green synthetic methods can be an alternative to the current chemical and physical synthetic methods which are mostly are expensive, require toxic solvents, and

generate harmful by-products. Furthermore, the green synthesis of nanoparticles using honey mediated methods is non-toxic, environmentally friendly, cost-effective, time-saving, and facile, where honey is both the reducing and stabilizing agents.

Honey mediated synthesis offers several advantages over the other green synthetic methods such as microorganism mediated methods, as it is a rapid process compared to the microbial methods. Also, microorganisms must be cultured with extreme care and there is a time lag for the conversion of nanoparticles by the microorganisms. Furthermore, the separation of nanoparticles from the microorganisms is a difficult task.

Fe_3O_4 NPs are one of the common types of NPs which have been extensively exploited, though Fe_3O_4 NPs are prone to oxidization. To overcome this problem, this study suggests that a structural composition which is handful for the protection of the core Fe_3O_4 NPs from the oxidation by Au NPs. The configuration of magnetic NPs covered with Au NPs is also possible, which in turn, results in a core-shell nanostructure that possesses both optical and magnetic properties simultaneously.

Basically, bare electrodes have poor sensitivity and selectivity; so, the chemical modification of the electrode surface has been widely used to overcome these problems in sensor and biosensor applications. Furthermore, to avoid additional modification steps for the immobilization of the ssDNA on the electrode surface of DNA biosensors, Fe_3O_4-Au core-shell NPs providing a suitable platform for the self-assembly of thiolated ssDNA on the gold shell of the SPCE-Fe_3O_4-Au core-shell NPs electrode is investigated in this study.

The two main DNA clinical techniques for the HPV detection are the Hybrid capture HPV DNA Test 2 (HC2) and polymerase chain reaction (PCR) combined with agarose electrophoresis. The Hybrid Capture 2 test requires simple handling, while the exact HPV type cannot be identified as “low-risk” and “high-risk”. Also, the analytical process of gel

agarose electrophoresis are time-taking, with tedious steps and require harmful elements such as ethidium bromide for gel staining and ultraviolet for band visualization.

1.3 Objectives of the study

The objective of this study is the synthesis and characterization of a novel, simple green, and cost-effective Fe_3O_4-Au core-shell nanoparticles and its application in biosensors. The following specific objectives of biosensor based on Fe_3O_4-Au core-shell nanoparticles are designed to achieve this goal:

a) To synthesize and characterize Fe_3O_4 nanoparticles with controllable size and shape using honey mediated green synthesis method.
b) To modify Fe_3O_4 nanoparticles by gold as a core-shell nanoparticle using honey mediated green synthesis method and controlling the shell thickness.
c) To modify electrodes with Fe_3O_4-Au core-shell nanoparticles for electrochemical biosensor application.
d) To study the electrochemical behavior of the modified Fe_3O_4-Au core-shell nanoparticles electrode.

1.4 Scope of the Study

To achieve the objectives, several scopes are outlined as follows:

a) The physical and chemical properties of the synthesized Fe_3O_4 NPs will be characterized through XRD spectroscopy, TEM, FESEM, EDX, FT-IR, and VSM for the optimized formulation of the nanoparticle.
b) The physical and chemical properties of the synthesized Fe_3O_4-Au core-shell NPs will be characterized through UV-vis spectroscopy, SAED, XRD spectroscopy, TEM, FESEM, EDX, FT-IR, and VSM for the best condition formulation of the

shell thickness in these core-shell nanoparticles to exploit the advantages of the gold layer.

c) Glassy carbon electrode (GCE) and Screen-printed carbon electrode (SPCE) surface are modified by the synthesized NPs using the drop-casting method. Electrochemical detection of dopamine (DA) and Human papillomavirus DNA type 16 (HPV-16) will be examined by using GCE and SPCE modified Fe_3O_4-Au NPs.

1.5 Novelty and limitation

The utilization of honey in the synthesis process of magnetic Fe_3O_4 NPs and core-shell NPs is considered a novel method due to the limited number of studies conducted on the usage of honey. Also, honey is rich in polyphenols with antioxidant effects and maybe a potential anti-cancer agent. It is believed that the presence of the antioxidant compound in honey helps in the surface modification of the NPs and core-shell thereby enhancing the anti-cancer properties.

The Fe_3O_4 NPs investigated in this work can be applied to the synthesis process of the core-shell Fe_3O_4-Au NPs. Also, the NPs can be used for the surface modification of GCE and SPCE. The Fe_3O_4-Au NPs have shown good sensitivity towards DA is a suitable platform for the immobilization of thiolated ssDNA on the surface of SPCE without further modification using the self-assembly of thiol group.

In this study, the immobilized DNA probe on the modified electrode is design for the bio-recognition of HPV-16. So, there is a limitation in this study when using this DNA electrochemical sensor for the detection of other types of HPV such as 18, 31, 33, 45, 52, 58.

The honey mediated green synthesis method has been extensively used in previous studies and characterized, however, there are no reports on the synthesis of Fe_3O_4 NPs and Fe_3O_4/Au core-shell NPs and their utilization in biosensors.

1.6 Thesis outline

The work presented in this thesis deals with the green synthesis of Fe_3O_4 and Fe_3O_4-Au core-shell NPs and its potential application as sensors for the detection of DA and HPV-16 DNA.

Chapter 1 describes the general introduction to research background about Fe_3O_4-Au core-shell nanoparticles, and their application in electrochemical sensors, besides problem statements and research motivation, objectives, scope, and novelty of this thesis.

Chapter 2 report the literature review on nanotechnology and nanoparticles including iron oxide nanoparticles and Fe_3O_4-Au core-shell nanoparticles, green synthesis of nanoparticles, biosensors and DNA biosensors including electrochemical DNA biosensors and metal oxide nanoparticles in electrochemical sensing and biosensing, chemically modified electrodes based on nanoparticles for detection of DA and cervical cancer as a major health problem including human papillomavirus as a cause of cervical cancer, current diagnostic of human papillomavirus and electrochemical DNA sensors for HPV detection. (This work has been published in Analytical biochemistry journal, September 2018, Volume 556, pp 136-144, doi: 10.1016/j.ab.2018.07.002)

Chapter 3 discusses the chemicals, materials, and techniques for the synthesis and characterization of nanoparticles in addition to the general procedures for the fabrication of the electrochemical sensors.

Chapter 4 reports the characterization and performance of each fabricated electrochemical sensor. Part 1 explains a new synthesis and characterization of Fe_3O_4 NPs

(This work has been published in the International Journal of Nanomedicine, October 2018, Volume 13, pp 6903—6911, doi: 10.2147/IJN.S158083). Part 2 demonstrates the synthesis and characterization of Fe_3O_4-Au core-shell NPs (This work has been published in the Journal of Cellular Biochemistry, October 2018, Volume 120, issue 4, pp 6624-6631, doi: doi.org/10.1002/jcb.27958). Part 3 reveals the performance of the Fe_3O_4-Au core-shell NPs for the oxidation of DA where the glassy carbon modified with the synthesized NPs improves the sensitivity of the DA sensor. Part 4 shows the ability of the Fe_3O_4-Au core-shell NPs for HPV-16 DNA sensing.

CHAPTER 2: THEORY AND LITERATURE REVIEW

A general literature review will be discussed in the following chapter. In section 2.1, 2.1.1 and 2.1.2, the introduction of nanotechnology, iron oxide nanoparticles, and core-shell Fe_3O_4-Au nanoparticles are discussed respectively, while the synthesis of direct Au coated Fe_3O_4 and synthesis of indirect Au coated Fe_3O_4 are explained in section 2.1.2.1 and 2.1.2.2. In section 2.2, the green synthesis of nanoparticles is elaborated. The biosensors and DNA biosensors such as electrochemical DNA biosensors and metal oxide nanoparticles in electrochemical sensing and biosensing are discussed thoroughly in sections 2.3, 2.3.1 & 2.3.2. Then, nanoparticles based modified electrodes for the detection of DA are discussed in section 2.4.

Cervical cancer as a major health problem in terms of the human papillomavirus as the cause of cervical cancer and the current diagnostic of human papillomavirus is presented in section 2.5.1 & 2.5.2. Furthermore, electrochemical DNA biosensors for HPV detection are discussed in section 2.5.3. Finally, the direct (label-free) electrochemical DNA detection and indirect (labeled) electrochemical DNA detection are presented in section 2.5.3.1 and 2.5.3.2.

2.1 Nanotechnology

Nanotechnology is the manipulation of matter on the atomic and molecular scales which has a profound impact on clinical medicine. In 1974, the earliest widespread description of the term nanotechnology was introduced by Norio Taniguchi, who gave a speech describing how the dimensional accuracy things are made had improved over time (Bayda, Adeel, Tuccinardi, Cordani, & Rizzolio, 2020; A. Z. Wang & Tepper, 2014). Taniguchi predicted correctly that the techniques will evolve to the degree that the dimensional accuracy of less than 100 nm is achievable by the late 1980s. The environmental protection agency (EIA) of the USA known nanotechnology as matter with sizes about 1-100 nm, where superior physical properties are manifested in these dimensions with unique applications (Mukhopadhyay & Sharma, 2013).

Nanoscience and nanotechnology have provided an affordable and easy method as a solution to significant expense productions and environmental cleaning operations. It is assumed one of the peerless interdisciplinary fields by converting different science fields and strongly related to pharmaceutical, food systems, environment, and agriculture. Nanotechnology is based on the addition of nano-size particles into larger compounds and systems, through monitoring the structure and characteristics of the modified new materials at the nanoscale level. In addition, NPs possess the wide-ranging characteristics of advanced biological compatibility with better photocatalytic properties, excellent medical performance, and easy preparation (Dastjerdi & Montazer, 2010; Khan, Saeed, & Khan, 2019). A higher surface area to volume ratio is the most crucial property of NPs which has a direct impact on their application and suitability in different fields such as electronics, photonics, drug delivery as well as sensors and biosensors.

NPs can be synthesized by two approaches, the top-down or bottom-up methods, which are shown in Figure 2.1. In the top-down approach, bulk materials are broken down to the nanometer scale, an appropriate starting material is smaller in size through mechanical or chemical methods. one of the advantages of this method is the opportunity of mass production in the industry. However, some disadvantages of this method are the longer consumption, wide range particle size distribution, and defects of the surface morphology (El-Sherbiny & Salih, 2018; Teow, Asharani, Hande, & Valiyaveettil, 2011). The bottom-up or the self-assembly method is defined as the construction of a structure through the defined arrangement of atoms or molecules. Chemical or biological methods can be used to assemble the atoms to form desired materials. The bottom-up method includes nanosphere lithography, chemical, photochemical, electrochemical, templating, sonochemical, and thermal reduction techniques (S. Kumar, Bhushan, & Bhattacharya, 2018; Shah et al., 2014).

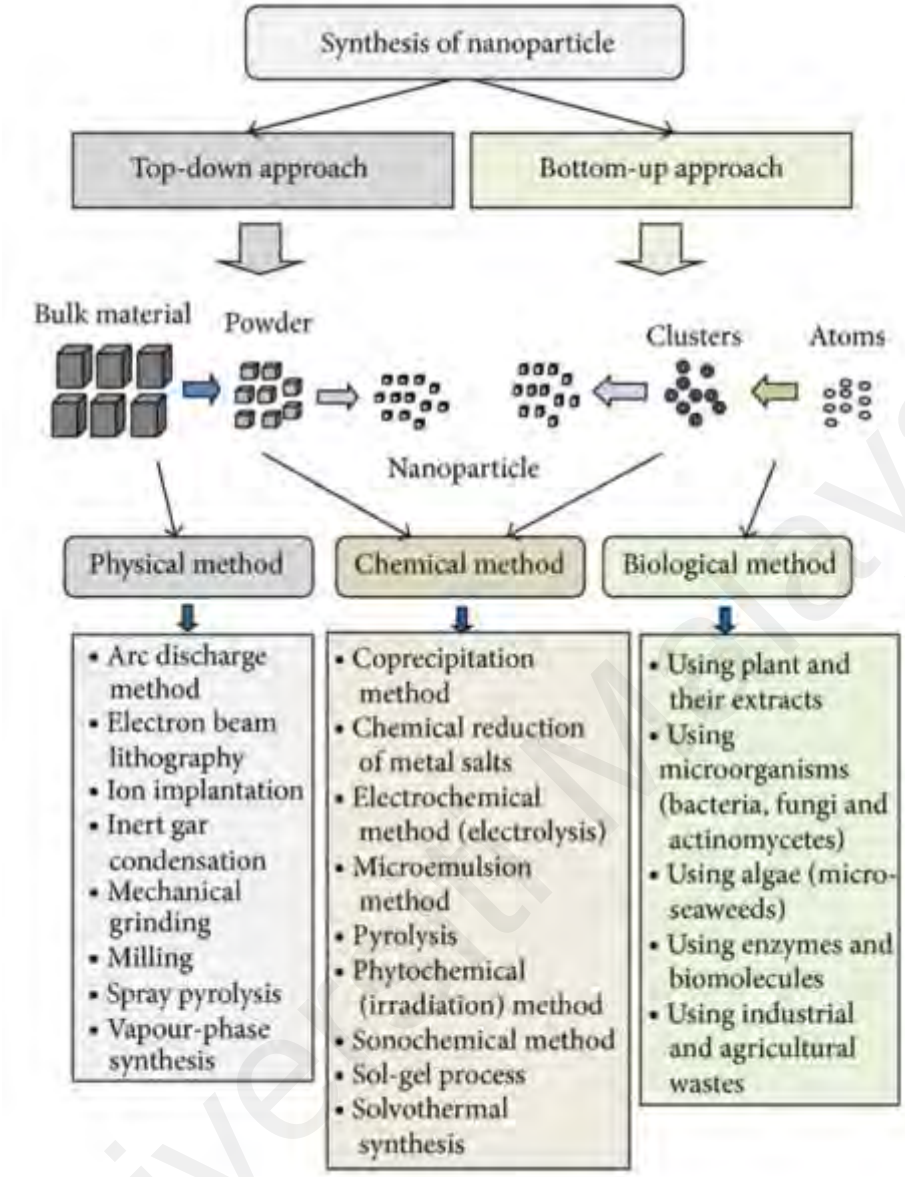

Figure 2.1: Different approaches and methods for synthesizing nanoparticles. reproduced with permission from the publisher (Patra & Baek, 2014)

The NPs are a few hundred nanometers smaller than the large biological molecules (enzymes, receptors, and antibodies). These NPs, which are 100 to 10,000 times smaller in size than the human cells, can present unprecedented interactions between both the biological molecules and the cells on the surface, as well as within the cells. Nanoparticle therapy can be revolutionary in the diagnosis and treatment of cancer (V. K. Chaturvedi, Singh, Singh,

& Singh, 2019). It is used in an extensive range of industries such as biomedicine, material sciences, pharmaceuticals, electronics, environmental analysis, catalysis, and cosmetics. Similar to other materials on earth, NPs are separated into inorganic materials (magnetic NPs, noble metal NPs, semiconductor NPs and quantum dots) and organic materials such as dendrimers and carbon nanotubes (Jeevanandam et al., 2018). Examples of these novel NPs are Au-NPs and Fe_3O_4-NPs that are widely used in advanced nanotechnology applications.

2.1.1 Iron Oxide Nanoparticles

Hematite (α-Fe_2O_3), maghemite (γ-Fe_2O_3), magnetite (Fe_3O_4) and iron (II) oxide (FeO) are the various forms of iron oxides which exist in nature. In fact, Fe_3O_4 NPs is one of the most favorable among noble magnetite NPs due to its unique properties in numerous field such as magnetic fluids (Wallyn, Anton, & Vandamme, 2019), catalysis (Shifrina & Bronstein, 2018), biotechnology/biomedicine (Guo et al., 2018; Vallabani & Singh, 2018), magnetic resonance imaging (Wallyn et al., 2019), data storage (García-Merino, Bringas, & Ortiz, 2021) and as remediation of the environment (B. Jiang et al., 2018; Su, 2017). In most of these applications, the critical size of the nanoparticles for the best performance is 10-20 nm. Magnetic nanoparticles, especially magnetite and maghemite nanoparticles with proven biological properties and excellent biocompatibility, have been the subject of various studies in the past ten years, due to the wide range of important biomedical and environmental applications such as cancer therapy (Mukherjee, Liang, & Veiseh, 2020), targeted drug delivery (Shen, Li, & Qiao, 2018), detoxification hyperthermia (Khan et al., 2019), enhanced magnetic resonance imaging (Avasthi, Caro, Pozo-Torres, Leal, & García-Martín, 2020) and magnetic separation. So far, the synthesis and preparation of iron oxide nanoparticle have been an important research priority, and it has been extensively studied and characterized.

Various synthetic methods have been reported for magnetic NPs such as co-precipitation (Shen et al., 2014), thermal decomposition(Chin, Pang, & Tan, 2011), microemulsion method (Salvador et al., 2021), sonochemical (Vijayakumar, Koltypin, Felner, & Gedanken, 2000; Yanmin Wang, Nkurikiyimfura, & Pan, 2015) and hydrothermal process (Torres-Gómez et al., 2019), which has a substantial effect on the shape, size control and distribution of these nanoparticles and add to their usefulness in different applications. However, there are still major challenges to produce a highly stable and completely protected magnetic nanoparticle which is suitable for biomedical applications.

A high surface to volume ratio of the magnetic iron oxide NPs results in agglomeration, a process that decreases the surface energy of the particles. Oxidation in the air and reactivity of the bare nanoparticles results in the loss of magnetism and the dispersion. Thus, it is imperative to come up with strategies that are aimed at stabilizing the nanoparticles for different applications. This means that the magnetic NPs need to be highly protected from degradation before or after the synthesis process. Some of the methods that are applied include coating with organic materials or grafting with polymers, or veneering using inorganic films such as carbon or silica. Different applications can also result in different uses of the stabilization strategies mentioned above. (Majidi, Zeinali Sehrig, Farkhani, Soleymani Goloujeh, & Akbarzadeh, 2016). Gold, platinum, carbon, iron, and palladium are applied as coatings to reduce the level of oxidation of the nanoparticles. It is, however, critical to ensure that the application of iron oxide (Fe_3O_4) nanoparticles is ascertained before coming up with the best metal or non-metal coating that should be utilized in the process. This is due to the different reactive processes that may occur, depending on the specific coating that may hinder the application of the nanoparticles, although the oxidation process decreases the saturation magnetization (Ms).

Table 2.1: Metal coated iron oxide (Fe_3O_4) and its properties

Nanoparticles	Properties (Magnetic/Thermal/Mechanical)	References
Au-Fe_3O_4	12 to 15 nm on *reduced graphene oxide* (rGO) sheets, Fe_3O_4-AuNPs were highly dispersed on reduced graphene oxide nanosheets to enhance the electrocatalytic activity of Fe_3O_4-AuNPs for the oxidation of methanol into CO_2.	(Atar, Eren, Yola, Karimi-Maleh, & Demirdögen, 2015)
Ag-SPIONs	Size of the bare superparamagnetic iron oxide nanoparticles (SPIONs), 6.2 nm. Size of Ag coated SPIONs 14.8 to 29.6 nm, the magnetic saturation of SPIONs was 32 emu/g, magnetic saturation value 9 emu/g	(Norouz Dizaji, Yilmaz, & Piskin, 2016)
Au-SPIONs	Size of the bare SPIONs 6.2 nm, size of Au coated SPIONs 10.1 to 12.1 nm. The magnetic saturation of SPIONs was 32 emu/g, magnetic saturation value 18 emu/g	(Norouz Dizaji et al., 2016)
Fe_3O_4-Au	Fe_3O_4 NPs size of 8.0 ± 2.0 nm with a spherical shape, core-shell Fe_3O_4-Au composite retained the spherical structure with a diameter of 20 ± 4 nm, the thickness of the Au shell 12 nm. Ms of Fe_3O_4 NPs and Fe_3O_4-Au is 53.765 and48.1 emu/g	(Fouad, El-Said, & Mohamed, 2015)
Pt-Fe_2O_3	Size 10 nm. Application in catalysis and as precursor materials for making magnetically active nanocomposites for ultrahigh data storage media applications	(Teng, Black, Watkins, Gao, & Yang, 2003)
Pd-Fe_3O_4	Size 8 nm, the Ms 29.6 emu/g $^{-1}$, in catalysis	(Zhifei Wang, Shen, Aihua, & He, 2005)
Ag-Fe_3O_4	230 nm, Ms of the sample is 15.7 emu g $^{-1}$	(D.-H. Zhang, Li, Li, & Chen, 2008)

2.1.2 Core-shell Fe_3O_4-Au Nanoparticles

The growing research focus is on the core-shell nanostructure because of its common compositions and structures (Bachhuka et al., 2015; Gawande et al., 2015; Ghosh Chaudhuri & Paria, 2011). In this nanostructure, the interaction among the core and shell may cause the development of new properties and functions (X. Wang et al., 2016; Z. Wang et al., 2016). To achieve varying physical properties and effects, various combinations between the organic and inorganic compounds can be utilize in nanostructure fabrication (Y. S. Kim et al., 2013). Ingredients used in the construction of the core-shell nanostructures and the physical properties of the ingredients may lead to the establishment of a new group of nanoparticles, which can be beneficial in a varied range of applications such as nanomedicine, biotechnology, magnetic device and others (Knopp, Tang, & Niessner, 2009; Mitsudome & Kaneda, 2013; Pustovalov, Astafyeva, & Fritzsche, 2012).

Recently, superparamagnetic iron oxide nanoparticles (SPIONs) have attracted extraordinary attention in many fields, such as bioseparation, magnetic recording media, target drug delivery, electrochemistry, and biochemical sensors (Xi Zhou et al., 2010). However, the biomedical applications of SPIONs are limited, due to high oxidation and aggregation of the magnetic nanoparticles (Papaphilippou et al., 2009; Shabatina, Vernaya, Shabatin, & Melnikov, 2020). To enhance their biomedical applications, the stability and dispersion must be improved; several coating methods have been utilized, for instance, coated SPIONs with polymers, silica, and noble metals (Dheyab, Aziz, Jameel, Noqta, & Mehrdel, 2020; Hoskins et al., 2012).

Over the past decade, gold-coated iron oxide nanoparticle (Au-Fe_3O_4) has received significant attention due to the enhanced mono dispersion, conductivity, selectivity, controlled oxidation, and stability of Fe_3O_4. The synthetic methods for this nanoparticle are

co-precipitation, thermal decomposition, microemulsion, sonochemical and hydrothermal process, which have a substantial effect on the shape, size control, and distribution of these nanoparticles. In most of these applications, the critical size of the nanoparticles for the best performance is 10-20 nm (Khan et al., 2019) . However, there are still major challenges to produce a highly stable and completely protected magnetic nanoparticle which is suitable for biomedical applications.

The preparation of Au-Fe_3O_4 nanoparticles imposes at least, a two-step method: the production of the magnetic core followed by the coating of gold. While the production of the magnetite NPs core is well established, (Adamiano, Iafisco, & Tampieri, 2018) the gold coating process has been more problematic, and several methods have been suggested, such as γ-radiation (Ghoreishian et al., 2019), laser ablation (Riedel et al., 2020), sonochemical reaction (Dheyab, Aziz, & Jameel, 2020), chemical reduction (De Souza, Nogueira, & Rostelato, 2019; Nikabadi, Shahtahmasebi, Rokn-Abadi, Mohagheghi, & Goharshadi, 2013) and layer-by-layer electrostatic deposition (Goon et al., 2009; Salgueirino-Maceira et al., 2006; Spasova et al., 2005). These methods can be divided into two general approaches: one of which involves the direct development of a gold shell on the iron oxide nanoparticles surface.

Mandal *et al*. (Mandal et al., 2005) have recounted that the Fe_3O_4 nanoparticles are detached, coated with metallic silver and gold via the reduction of Au^+ and Ag^+, to attain steadiness of the magnetic nanoparticles for an extended time. This route produced nanoparticles of 18 to 30 nm in size, where the nanoparticles have a distinct core-shell structure, although the transmission electron microscopy (TEM) micrograph does not reflect such morphology. The data also revealed that the Ms of gold-coated is 38 emu g^{-1} (T = 10 K) and decreases by 57.6% of the bulk Fe_3O_4 nanoparticles (92 emu g^{-1}, T = 10 K). Usually,

this method often applies to the preparation of the core-shell type of nanoparticles, but it is inclined to preserve the magnetic properties of the bare iron oxides. This is the most common method for the preparation of the metallic functionalized iron oxide nanoparticles by a single-metal ion reduction process on small molecule surface, SiO_2 or polymer functionalized iron oxide nanoparticles, as well as the connection of gold nuclei followed by the coalescence and development of the nuclei into a whole shell.

In recent years, a method has been used to formulate the nanoparticles of monodispersed gold-coated Fe_3O_4 through the sonolysis of a mixture of amino-modified Fe_3O_4 nanoparticles and gold ions with an additional drop-inclusion of the reducing agent. The composite nanoparticles are of 30 nm in diameter, and their saturation magnetization is approximately 63 emu g^{-1}, and it is abridged only by 0.03% from the bulk Fe_3O_4 nanoparticles (65 emu g^{-1}, T = 10 K). Thus, this method is useful to preserve the Ms of the initial bare magnetite nanoparticles(W. Wu, He, Chen, Tang, & Nie, 2007).

Yu et al. (H. Yu et al., 2005) also described the production of dumbbell-like double-functional Au-Fe_3O_4 nanoparticles through epitaxial development of iron oxides on the seeds of Au. A combination of Au nanoparticles, 1-octadecene solvent, oleic acid, $Fe(CO)_5$ and oleylamine, was heated and refluxed at 300 ºC followed by room temperature oxidation in air. Using these procedures, the dumbbell-like nanoparticles have adjustable sizes ranging between 3 to 15 nm.

Stoeva *et al*. (Stoeva, Huo, Lee, & Mirkin, 2005) also made use of the shell-core functionalized iron oxide nanoparticles (SiO_2/Fe_3O_4 nanoparticles). The electrostatic attraction of 1 to 3 nm gold NP nuclei acts in a consequent stage, as the nucleation spot for

the creation of an uninterrupted gold shell surrounding the shell-core nanoparticles upon the $HAuCl_4$ addition (W. Wu et al., 2007). It is also established that these three-layered magnetic nanoparticles could be functionalized with DNA, after artificial techniques for pure gold nanoparticles and amassed reversibly into macroscopic collections, through the use of complementary connecting oligonucleotides.

O'Connor *et al*. have produced iron NPs that are gold-coated with 11 nm core size as well as a gold shell with a thickness of approximately 2.5 nm (Ban, Barnakov, Li, Golub, & O'Connor, 2005). The gold coated iron nanoparticles are stable under acidic and neutral solutions. The coating was attained through a restricted additional reaction through the use of a polar aprotic solvent.

Briefly, a $FeCl_3$ yellowish solution, liquefied in 1-methyl-2- pyrrolidinone (NMPO), was poured into a dark green liquid of NMPO encompassing naphthalene and sodium under rigorous stirring at room temperature (W. Wu et al., 2007). Therefore, the Fe^{3+} ions were condensed with sodium to create the metallic cores. Following the elimination of sodium chloride through centrifugation, as well as the inclusion of the capping agent, 4-benzylpyridine at high temperature, the iron NPs were smeared with gold by adding dehydrated $HAuCl_4$ into the NMPO solution.

An inverse microemulsion technique can also form the gold-coated iron NPs. The reverse micelles were fabricated with CTAB as the surfactant, 1-butanol as a co-surfactant, and octane as the continuous oil phase. $NaBH_4$ reduced the $FeSO_4$, and the gold coating on the iron NPs was established from the reduction of $HAuCl_4$ (Q. Liu, Xu, Finch, & Egerton, 1998).

Zhang *et al*. described a new technique for the preparation of gold-coated iron magnetic core-shell NPs through the unification of laser irradiation and wet chemistry. The gold powder and iron NPs in a liquid medium were illuminated by a laser, to set down the gold shell (J. Zhang et al., 2006). The body-centered cubic (bcc) (18 nm) iron mono-domain magnetic cores are enclosed by a partly merged gold shell of around 3 nm in diameter, of the face-centered cubic (fcc) gold-coated NPs. The core-shell particles usually are superparamagnetic at room temperature. The blocking temperature (TB) is roughly 170 K. Following four-month shelf storage in a typical laboratory setting, the magnetization standardized to the iron content was found to be 210 $emug^{-1}$, approximately 96% of the value of bulk iron, which designates the high steadiness.

2.1.2.1 Synthesis of direct Au coated Fe_3O_4

Keung Lo *et al*. (Lo, Xiao, & Choi, 2007) synthesized small Fe_3O_4 (12.3 nm) nanoparticles from the co-precipitation of $FeCl_3$ and $FeCl_2$ in diluted NH_3 solution. Next, a $HAuCl_4$ solution was boiled with the addition of Fe_3O_4 nanoparticles, followed by the addition of sodium citrate as the reducing agent for the Au shell formation. L-Homocysteine was added into the boiling solution to form Fe_3O_4-Au-homocysteine nanoparticles. These nanoparticles are well dispersed in water, which is essential for biomedical applications. Moreover, the surface functionalization with homocysteine is useful for the further functionalization of the Fe_3O_4-Au nanoparticle surface. Amine and carboxylate groups on the nanoparticle surface may allow subsequent transformations, as shown by the Au nanoparticle ligand sphere (Templeton, Wuelfing, & Murray, 2000) and carboxylated Fe_3O_4-Au nanoparticles (Kouassi & Irudayaraj, 2006). According to the TEM data, the nanoparticles are sphere-shaped, with small average sizes of 12.3 nm.

Fe_3O_4 nanoparticles can also be coated with gold by using $NaBH_4$ reduction of $HAuCl_4$ with sonication. The sonication procedure leads to an improved nano-particle monodispersity and avoids the agglomeration attributable to the ionic interactions. The obtained core/shell nanoparticles are also small, with a mean size of 12.573 nm (Tamer, Gündoğdu, Boyacı, & Pekmez, 2010).

The other approach to the Fe_3O_4 coating with gold is the $HAuCl_4$ reduction using sodium citrate and hydroxylamine hydrochloride. This reduction procedure involves a longer time duration than other approaches up to 5h. The resulting NPs are spherical, with a mean diameter of 20 nm (X. Zhao, Cai, Wang, Shi, & Jiang, 2008). The magnetite surface is often modified to attract Au ions. One of the modifications is through a sodium citrate coating of Fe_3O_4. The Fe_3O_4-Au NPs with a diameter of 15 to 40 nm were obtained with this approach. Magnetite NPs can be prepared by the co-precipitation method. Sodium citrate was added into the mixture with stirring, to form the precipitate. Then, the Fe_3O_4 citrate coated nanoparticles were added to the $HAuCl_4$ boiling solution(Elbialy, Fathy, & Khalil, 2014). The proposed reactions are quick and convenient as they are performed in an aqueous medium.

There are also other procedures of Fe_3O_4-Au synthesis in organic media. For example, small Fe_3O_4 nanoparticles with a diameter of 10 nm (Xu, Hou, & Sun, 2007) and 6.770.7 nm (Robinson, Tung, Maenosono, Wälti, & Thanh, 2010) were produced through the thermal decomposition technique. The reduction of $Fe(acac)_3$ by 1,6-hexadecanediol in oleic acid and oleylamine as the capping agent resulted in Fe_3O_4 nanoparticles with amine functional groups on the surface. Thus, these amine groups are utilized as a template to attach the Au^{3+} ions. In another approach, the Au shell was formed by the reduction of $Au\ (Ac)_3$ using 1,2-hexadecanediolinin with the presence of oleic acid, oleylamine, and magnetite. The solution

was heated between 180 and 190 °C for 90 minutes. To form the water-soluble shell/core NPs, they were dissolved in tetramethylammonium hydroxide and tri-sodium citrate solution (Robinson et al., 2010).

In another experimentation, the Au shell was shaped through the reduction of $HAuCl_4$ by oleylamine in the presence of magnetite (Xu et al., 2007). These nanoparticles are well dispersed in nonpolar solvents. To form the water-soluble shell/core NPs, they were dissolved in CTAB and a sodium citrate aqueous solution under sonication. The as-prepared nanoparticles were used as seeds for the development of the Au shell using ascorbic acid for reduction of $HAuCl_4$ designed for 6 hrs to deposit an extra 0.5 nm layer of gold. Therefore, the resulted nanoparticles have a core diameter of 10 nm and shell diameters of 1 nm, 1.5 nm, 2 nm, 2.5 nm, and 3 nm. However, this method allows for the regulation of the thickness of the Au shell. The dissolution in different solvents is required to make the Fe_3O_4-Au nanoparticles water-soluble.

2.1.2.2 Synthesis of indirect Au coated Fe_3O_4

The gold coated magnetic nanoparticles can also be freely functionalized using biomolecules due to the conjugation of protein and nucleic acids on the gold surface (Lim et al., 2008; Lu et al., 2006). Silica layer covering is necessary after the production of the Fe_xO_y core due to its capacity to stabilize the Fe_xO_y core, as well as to avert its accretion. To coat a layer of silica on the Fe_xO_y NPs, tetraethylorthosilicate (TEOS) is generally utilized in the sol-gel process. In the course of the production of Au–Fe_xO_y nanocomposites, the introduction of the silica layer is necessary to ensure the stability and the size increase of Fe_xO_y. Huang *et al*. reported that Fe_xO_y NPs are initially covered with a silica layer so that

the construction of the core/shell and the core/satellite structures can take place (Yougbaré et al., 2020).

Lee *et al*. (J. Lee et al., 2008) synthesized multifunctional magnetic gold nanocomposites (MGNCs) for coordinated cancer diagnosis and therapy by magnetic resonance imaging (MRI). The monodispersed $MnFe_2O_4$ magnetic nanocrystals (MNCs), soluble in organic solvents, were produced by a formerly described thermal decomposition method. Aggregates of MNCs were prepared by a nano-emulsion technique to form the magnetic kernels (MKs). The prepared MKs are covered with a silica layer via the tetraethylorthosilicate (TEOS) hydrolysis. The magnetic silica nanoparticles (MSNPs) surface was further adjusted with trimethoxysilane for the efficient nucleation of gold nanoparticle (Au-NP) to the amine-terminated surface of silica. They eventually fabricated an MGNCs with a gold nanolayer by the reduction of $HAuCl_4$. Laser scattering confirmed that the MGNCs had a magnitude between 120 ± 13.8 nm. A silica layer coating can form a double-layered Au shell on the inner Au shell, and an additional coating of Au shell placed on the outer silica layer.

A multilayer of Fe_3O_4-SiO2-γ- AlOOH-Au nano/micro flowers were prepared by K Cham-Fai Leung *et al*. (Xuan et al., 2011) with a superparamagnetic Fe_3O_4 microsphere (200 nm) (Ge & Yin, 2008), and a layer of SiO_2 (25 nm) (Xuan, Wang, Yu, & Cham-Fai Leung, 2009), to form a spherical Fe_3O_4-SiO_2 core/shell particle. The SiO_2 coating not only protects the Fe_3O_4 core but also alters the surface features, which is favorable to the ensuing solvothermal reaction of the tiered γ-AlOOH nanosheets, to bring about the nano/micro flower structures. Then, the nanoflowers are altered using 3-aminopropyltriethoxysilane to activate the particles with amine practical clusters and protonated into the ammonium clusters.

Citrate-protected Au NPs that are negatively charged were efficiently gathered onto the nanoflower surface, which is positively charged. This is possible through the electrostatic attraction (Fang et al., 2008; Xuan, Wang, Yu, & Leung, 2009). The scanning electron microscope (SEM) image shows an emblematic sample that encompasses numerous similar and flower-like architectures of about 500 nm in diameter and also reveals that the structure's periphery is composed of various nanosheets which are 5-10 nm thick and 100-300 nm wide. The formed nano-flowers are mono-dispersed, and in the absence of a large aggregation, they can be well dispersed in the solution. In this study, it was discovered that the magnetic micro/nano-structures were engaged to remove/immobilize bovine serum albumin (BSA) protein. Ultimately, this material can be relevant to enzyme immobilization for a particular catalytic purpose, drug or gene delivery, as well as discriminatory biomolecules capture for water purification. Additionally, they have an efficient magnetic targeting and separation features.

Oleic-acid functionalized magnetite NPs of magnitude 4.8 ± 1.1 nm were prepared from $Fe(acac)_3$ thermal decomposition in the presence of oleylamine and oleic acid, based on the process established by Sun *et al*. (S. Sun et al., 2004) The resulting NPs are considerably larger, with a magnitude of 20.6 ±7.8 nm, and more spherical-shaped unlike the regularly cubic oleic acid-coated iron oxide preliminary material. The upsurge in the magnitude of the nanoparticles relates to the incorporation of a gold layer thickness of 7.5 nm. It is imperative to note that this process does not make it possible for a uniform coating of gold with the same thickness onto each NP. Consequently, there is a polydispersity detected in the ultimate product. Magnetic nanoparticle's gold coating is particularly fascinating because the gold surface can be extensively functionalized by the thiol clusters. This action allows the

connection of practical ligands which may generate the resources suitable for optical and catalytic applications (Amina & Guo, 2020).

Metallic NPs have an advanced level of magnetization compared to their oxides. Nevertheless, the high toxicity and reactivity make them inappropriate for direct use in biotechnology and biomedicine. Hence, metallic NPs must be covered with an insulating shell for protection and silica, or a polymer layer coating is regularly utilized for this purpose. However, the polymer-coated magnetic NPs are unstable when exposed to high temperature due to the core volatility of the polymers and is unfavorably impacted by the catalytic nature of the NPs. It is hard to accomplish a wholly nonporous and dense silica coating of the silica-coated magnetic NPs. This means that it is challenging to maintain the high stability of these NPs under alkaline environmental conditions (Catalano et al., 2017). There is still a necessity to explore novel synthetic techniques to strengthen the magnetic NPs' stability in alkaline and acidic conditions and under high temperatures.

Table 2.2: Summary comparison of the Fe_3O_4-Au synthetic methods. Adapted with (Salihov et al., 2015)

Synthesis techniques Core	Synthesis techniques shell	Size (nm) Core	Size (nm) Particle	Surface modification	Application	Ref.
Co-precipitation	Reduction by citrate	N/A	30	Homocysteine	Unspecified	(Rudakovskaya, Beloglazkina, Majouga, & Zyk, 2010)
Co-precipitation	Reduction by citrate	20	22	N/A	T2 Contrast Agent MRI	(T. Ahmad et al., 2012)
Co-precipitation	Reduction by citrate	N/A	12.3	N/A	Unspecified	(Lo et al., 2007)
Co-precipitation	Reduction by $NaBH_4$ Ultrasound	9.5± 3	12.5± 3	Boronic oxide+ fructose	Biomolecule Immobilization and detection	(Tamer et al., 2010)
Co-precipitation	Reduction by hydroxylamine hydrochloride and citrate	N/A	20	11-mercaptoundecanoic acid11-dodecanethiol	Interaction with target molecules	(X. Zhao et al., 2008)
Co-precipitation	Reduction by citrate	N/A	100	3′-(alkanethiol) oligonucleotide	Biosensor	(Pang et al., 2007)
Co-precipitation	Reduction by citrate	11 ± 3.2	24.06 ± 1.5	Thiol-terminated polyethylene glycol	Doxorubicin delivery	(Elbialy et al., 2014)
Co-precipitation	Reduction by citrate	10	22-30	3′-alkanethiol-modified oligonucleotides	DNA detection	(H. Zhou et al., 2012)
Co-precipitation	Reduction by citrate	N/A	15–40	Protein immunoglobulin G	Biological separations	(Pham, Cao, & Sim, 2008)
Co-precipitation	Reduction by Hydroxylamine	N/A	30	Different antibodies and proteins	Ultrasensitive detection of carbohydrate protein interactions	(Liang et al., 2009)
Thermal decomposition	Thermal decomposition from Au (Ac)3, oleic acid and oleylamine (organic medium)	6.7 ± 0.7	9.2 ± 1.3	Thiolated DNA	Unspecified	(Robinson et al., 2010)

Table 2.2: Summary comparison of the Fe_3O_4-Au synthetic methods. (continued)

Synthesis techniques		Size (nm)		Surface modification	Application	References
Core	shell	Core	Particle			
Thermal decomposition	Reduction by Oleylamine (organic medium)	10	12	No	Unspecified	(Xu et al., 2007)
Reversed micelle technique	Reduction by NaBH4	N/A	18±4	No	T1 and T2 weighted imaging	(S.-J. Cho, Jarrett, Louie, & Kauzlarich, 2006)
Water-in-oil inverse nanoemulsion procedure	Reduction by NaBH4	9 ±2	13±3	No	Unspecified	(Maleki, Simchi, Imani, & Costa, 2012)

An extensive range of studies has been performed to synthesize core-shell nanoparticles through successive reduction techniques, with the quest of genuine multifunctionality in a single nanostructure. With regards to the cores and shells using noble metals, gold is an excellent candidate, owing to the high chemical stability, low reactivity, and biocompatibility (Mahato et al., 2019). It also provides the functionalization with amine or thiol functional groups via covalent bonds (Rao et al., 2019). Au coated Fe_3O_4-NPs provide a suitable platform for the combined iron oxide magnetic properties and gold shell properties, to be utilized for biotechnological and biomedical applications.

2.2 Green Synthesis of Nanoparticles

Various procedures are used for the synthesis of nanoparticles, such as physical and chemical approaches. The physical method involves a top-down approach, whereas the chemical method includes a bottom-up approach. Previously, the top-down approach was used widely, which employ physical and chemical means to reduce the bulk material into nanosized structures (Tarafdar, Sharma, & Raliya, 2013). However, such methodologies are associated with a large number of materials and energy consumption, hence, they are not preferred. Nowadays, the bottom-up approach has become more popular and is used more commonly, though mostly in smaller scales.

The wet chemical methods often employ reducing agents or capping agents for the synthesis of nanoparticles (Baruwati & Varma, 2009; Nadagouda & Varma, 2008; Nikam, Prasad, & Kulkarni, 2018). Although they control the size, morphology, and composition of nanoparticles, yet most of these capping agents are highly toxic and do not degrade quickly and remain in the environment for several years, thereby contributing to environmental pollution (X. Li, Xu, Chen, & Chen, 2011). Such processes utilize the sol-gel, solvothermal,

hydrothermal, electrodeposition and spray pyrolysis techniques (Fan, Feng, Tang, & Li, 2015; Mani & Rayappan, 2015; Sonker, Sabhajeet, Singh, & Yadav, 2015; Suntako, 2015; M.-H. Wang, Ma, & Zhou, 2015).

Since the evolution of nanoscience and technology, various reducing agents have been used for the synthesis of nanoparticles, such as hydrazine (Musza et al., 2019), sodium borohydride (Ramos et al., 2020), potassium bitartrate (Tan, Dai, Li, & Zhu, 2003), and methoxy polyethylene glycol (Titkov et al., 2019). Toxicities of representative capping agents, reducing agents, and solvents using in nanoparticle synthesis is summarized in Table 2.3:

Table 2.3: Toxicities of representative capping agents, reducing agents, and solvents using in nanoparticle synthesis (Duan, Wang, & Li, 2015).

Toxicities	Capping agents[a]	Reducing agents[b]	Solvents[c]
Harmful	PPI, PEI, CTAB	EG, vitamin C	Ethanol, toluene, ODE
Irritant	PEG, PAA, linoleic acid, TOPO, TOP, OA, ODA	Citric acid	
Corrosive	PAA, TOP, OAm, DDA	Citric acid, NaBH4, OAm	OAm
Toxic	PAA, PAMAM, OA	Formaldehyde, CO, N2H4, NaBH4	Ethanol, DMF, toluene
Highly flammable		Ethanol, N2H4	Ethanol, toluene
Extremely flammable		CO	
Dangerous for the environment	CTAB, OAm, DDA	N2H4, NaBH4, OAm	OAm

[a] The full names of listed abbreviations are given as: PPI: poly(propyleneimine). PEI: polyetherimide. CTAB: hexadecyltrimethylammonium bromide. PEG: polyethylene glycol. PAA: polyacrylic acid. TOPO: trioctyl-phosphine oxide. TOP: tri-n-octylphosphine. OA: oleic acid. ODA: octadecylamine. OAm: oleyl amine. DDA: dodecylamine. PAMAM: poly(amidoamine). [b] EG: ethylene glycol. [c] ODE: 1-octadecene.

Due to the hydrophobicity of the capping agents, such as oleic acid and thiols, a large amount of toxic organic solvents must be employed in the wet chemical synthesis processes, which accounts for major reasons for the steep increase in environmental pollution (Mondal et al., 2011). These solvents are carcinogenic, health-hazardous, and corrosive. Moreover, chemical methods usually involve high-temperature conditions (Nikam et al., 2018). The

processes, which can be operated at ambient temperature, are appreciated as they are energy-saving and can be employed efficiently for industrial purposes.

On the other hand, various physical methods for the synthesis of nanoparticles include flame pyrolysis (Solero, 2017), electric discharge (Bulychev, 2021), ball milling (J. Zhang et al., 2018) and laser ablation (Menazea, 2020). No doubt that these physical techniques do not involve harmful chemical reagents, but high temperature and pressure are essential, which can only be maintained at the cost of energy consumption, thus, it is not an economical approach (Thakkar, Mhatre, & Parikh, 2010). Therefore, the development of wet chemical processes, which operate at ambient temperature and atmospheric pressure, involve relatively less hazardous solvents and reagents. Such processes give high yield with minimum size. Thus, the process of green chemistry becomes essential.

The term 'Green Chemistry' was termed with the main objective of reducing the use of hazardous substances/reagents and replacing them with natural reagents from nature (Linthorst, 2010). An extended inspection reveals that there are at least three significant factors where green chemistry can be applied to remove the yet common problems: choice of capping agents/stabilizers, choice of reducing agents, and choice of solvents (Parveen, Banse, & Ledwani, 2016). Nowadays, a wide range of studies has emerged, which focuses on the use of principles of green chemistry for the development of different types of nanomaterials. Green chemistry aims at carrying out the reactions under ambient conditions, utilizing renewable resources, and minimizing the experimental risks, which enables minimum environmental hazards, unintended risks to human health, and next-generation enhanced applications (Lancaster, 2020). In green synthesis, mainly three factors are

dominant i.e. the choice of green alternative solvent, non-hazardous reductant, and environmentally friendly stabilizing agent.

2.3 Biosensors and DNA biosensors

Biosensors are integrated receptor-transducer devices which integrate a biological component with a detector component that has three main parts (Yoon, 2016):

(1) A biologically derived material as the sensing element. (2) A transducer or detector element for the conversion of the biochemical signal from the recognition element into a readable and quantified output. (3) A signal processor that displays the transformed signal.

In 1962, Clark and Lyons reported their innovative work on glucose sensors for the detection of glucose in samples from diabetic patients (Clark Jr & Lyons, 1962). Currently, the research interest towards biosensors is growing steadily due to their advantages such as sensitivity, specificity, rapid response, and simplicity without prolonged experimentation processes and purification requirements. Biosensors are commonly classified into two categories: i) the bioreceptor (whole cells, antibodies, peptides, nucleic acids, and aptamers) and ii) the transducer; and in some cases, the bioreceptor is coupled with the transducer (Shukla, Govender, & Tiwari, 2016).

The different types of transduction-based biosensors are electrochemical, optical, mass, and electrical biosensors. The sensitive element in nucleic acid-based biosensors generally comprises of a single-stranded DNA (ssDNA) molecule which allows the particular binding of nucleic-acid sequences on a surface before the hybridization with the complementary target nucleic acid (Elbaz, Tel-Vered, Freeman, Yildiz, & Willner, 2009; Sohrabi, Valizadeh, Farkhani, & Akbarzadeh, 2016). There is a direct proportionality between the amount of

target and the level of hybridization with the signal intensity, which influences the sensor response (Beattie et al., 1995).

The synthesis of DNA sequences with functionalized end groups is commonly reported; furthermore, DNA purification from biological or clinical samples is more facile compared to protein, as the former is a more stable molecule. The rapid and reversible hybridization of ssDNA and target nucleic acid in electrochemical DNA biosensors allow the regeneration of the sensor, which offers rapid detection, simplicity, low cost, and stability. The detection of DNA sequences represents a promising strategy for the early screening and detection, as well as the early diagnosis of diseases (Dwivedi et al., 2017; Chensu Wang et al., 2011). Due to the deficient screening options and exceedingly high fatality rates in developing countries, the fabrication of rapid and economical detection devices is profoundly critical.

Numerous methods such as radiochemical, enzymatic, fluorescent, surface plasmon resonance spectroscopy and quartz crystal microbalance have been utilized for DNA detection (L.-s. Liu, Wu, & Zhang, 2017; Sarika Pal, Verma, Raikwar, Prajapati, & Saini, 2018; H. Zhang et al., 2020). Besides, it is also crucial to develop ultrasensitive devices for samples with a lower concentration of HPV DNA. Several ultrasensitive sequence-specific DNA detection techniques such as polymerase chain reaction (Zou & Ling, 2018), rolling circle amplification (RCA) (Deng, Li, Huang, & Li, 2017; Y. Gao et al., 2020; Xingxing Zhou, Guo, Gao, Zhao, & Xu, 2017) and nucleic acid sequence-based amplification (Bodulev & Sakharov, 2020) are described, but most of these techniques involve complex operation, expensive reagents, dedicated instrumentation and exhaustive labels (Xian Chen et al., 2012). Also, biosensors commonly involve the use of a wide range of transduction mechanisms such as optical, electrochemical, electrical, and mass-based mechanism.

2.3.1 Electrochemical DNA biosensors

The focus on electrochemical DNA biosensors has been increasing recently as they are low cost, portable, less complicated, offer rapid detection with higher sensitivity via signal amplification, and are compatible with mass production with the help of microfabrication technologies. Besides, other methods of detection involve expensive signal transduction tools compared to the electrochemical detection of analytes which is the result of direct electronic signals, mainly the current (Amps) (Chalklen, Jing, & Kar-Narayan, 2020). Moreover, few electronic instruments could record very low currents down to several pico-Amps which improve the sensitivity of detection.

Electrochemical DNA biosensors are based on the hybridization of a target nucleic acid with their complementary DNA probes or ssDNA (Campos-Ferreira et al., 2013; Rashid & Yusof, 2017). Over the recent years, numerous innovative advancements have been achieved with improved biorecognition and interfacial procedures on solid state devices and in solution. Biosensing provides some extraordinary prospects for genetic screening and recognition with the capability to produce features on solid substrates with nanoscale accuracy. Lately, some innovative improvements have been achieved in electrochemical DNA biosensors. The crucial role of the sensor is to facilitate the formation of the probe-target complex, where the coupling process generates a detectable signal into an electronic readout.

In DNA biosensors, the single-strand DNA (ss-DNA) molecules or the probe DNAs are the biological recognition element. This general concept is built upon the hybridization of the ss-DNA probe with the complementary target DNA. The hybridization leads to changes in the mass transport, light emission or absorption, or proton concentration which generates the signal. The generated signal is transformed into a quantifiable response through a suitable

transduction element such as thermal, optical, or electrochemical, which converts the signal into current, light, or potential (Karunakaran, Rajkumar, & Bhargava, 2015).

An electrochemical DNA biosensor consists of the working, reference, and counter electrodes similar to a conventional three-electrode electrochemical cell (H. Kumar & Neelam, 2016; Ronkainen, Halsall, & Heineman, 2010). The immobilization of the ss-DNA or DNA-analog probe onto the electrode surface is the first principle of an electrochemical DNA biosensor. The hybridization of ss-DNA probe with the target DNA induces a variation in the electrochemical signal of the electroactive labels/indicators linked to the probes (Abi & Ferapontova, 2012; Kang et al., 2012; Luo, Lee, & Hsing, 2008). Electrodes such as gold, hanging mercury drop electrode, platinum and various types of carbon electrodes modified with the probe ss-DNA molecules are the most common working electrodes (WE), while a saturated calomel electrode (SCE) and platinum wire are the references and counter electrodes, respectively (Labuda et al., 2010).

Electrochemical techniques are well suited for DNA diagnostics because direct recognition is achieved through techniques such as voltammetry, potentiometry, amperometry, and electrochemical impedance spectroscopy (EIS). Therefore, there is no requirement for advanced and expensive signal transduction equipment. Also, the immobilized probe sequences could be established on different electrode substrates, and detection could be performed with an electrochemical analyzer (I.-H. Cho et al., 2020).

2.3.2 Metal oxide nanoparticles in electrochemical sensing and biosensing

Highly sensitive novel electroanalytical sensors fabricated on nanostructured metal oxides are cost-effective and will improved selectivity when attached to the biorecognition molecules (George, Antony, & Mathew, 2018). Metal oxide nanoparticles (MO NPs) with

diverse morphologies have been synthesis over versatile methods. These MO NPs show different sorts of electrical and photochemical properties as a result of their size, stability, and high surface area. The key functions of metal nanoparticles in electroanalysis include the toughening of the conductive sensing interface, the catalytic properties of nanoparticles allowing the expansion with metals, and the electrical contact of redox-centers in proteins with the surface of the transducers (Malekzad, Zangabad, Mirshekari, Karimi, & Hamblin, 2017).

The rapid electron transfer between the transducer and analyte molecule in the presence of metal nanoparticles considered them as "electronic wires" and "electrocatalysts" due to the nanosize dimension and structure (Baig, Kammakakam, & Falath, 2021). The biocompatible MO NPs are commonly utilized to immobilize the biomolecules for the fabrication of immunosensors, enzyme sensors, and DNA sensors, while semiconducting nanoparticles are mostly used as markers and tracers in the electrochemical study (Pan et al., 2017). The strong affinity of MO NPs to the surface of the working electrode can be obtained through several techniques including physical adsorption, electrodeposition, chemical covalent bonding, and electropolymerization (Adarakatti & Kempahanumakkagari, 2018).

Magnetite (Fe_3O_4) nanoparticles introduce a novel area in electrochemical sensing. The electron hopping processes between the Fe^{2+} and Fe^{3+} ions result in the higher electrical conductivity of Fe_3O_4 at room temperature. Iron oxide nanoparticles are broadly used to modify electrodes in the detection of many analytes like H_2O_2, glucose, heavy metals (Pb (Chauhan & Pundir, 2011; S. Lee, Oh, Kim, & Piao, 2016), Zn (S. Lee et al., 2016), Cd (S. Lee et al., 2016)), nitrites and nitrates (Absalan, Akhond, Bananejad, & Ershadifar, 2015; Bonyani, Mirzaei, Leonardi, Bonavita, & Neri, 2015; Erogul, Bas, Ozmen, & Yildiz, 2015;

B.-Q. Li, Nie, Sheng, & Zheng, 2015; Radhakrishnan, Krishnamoorthy, Sekar, Wilson, & Kim, 2014; Teymourian et al., 2013; Yuan et al., 2016) and many organic entities (urea (Sousa et al., 2017), dopamine (Adekunle, Agboola, Pillay, & Ozoemena, 2010; Fernandes et al., 2014), bisphenol A (Alkasir, Ganesana, Won, Stanciu, & Andreescu, 2010; Hou, Tang, Zhang, Wang, & Zhu, 2014; Y. Zhang et al., 2013)). It also senses many biocompatible drugs in efficient ways. In numerous cases, bare iron oxide (Fe_2O_3/ Fe_3O_4) nanoparticle with appropriate shape and size are used for the electrode modification (Magro & Vianello, 2019; Z. Zhang, Zhu, Wang, & Yang, 2011).

Rather than using iron oxide unaccompanied, some modifications were made to enhance the sensitivity and detection limit of the working electrode. Iron oxide nanoparticles were made into the core-shell bimetallic structures which improve the performance due to their synergistic effect. Metals like Au, Zr, Ag and cobalt hexacyanoferrate were incorporated with iron oxide to fabricate core-shell modifications (Arvand, Orangpour, & Ghodsi, 2015; Bonyani et al., 2015; Chandra, Lang, & Bahadur, 2013; Fernandes et al., 2014; N.-N. Li, Kang, Zhang, Lu, & Cheng, 2015; Wen et al., 2014; M. Zhang, Sheng, Nie, & Zheng, 2014; W. Zhu et al., 2015).

Iron oxide combined with metals, organic moieties and some carbonaceous entities like carbon nanotubes (CNT) and graphene oxide (GO) to form multicomponent composites and exhibited high electrocatalytic performance towards many analytes (Arvand et al., 2015; Ali Benvidi, Jahanbani, Mirjalili, & Zare, 2016; Chauhan & Pundir, 2011; Hou et al., 2014; S. Lee et al., 2016; B.-Q. Li et al., 2015; LOPEZ, 2016; Madrakian, Maleki, Heidari, & Afkhami, 2016; Radhakrishnan et al., 2014; Ran, Chen, & Xia, 2017; Teymourian et al., 2013; Y. Zhang et al., 2013). In most of these nanocomposites, carbon matrix acts as a

support to ensure the size-shape selectivity of nanoparticles by avoiding agglomeration and offer a surface to volume ratio for electrocatalytic improvement. The carbon matrix also shows great surface area, high mechanical strength, rapid electron transfer rate, outstanding thermal and electrical conductivities which in turn improve the electrocatalytic activity (Y. Zhang et al., 2013; Zheng et al., 2020).

2.4 Nanoparticles based modified electrodes for detection of DA

Dopamine (DA) is a neurotransmitter that has a very crucial role in sustaining functional activities of central nervous, cardiovascular, and hormonal systems. DA has an important role in the regulation of cognitive functions such as stress, behavior, and attention. DA is present as organic cations in body fluids and brain tissues and its abnormal concentrations are associated with many diseases (Worley, 2017). For the diagnosis of these diseases, very precise measurements of DA in biological samples are required. Being electrochemically active, DA is sensed using electrochemical techniques.

Electrochemical methods are most extensively used for the detection of DA, ascorbic acid (AA), and uric acid (UA). Low cost associated with electrochemical instrumentation is a huge advantage; however, a perception of low sensitivity and selectivity when dealing with real samples is somehow justifiable. With the growth of new materials, researchers have tried chemically modified electrodes for the detection of DA in the presence of significant concentrations of UA and AA. Very low detection limits have been reported with modified electrodes whereas such detections were not possible with the bare electrodes. These materials include but not limited to carbon nanotubes (J. Cheng et al., 2020; Eom et al., 2019; Hatefi-Mehrjardi, Karimi, Soleymanzadeh, & Barani, 2020; Yang, Li, & Zhu, 2019; C. Zhang et al., 2018; X. Zhang & Zheng, 2020), nanoparticles and nanocomposites (G. Han et al., 2021; G. Li et al., 2019; Venu et al., 2018; C. Zhang et al., 2018), polymeric materials

(Filik, Avan, Aydar, & Arpacı, 2014; K. Jiang et al., 2017; Xiaofang Liu et al., 2014; Y. Liu et al., 2017), and ionic liquids (L. Cheng, Fan, Shen, & Liang, 2019; Jianbo Li et al., 2017; Thakur et al., 2018).

Modified electrodes are made for a particular application which is not feasible with the bare conductive electrode. The deliberate covering of the conductive substrate may result in improved electron transfer kinetics. Modifications carried out on a conductive substrate include irreversible adsorption, self-assembled layers, covalent bonding, electropolymerization, and many others. Surface modifications play the role of catalyst and minor details of surface morphology assess the sensitivity of measurement in electroanalytical applications.

Glassy carbon electrode (GCE) is the most used substrate for modification because it offers a wide potential window, gives low background currents, and chemically stable. Chemically modified electrodes are selective, sensitive, and able to detect DA in the presence of other interferences by the reduction of ohmic resistance associated with a wide potential window. Issues that may affect the response of a modified electrochemical sensor include the properties of the coated material, synthesis process of the coating material, use of mediators, electrode coating method, and nature of sample matrix.

Nanoparticles (NPs) have better physical, chemical and electronic properties than the bulk. Properties of NPs are extremely related to the nature of the material from where they are synthesized. Mostly, NPs are prepared through chemically reduction method of metal salts in the presence of a stabilizer that attaches to the surface of NPs and contributes to their charge, solubility, and stability. NPs are extremely sensitive to the changes on their surface.

The main advantages obtained from modified electrodes with NPs are enhanced electrode kinetics by providing greater surface area, increased mass transport rates, better control of NPs surface, and controllable functionalization of the desired groups.

Recently, metal nanoparticles (MNPs) have received great attention in the area of electrocatalysis because of their unique physical and chemical behavior. MNPs modified electrodes display reasonably fast redox activity towards the compounds which improve the sluggish electrode kinetics at the bare electrodes. In several cases, the use of MNPs modified electrodes was useful in resolving overlapped peaks of analytes with close oxidation potentials. Also, such modified electrodes provide good peak to peak separations(Sajid et al., 2016).

2.5 Cervical Cancer as a Major Health Problem

2.5.1 Current Diagnostic of Human Papilloma Virus

The visible epidermal manifestations such as warts or condylomas occur only in 1% of the infected patients. Therefore, the diagnosis of HPV infection requires specialized equipment to pinpoint the internal lesions at the mucous membranes. The Papanicolaou test is another type of analysis for proven cervical injury cases. In this test, the cervical cells are collected using swabs, followed by staining with the Papanicolau staining technique (Baydar, Kulac, Ozagari, & Tezel, 2013). A molecular diagnosis is essential for the accurate differentiation of various HPV strains, which are categorized according to their low, intermediate, or high oncogenic risk.

The differentiation of various HPV strains is a challenging task since all HPV strains are closely related. The protein expression ratio analysis could provide some differentiation of

the various HPV strains through molecular fingerprinting of the oncogenic potential in histopathological samples (Frías, Avelino, Silva, Andrade, & Oliveira, 2015; Rossi et al., 2013; Salimović-Bešić, Tomić-Čiča, Smailji, & Hukić, 2013). DNA analysis is another essential method of identification of the different types of HPV strains, which is based on the complementary principle of the DNA strands. For example, the signal amplification of a fragment of target nucleic material can be identified by the polymerase chain reaction (PCR) method and signal amplification of an oligonucleotide hybridization assay (Abreu, Souza, Gimenes, & Consolaro, 2012b; Vince & Lepej, 2010). At present, HPV diagnosis is based on molecular biological techniques which are categorized into nucleic acid-hybridization assays, signal amplification assays, and nucleic acid amplification (Figure 2.3 and Table 2.4) (Abreu, Souza, Gimenes, & Consolaro, 2012a; Burd, 2016).

Southern blotting, *in situ* hybridization, and dot-blot hybridization use radio-labeled nucleic acid hybridization assays to detect HPV infection in cervical samples. Low sensitivity, large amounts of purified DNA, and time-consuming procedures are disadvantages of these techniques. However, high-quality information is the benefit of using these techniques (Abreu et al., 2012a).

The Hybrid Capture® 2 (HC2) distinguishes between the high-risk and low-risk groups but is not designed for genotyping single HPV (Hwang & Shroyer, 2012; Katanga et al., 2019). The Cervista® HPV identifies the presence of 14 HR-HPV types and also utilizes a signal amplification method for the detection of specific nucleic acids. The Cervista® assay demonstrated 100% sensitivity in the detection of CIN III and 98% sensitivity in the detection of CIN II compared to hc2 (Johnson et al., 2008). Lower false-positive rate and high sensitivity and specificity to genotyping HPV -16/18 are other properties of this assay

(Bartholomew, Luff, Quigley, Curtis, & Olson, 2011; Einstein et al., 2010). However, these techniques involve complex protocols and require specialized skills for the correct instrument operation as these techniques do not fulfill the requirements of point-of-care clinical diagnostics and generally lack the required sensitivity and rapidity (Tardif, Simmon, Kommedal, Pyne, & Schlaberg, 2013).

The early diagnosis of the disease is highly desirable, due to the dangers posed by the presence of HPV in the human body; thus more efficient techniques for the detection of the HPV virus are needed (Cubie, 2013). The most widely used techniques for the screening and diagnosis of HPV infections are the Digene hybrid capture assay (HC2), pap-smear test and polymerase chain reaction with generic primers (Gravitt & Jamshidi, 2005; Melo, Ribeiro, & Canevari, 2018).

However, the first two techniques have some disadvantages. These methods involve the use of expensive instrumentation and expert analysis, yet display low specificity and sensitivity, hence are time-consuming and complicated. Therefore, these techniques are unsuitable with limited resources and personnel (Villa & Denny, 2006). Recently, some new detection techniques such as leaky surface acoustic wave, piezoelectricity, and fluorescence spectroscopy, have been utilized for the detection of HPV virus, but these are also still expensive and require complicated instrumentation (Mahmoodi et al., 2019; Yunxia Wang et al., 2009).

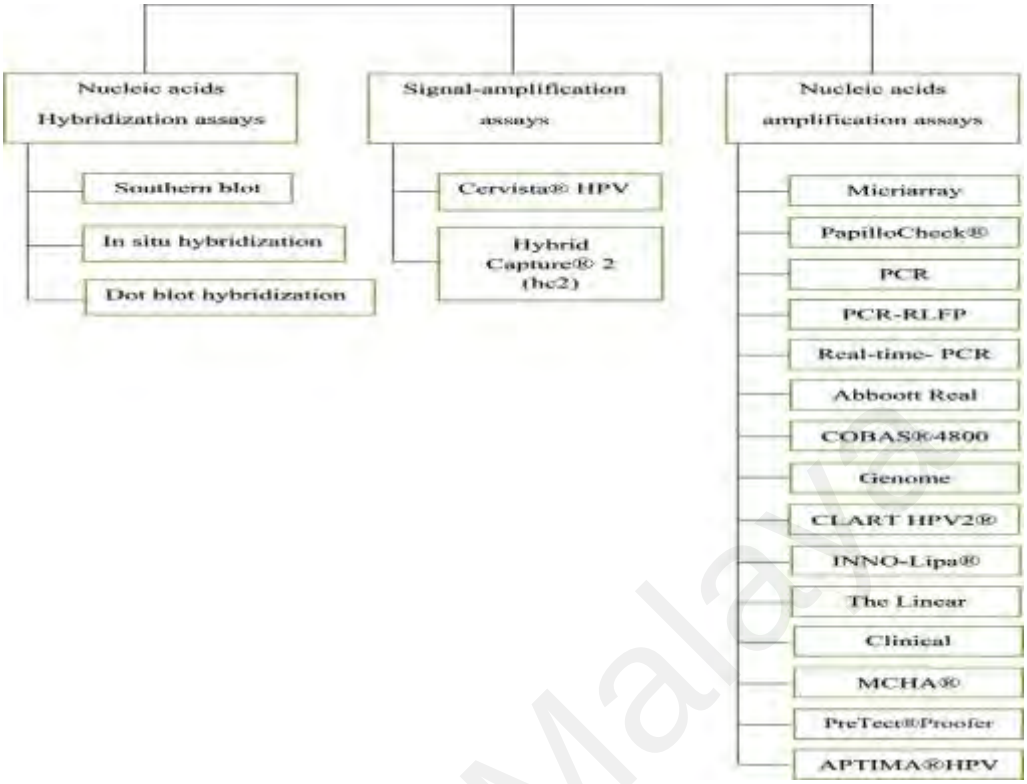

Figure 2.2: Classification of molecular-biology techniques for HPV diagnosis

Table 2.4: Advantages and Disadvantages of the HPV detection of molecular methods.

Methods	Advantages	Disadvantage
Nucleic acids hybridization assays	• Southern blot is the gold standard for HPV genomic analysis. •Presence of HPV in association with morphology	• Low sensitivity, time-consuming, relatively large. • Southern blot and hybridization cannot use degraded DNA • Purified DNA amount
Signal amplification Assays	• Quantitative • FDA-approved test (hc2) • Lower false-positive rate •High sensitivity to genotyping	• Licensed and patented technologies • Cannot use for genotyping individual
Nucleic acids amplification assays	• Flexible technology • Very high sensitivity • Multiplex analysis	•Lower amplification signals of some HPV genotypes • Contamination with previously amplified material can lead to false positives

2.5.2 Human Papilloma Virus as Cause of Cervical Cancer

One of the most common sexually transmitted infections is the human papillomavirus (HPV) which affects millions of people worldwide. Thus it has gathered huge attention due to increased focus on vaccine development and cancer-screening recommendations for early prevention of the disease (Forcier & Musacchio, 2010). While some common dermatological and sexually transmitted diseases are easily attributed to the presence of the HPV virus, there is still no cure for HPV (CC Wang & Palefsky, 2016), though a healthy immune system could offer sufficient protection from the virus itself. Around half of the world's population is exposed to the risk of HPV infection at least once in their lifetime (M. Z. Handler, N. S. Handler, S. Majewski, & R. A. Schwartz, 2015).

Cervical cancer, from the contamination of high-risk HPV, is the third most prevalent type of cancer in occurrence and fourth in the death rate among women worldwide (Steenbergen, Snijders, Heideman, & Meijer, 2014). The HPV-16 and HPV-18 are two of the most dangerous cancer-causing HPVs which contain the E6 and E7 oncogenes, are responsible for almost 70% of all cervical cancers. The HPV-16 is associated with squamous cell carcinoma, while the HPV-18 is associated with adenocarcinoma, a less common disease despite being more dreadful than the latter. Both the HPV 16 and HPV 18 are preventable by vaccination (CC Wang & Palefsky, 2016). Around 26,900 new cases of HPV-associated cancers are diagnosed each year between 2004 and 2008, with 4100 women deaths from cervical cancer in the United States alone (N. S. Handler, M. Z. Handler, S. Majewski, & R. A. Schwartz, 2015). The National Program of Cancer Registries (NPCR) and the Surveillance, Epidemiology, and End Results (SEER) program shows that an average of 33,369 diagnosed HPV-associated cancers is detected annually, including 12,080 males (8.1 per 100,000) and 21,290 females (13.2 per 100,000). The HPV virus is believed to be responsible for 96% of

cervical cancers, 93% of anal cancers, 64% of vaginal cancers, 51% of vulvar cancer, 36% of penile cancers and 63% of oropharyngeal carcinomas (Cobos et al., 2014).

2.5.3 Electrochemical DNA sensors for HPV detection

The electrochemical recognition of HPV-DNA sequences has been developed recently (Espinosa, Galván, Quiñones, Ayala, & Durón, 2019; Jampasa et al., 2018; Teengam et al., 2017). The increased sensitivity, small sample volume, low cost, simplicity, and portability make the electrochemical detection an excellent candidate for point-of-care DNA diagnostics. Although the electrochemical detection of DNA is already an established method with an increasing number of publications annually, most of the reports suffer from the lack of analyzing real human samples, and their assessment with standard approaches (Palecek & Bartosik, 2012). Figure 2 shows the DNA detection of both synthetic oligonucleotides (HPV16E7p and HPV45E6) performed using the so-called sandwich type format (L Civit, Fragoso, & O'Sullivan, 2010).

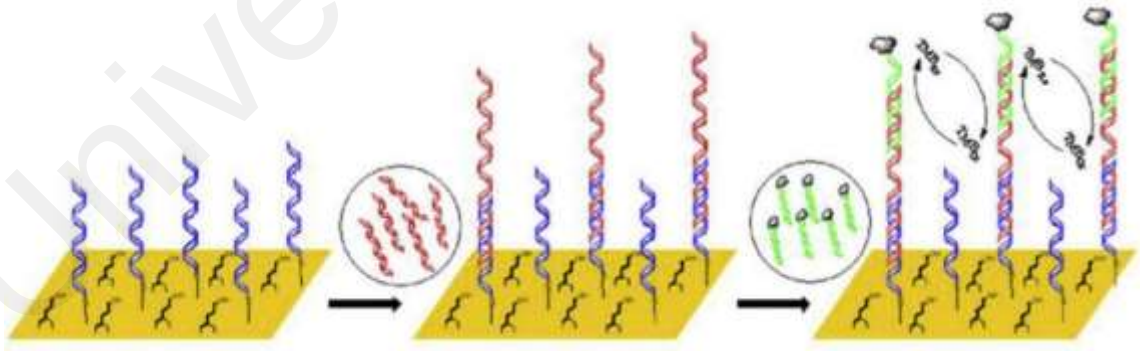

Figure 2.3: Schematic description of the developed assay based on the co-immobilization of the thiolated probe with backfiller, hybridization process, and electrochemical detection. Reproduced with permission from the publisher

2.5.3.1 Direct (label-free) electrochemical DNA detection

A label-free electrochemical DNA detection is a direct method of measuring the physicochemical variations on the surface of the transduction device due to the DNA hybridization. The electrical transduction could be combined with advances in nanotechnology which gives rise to electrochemical DNA nanosensors, as it is portable and more economical compared to the label-free physical and optical transduction (Arif & Khan, 2020; Cagnin et al., 2009). This method excludes the requirement for an additional marker (label) step which allows more simple sensing protocol (Labuda et al., 2010; Vagin, Karyakina, Hianik, & Karyakin, 2003; Vagin, Trashin, Karyakin, & Mascini, 2008).

In 2008, Liepold *et al*. introduced a new electronic microarray format that could display the hybridization of amplicons in a few minutes (Liepold et al., 2008). Dipstick-type microelectrode arrays consisting of 32 gold microelectrodes on silicon, was applied directly to the amplification reaction without any labeling or washing steps. Initially, the gold microelectrodes were functionalized with the probe DNA and followed by the hybridization of ferrocene-modified DNA.

Immobilization procedure, accessibility of the capture probes, and prevention from nonspecific target adsorption are a prerequisite for a robust and reliable performance of the sensor, and these aspects are demonstrated in this research. The minimal equipment needed in this proposed sensor is suited for clinical and medical diagnostic tests and it is easy to handle. The labeling or washing steps are not needed in this work. The target DNA was hybridized with the probe DNA as the sensor was dipped into the sample. With this approach, the target DNA could be measured as a decrease in the electrochemical signal. The HPV-6 target DNA could be measured down to 30 pM accuracy using this method.

In another investigation, Zari *et al*. determined a 20-mer oligonucleotide of HPV virus adsorbed on screen-printed gold electrodes (SPGE) for the direct monitoring of DNA hybridization with the absence of labeling or an external redox indicator (Zari, Amine, & Ennaji, 2009). The electrochemical oxidation of purines (guanine and adenine) and DNA fragments at various electrode surfaces (carbon paste, glassy carbon electrode, and gold) were investigated by square wave voltammetry (SWV). The guanine and adenine bases could be quantitatively determined by SWV for a deoxyribonucleic acid sample after the acid hydrolysis. The gold electrodes showed the highest sensitivity. The order of peak currents was found to increase as follows: hybrid-modified SPGE < 11-base mismatched modified SPGE < 18-base mismatched SPGE < probe modified SPGE. The selectivity of the proposed DNA biosensor was examined by the non-complementary oligonucleotides. Under optimal conditions, this sensor shows a good calibration range with an HPV DNA sequence detection limit of 2 pg ml-1 (S/N = 3). The proposed protocol is very simple and relatively rapid. The main advantage of this method is the suitability of microarray fabrication, as electrochemical microarrays are easily fabricated using a gold electrode, while the carbon or mercury-based electrodes are unsuitable.

For the first time, Piro *et al*. revealed a technology based on the application of conjugated copolymer poly (5-hydroxy-1,4-naphthoquinone-co-5-hydroxy-2-carboxyethyl-1,4-naphthoquinone) for the detection of HPV infection (Piro et al., 2011). The proposed immunosensor acts as the immobilization and transduction element and can identify the interaction between the antigenic peptide L1 from the HPV-16 major capsid protein, a dominant epitope involved in viral infection, as well as in prophylactic vaccine and the relevant antibody. The HPV-16-L1 was grafted as the probe to detect the HPV-16 antibody. The SWV of the poly(HNQ-co-HNQ-COOH) recorded in PBS before and after the grafting

process, as well as after the complexation with anti-ovalbumin (αOVA) and alpha-papillomavirus (αHPV). The anti-OVA induces a weaker signal drop compared to the anti-HPV (available in serum). The significant advantage of this technique is that the antigen-antibody complex formation takes place without any intermediate steps or reagents by monitoring the electrochemical response of the polymer by SWV. Moreover, the steps to replace the Ag probe (in this case, HPV virus) by much smaller fragments such as an oligopeptide of a few tens' amino acids, which presents a much smaller size than a bulky antigen was studied. By this approach, the system in terms of sensitivity and stability might improve. This report was based on the use of synthetic DNA.

In a similar work, the analytical performance of polyaniline-multiwalled carbon nanotube film (PANi–MWCNT) on interdigitated platinum electrode arrays (IDA) for the detection of HPV virus was reported by Dai Tran *et al*. (Dai Tran, Nguyen, Nguyen, Do, & Le Nguyen, 2011). They reported a sensitivity of 1.75 ± 0.2 μA nM−1 (r2 = 0.997) between 10 and 50 nM of anti-HPV concentration with a limit of detection (LOD) of 490 pM. This work highlights the ability of the arrays to control the technical and biological variation. However, further studies are required to determine the viability of the assays for clinical applications.

Wang *et al*. fabricated an ultrasensitive biosensor by electrochemical deposition of gold nanoparticles on single-walled carbon nanotubes (SWCNTs) arrays for the detection of human hepatitis B and papillomaviruses (S. Wang et al., 2013). They examined both the aligned and random SWCNTs' arrays upon the immobilization of ss-DNA probe onto the SWCNTs/Au surface by a self-assembly method (L. Li, Wang, Yang, Huang, & Wang, 2012). The experimentally achieved detection limits are almost the same for the random and the aligned SWCNTs/Au arrays; the electrochemical detection of the HPV virus was performed by electrochemical impedance spectroscopy (EIS). The hybridization detection of

a 24-base papillomavirus ss-DNA showed great stability where the charge transfer resistance dropped to less than 1% after a month of storage between 4 and 8 °C. In this research horizontally aligned SWCNTs array coated with Au NPs is a very promising platform for DNA detection but making parallel SWCNTs array represents a huge challenge in practice, it requires a very steady and stable laminar gas flow, and it is easier to fabric the random SWCNTs array. The remarkable improvement of SWCNTs/Au platforms over those utilizing SWCNTs or Au NPs alone indicates the synergistic interactions of SWCNTs array and Au NPs. Moreover, the good regeneration ability of the proposed biosensor in hot water makes it a valuable candidate for achieving an early diagnosis of gene-related diseases. The considerable advantage of this work is the very low limit of detection (LOD) compared to the previous report. This report was also based on the use of synthetic DNA.

In another report, Huang *et al*. constructed an enzyme-free and label-free electrochemical biosensor based on graphene/Au nanorod/ polythionine (G/Au NR/PT) modified glassy carbon electrode (GCE) for the ultrasensitive detection for HPV DNA. A ruthenium complex, $[Ru(phen)_3]^{2+}$ was selected as the redox indicator (H. Huang, Bai, Dong, Guo, & Liu, 2015). The proposed DNA biosensor demonstrated great selectivity and a LOD of 1.0×10^{-13} to 1.0×10^{-10} M and 4.03×10^{-14} M, respectively, for the detection of HPV DNA. The presence of graphene enhances the electrode surface area and electrical conductivity. The enhanced immobilization of the probe DNA and the ability for hybridization is due to the presence of Au NRs. The proposed biosensor showed a very low detection limit, and the experiment was optimized by different factors, and the target DNA was also detected in the complex human serum sample. The fabricated biosensor shows good potential for clinical applications.

Campos-Ferreira *et al*. proposed a label-free electrochemical DNA biosensor for the identification of a target gene cloned into a plasmid (Campos-Ferreira et al., 2016). A 23-mer guanine-free oligonucleotide was immobilized on pencil graphite electrode for the detection of the E6 gene (due to its clinical importance) from the HPV type 16 virus. The LOD is 16 pg/μL and suggests that the electrochemical method is more sensitive and specific compared to the agarose gel electrophoresis assay (1500-fold lower in concentration) which can be postulated as a new and alternative method for cloning analysis in plasmids. The DNA biosensors are less commonly explored for cloning analysis and the considerable advantage of this novel; simple, inexpensive, stable electrochemical DNA biosensor is the ability to detect the HPV 16 E6 gene cloned in the expression vector.

Karimizefreh *et al*. reported a label-free electrochemical impedance biosensor for the recognition of HPV type 16 (Karimizefreh, Mahyari, VaezJalali, Mohammadpour, & Sasanpour, 2017). Instead of using a common gold disk electrode, they utilized a modified glassy carbon/ gold nanosheet electrode to improve the performance of the DNA biosensor because, among different morphologies of gold nanostructures, gold nanosheets have many edges and corners as the active sites for catalysis compared to spherical nanoparticles. This electrode was immobilized with a thiolated single-stranded 25-mer oligonucleotide (synthetic thiol-ss-DNA) and gave a LOD of 0.15 pM. Moreover, the biosensor showed one base pair mismatch detection limit with good selectivity. The biosensor has a great potential in HPV DNA diagnostics and clinical analysis.

Kowalczyk *et al*. for the first time, investigated the role of mercury (II) in the nitrogen base for the voltammetric detection of specific DNA sequences characteristic of the HPV type 18 in thymine bases without the labeling step (Kowalczyk & Nowicka, 2016). The

detection of the target DNA sequence was based on the electrochemical reduction of mercury (II) ions bonded with opposite thymine bases (mispairs) in the DNA helix. The laser ablation technique, coupled with inductively coupled plasma mass spectrometry and circular dichroism, was also utilized in this detection. This fabricated biosensor is convenient, low cost, less construction procedure and showed very low LOD and quantification limit of (1.2 ± 0.2) $\cdot 10^{-14}$ and (7.5 ± 0.1) $\cdot 10^{-14}$ M, respectively, and have a great potential in HPV DNA diagnostics. Limited success has been achieved for the commercialization of the above biosensors.

2.5.3.2 Indirect (labeled) electrochemical DNA detection

Although the label-free DNA detection allows an easier screening step and decreases the time consumption and expenses, it does not achieve the sensitivity of the labeled DNA detection. The indirect technique improves the sensitivity to attomolar concentrations of the target DNA (Armistead & Thorp, 2002; Q. Wu et al., 2019). The indirect techniques also need mediators to simplify the electron transfer step between them and the electrode. The most common electron mediators are $Fe[(CN)]_6^{3-/4-}$, $Os(bpy)_3^{3+/2+}$ $Ru(bpy)_3^{3+/2+}$, ferrocene and methylene blue (MB). Nanomaterials such as metal nanoparticles could also be utilized as indirect electrochemical sensors, which represent a large redox reservoir (Rasheed & Sandhyarani, 2017).

In 2008, Sabzi *et al*. utilized MB as an electroactive label on a pencil graphite electrode (PGE) to provide a well-defined recognition interface for the detection of HPV target DNA (Sabzi, Sehatnia, Pournaghi-Azar, & Hejazi, 2008). Five non-complementary DNAs corresponding to the human, hepatitis C virus (HCV), fungi, and bacterial genomes were investigated to confirm the selectivity of the biosensor towards HPV DNA detection in the presence of other DNAs. The data showed that the fabricated electrode detects the target

DNA with a LOD of 1.2 ng/µl. The authors attempted to discriminate the HPV universal region from the mixed oligousenucleo HCV universal, bacterial 16S rDNA, and fungi 5/18s rDNA regions by using DNA biosensors in the future work. In a similar study, MB was utilized as an electrochemical intercalator to monitor the DNA hybridization process (Souza et al., 2014). The MB binds specifically to guanine bases in the ssDNA, and a lower current signal was observed upon the DNA hybridization. Souza *et al*. fabricated an electrochemical DNA biosensor for specific sequence detection of the E1 HPV type 16, using MB as the hybridization indicator utilizing the DPV technique. To examine the selectivity of the biosensor, some hybridization experiments with non-complementary oligonucleotides (target and probe DNAs were the synthetic oligonucleotides) were performed. They reported that the DNA biosensor could be utilized for the detection of E1 HPV gene due to enhanced selectivity of the DPV technique. The LOD of the probe immobilized on the electrode to its complementary sequence was 1.49 nM.

In another fabricated biosensor, L-cysteine was first electrodeposited on the gold surface to form the L-cysteine film and followed by the immobilization of HPV16-specific probe on the modified surface (Campos-Ferreira et al., 2013). The DPV technique was used to investigate the reduction signals of MB. The effect of probe concentration was analyzed, and the best performance was obtained at 1000 nM. The biosensor demonstrated great sensitivity and comprehensive linear response to the target concentration (18.75 nM and 250 nM) with a LOD of 18.13 nM. The biosensor performance indicated high sensitivity and selectivity towards HPV-16 detection and distinguished it from the other types of HPV. This allows the possibility of developing new portable detection systems for different types of HPV viruses and could be the first step for effective diagnosis during the early stages of infection.

Hematoxylin was utilized as the biological stain in biomedical research and diagnostic procedures (Sioi, Bolosis, Kostopoulou, & Poulios, 2006), as well as a pivotal agent in the histopathology of prostate cancer (Lunn & Sansone, 2012). Nasirzadeh *et al*. studied the electrochemical properties of hematoxylin modified electrodes as an electrochemical sensor for the detection of NADH (Zare, Nasirizadeh, Mazloum-Ardakani, & Namazian, 2006), hydrazine (Zare & Nasirizadeh, 2007) and other biological compounds (Nasirizadeh & Zare, 2009) in their previous works.

In another report, Nasirzadeh *et al*. introduced a new electrochemical biosensor based on the interaction of hematoxylin with 20-mer deoxyoligonucleotides of HPV through hybridization (Nasirizadeh, Zare, Pournaghi-Azar, & Hejazi, 2011). In this research, the best method for the self-assembly of DNA probes is the drop-casting self-assembly method, while the best hybridization is the solution-based hybridization method. The electrochemical techniques utilized in the detection were cyclic voltammetry (CV) and differential pulse voltammetry (DPV). The electrical signal under optimum conditions shows a linear relationship with the concentration of target DNA, ranging from 12.5 nM to 350.0 nM with a LOD of 3.8 nM. Although the miniaturization and economic cost are the key elements for an ideal biosensor, the simultaneous detection of multiple analytes is also much desired. For this reason, Civit *et al*. developed an electrochemical genosensor array for the simultaneous detection of three specific high-risk HPV sequences, HPV-16, 18, and 45 (Laia Civit, Fragoso, Hölters, Dürst, & O'Sullivan, 2012). In this work, the parallel detection of multiple targets and multiplex studies were made possible by 16 gold WE sensor arrays, through the immobilization of three thiolated HPV probes on alternating electrodes. This work highlights the high specificity of the sensor arrays and no significant cross-hybridization between the three high-risk sequences was observed. Moreover, real samples obtained from cervical

scrapes were amplified and were utilized to investigate the genosensor performance in real clinical applications, where an excellent correlation was obtained compared to the response of HPV genotyping carried out in a hospital laboratory.

Jampasa *et al*. designed a selective electrochemical biosensor for the detection of HPV type 16 DNA, based on the immobilization of anthraquinone-labeled pyrrolidinyl peptide nucleic acid (AQ-PNA) probe (Jampasa et al., 2014). The probe was immobilized onto a chitosan-modified disposable screen-printed carbon electrode via a C-terminal lysine residue using glutaraldehyde as the cross-linking agent. They obtained a linear range between 0.02 and 12.0 μM, with a LOD and limit of quantification (LOQ) of 4 and 14 nM, respectively. The fabricated biosensor showed high selectivity against non-complementary 14-base oligonucleotides, such as the HPV types 18, 31, and 33 DNA. The ease of electrode preparation and probe immobilization with small sample volumes are the main advantages of this platform. The excellent specificity under nonstringent hybridization conditions and simple instrumental set-up are some advantages of this technique for HPV screening in the developing countries. On the other hand, the requirement of DNA probe immobilization, the non-reusability, and detection limits (LOD) higher than the standard DNA detection are some disadvantages of the proposed biosensors. Nevertheless, the detection limit is still acceptable to facilitate the detection of HPV type 16 DNA from PCR samples.

In 2015, Bartolome *et al*. modified glassy carbon electrodes (GCE) with stable dispersion of pristine carbon nano-onion (CNOs) which were functionalized by diazonium salts possessing carboxylic acid or maleimide groups, using the electrografting technique (Bartolome, Echegoyen, & Fragoso, 2015). They described two sensing platforms: i). GC/CNO/phenylacetic acid (PAA) immobilized with streptavidin and biotinylated capture

DNA sequence and ii). GC/CNO/phenyl maleimide (PM) immobilized with a thiolated DNA probe. Both the fabricated biosensors (sandwich-type assay with a peroxidase-labeled DNA reporter probe) were utilized for the HPV DNA sequence detection using the amperometry technique. The results distinctly showed better sensitivity and lower LOD of the amperometric assays achieved on the GC/CNO-modified surface compared to the bare GC electrodes. The proposed electrochemical DNA biosensor gave a sensitivity and LOD of 0.91 μA nM^{-1} and 0.54 nM for the GCE/CNO/ PAA (in the absence of CNO, sensitivity = 0.21 μA nM^{-1}; LOD = 3.9 nM) and 0.41 μA nM^{-1} and 0.50 nM for the GCE/CNO/PM (in absence of CNO, sensitivity = 0.11 μA nM^{-1}; LOD = 1.4 nM), respectively. The results showed that the incorporation of CNOs on the surface resulted in higher sensitivities and lower detection limits, due to the enhanced electron transfer process at the CNO-modified electrodes. These observations confirm the promising and versatile role of the CNO-modified surfaces for the development of different and effective analytical sensor systems.

Bartosik *et al.* developed an electrochemical-chip based assay using an anti-digoxigenin-peroxidase detection system on carbon screen-printed electrode chips (Bartosik et al., 2016). They used a magnetic bead-modified DNA probe to capture the target HPV DNA. The designed HPV DNA biosensor showed high sensitivity in the attomolar range. This biosensor also demonstrated the selective discrimination of HPV-16 from HPV-18, which is highly significant for HPV-16-1961 and HPV-18-2031 targets in their relevant genomes, where around 75% of their sequences possess resemblance. Since the majority of assays still lack validation using real human samples ideally from patients, along with the comparison with standard methods, one of the most significant aspects of this assay is that the proposed biosensor could be an effective tool for the detection of HPV DNA directly from cervical

samples. The assay was successfully utilized for the detection of DNA not only from cancer cell lines but also from human cervical brush smears from HPV patients.

Very recently, Teengam *et al*. developed a novel paper-based electrochemical DNA biosensor for the determination of high-risk HPV type 16 using pyrrolidinyl peptide nucleic acid (AQ-PNA) probe immobilized on a graphene-polyaniline (G-PANI) modified electrode (Teengam et al., 2017). The AQPNA immobilization and target HPV-16 DNA hybridization were confirmed by EIS and SWV techniques. The biosensor gave a LOD of 2.3 nM with a linear range between 10 and 200 nM. The designed biosensor effectively detected the PCR amplified DNA from HPV-16 positive SiHa cells. The proposed biosensors showed some improved features compared to previous works. The electrochemical paper-based analytical devices (ePAD) provide a low-cost, disposable biosensor for point-of-care (POC) applications. Moreover, the G-PANI modified electrode is attractive relative to the covalent immobilization because of its inherent simplicity. Another advantage of this sensor is the possibility for mass production while limiting the variation among individual sensors, which is crucial for a disposable biosensor. Table 2.5 summarizes the electrochemical DNA biosensors for HPV detection. As can be seen, the suggested electrochemical sensor platforms have a low LOD and a wide linear range, compared to other types of DNA biosensors.

Table 2.5: Comparison of electrochemical biosensor for HPV Diagnostics

Electrode	Electroactive Indicator	Electrochemical Technique	Linear range	Detection limit (LOD) (nM)	Ref.
L-cysteine film/Gold electrode	Methylene blue	DPV	18.75–250 nM	18.13	(Campos-Ferreira et al., 2013)
Oligonucleotide/Gold electrodes	Horseradish peroxidase	Steps & Sweeps	0.1–10 nM	490 pM	(L Civit et al., 2010)
Gold electrodes	Horseradish peroxidase	Steps & Sweeps	0.1–10 nM 0.1–12 nM	220 pM 170 pM	(Laia Civit et al., 2012)
Pencil Graphite Electrode	Methylene blue	SWV	0–10 ng/µL	1.2 ng/µL	(Sabzi et al., 2008)
Carboxyphenyl layer/GCE	Mercury(II)	SWV	10^{-15}-10^{-6}M	$1.2 \cdot 10^{-5}$	(J. Wang, Jiang, & Mukherjee, 1999)
Dipstick-type microelectrode gold arrays	Ferrocenium	ACV&CV		30 pM	(Liepold et al., 2008)
Screen-printed gold electrode	Free-indicator	SWV	0–5 ng ml^{-1}	2 pg ml^{-1}	(Zari et al., 2009)
Poly(HNQ-co-HNQ-COOH) film/GCE	Free-indicator	SWV	50 nM		(Piro et al., 2011)
Interdigitated platinum electrode arrays/Polyaniline/Multiwalled Carbon Nanotube film	Free-indicator	CV & SWV	10–50 nM	490 pM	(Dai Tran, Nguyen, Nguyen, et al., 2011)
Single walled carbon nanotube arrays/Au nanoparticles/SiO2/Si Substrate	Free-indicator	EIS	10^{-9} - 10^{-3} nM	10^{-9}	(S. Wang et al., 2013)
Graphene/Aunanorod/Polythionine/GCE	([Ru(phen)3] 2+)	DPV	10^{-4} -10^{-1} nM	$4.03*10^{-5}$	(H. Huang et al., 2015)
Pencil Graphite Electrode	Free-indicator	DPV	40–5000 pg/µL	16 pg/µL	(Campos-Ferreira et al., 2016)
Glassy carbon electrode/Gold nanosheets	Free-indicator	EIS	1 pM^{-1} µM	0.15 pM	(Karimizefreh et al., 2017)
Graphite electrode	Methylene blue	DPV	2–10 nM	1.49	(Souza et al., 2014)
Gold electrode	Hematoxylin	CV & DPV	12.5–350 nM	3.8	(Nasirizadeh et al., 2011)
Screen-printed carbon/Chitosan	Anthraquinone	SWV	0.02–12 µM	4.0	(Jampasa et al., 2014)
Graphene/Polyaniline	Pyrrolidinyl	EIS & SWV	10–200 nM	2.3	(Teengam et al., 2017)

CHAPTER 3: EXPERIMENTAL AND CHARACTERIZATION METHODS

This chapter discusses the experimental methods and material utilized in this study. The materials and reagents are described thoroughly in section 3.1. The overall methodology is presented in section 3.2 while the preparation of the general solution is presented in section 3.3. This is followed by the synthesis process of nanoparticles such as iron oxide nanoparticles and iron oxide-gold core-shell nanoparticles, and the characterization of synthesized nanoparticles in sections 3.4 and 3.5, respectively. Electrochemical measurements and the preparation of core-shell Fe_3O_4-Au NPs modified electrodes are presented in sections 3.6 and 3.7, respectively. Finally, the electrochemical detection procedures for human papillomavirus and dopamine are presented in sections 3.8 and 3.9, respectively.

3.1 Materials and reagents

3.1.1 Chemical, solvents and biological reagents

In this study sterilized ultrapure deionized (DI) water (Mili-Q ultrapure water system, USA) used to prepare all aqueous reagents. Table 3.1 shows the complete list of substances.

Table 3.1: General list of chemical and biological reagents used in this study

CHEMICALS AND BIOLOGICAL REAGENTS		SUPPLIER
Chemicals		
Ferric chloride hexahydrate	$FeCl_3 \cdot 6H_2O$	Merck, Germany
Ferrous chloride tetrahydrate	$FeCl_2 \cdot 4H_2O$	Merck, Germany
Natural honey		Polleney-highlands of Northeastern China
Sodium Hydroxide	NaOH (99.0%)	Merck, Germany
GOLD(III) CHLORIDE TRIHYDRATE	$HAUCL_4.3H_2O$ (≥49.0%) W	SIGMA-ALDRICH, USA

Table 3.2: General list of chemical and biological reagents used in this study (continued)

CHEMICALS AND BIOLOGICAL REAGENTS		SUPPLIER
Dopamine	$C_8H_{11}NO_2$	Sigma-Aldrich, USA
Acetone, >99%	C_3H_6O	Sigma-Aldrich, USA
Potassium hexacyanoferrate III	$K_3Fe(CN)_6$	R&M Chemicals, UK
Tris-sodium citrate	$Na_3C_6H_5O_7$	R&M Chemicals, UK
Ethylenediaminetetraacetic acid (EDTA)	$(HO_2CCH_2)2NCH_2$ $CH_2N(CH_2CO_2H)_2$	Sigma-Aldrich, USA
Sodium chloride	NaCl	PROLABO, Paris
Potassium chloride	KCl	Sigma-Aldrich, USA
Sulfuric acid	H_2SO_4	
Magnesium sulfate	$MgSO_4$	
Sodium sulfite	$NaSO_3$	
Glucose	$C_6H_{12}O_6$	
Ascorbic Acid	$C_6H_8O_6$	
Uric acid	$C_5H_4N_4O_3$	

3.1.2 Synthetic oligonucleotide sequences

The synthetic oligonucleotide of the human papillomavirus (type 16) DNA sequence was purchased from TAG Copenhagen, Frederiksberg, Denmark, with the following base sequences in Table 3.2.

Table 3.3: Synthetic oligonucleotide sequences

SYNTHETIC OLIGONUCLEOTIDE	DNA SEQUENCES
Thiolated ssDNA probe	5'SH-$(CH_2)_6$-CATACACCTCCAGC -3'
Complementary target (type16) ssDNA	5' -GCTGGAGGTGTATG -3'
One-base mismatch	5' -GCTAGAGGTGTATG -3'
Three-base mismatch	5' -GCTAGAGATGCATG -3'
Non-complementary	5' -GGATGCTGCACCGG -3'

3.2 Overall Methodology

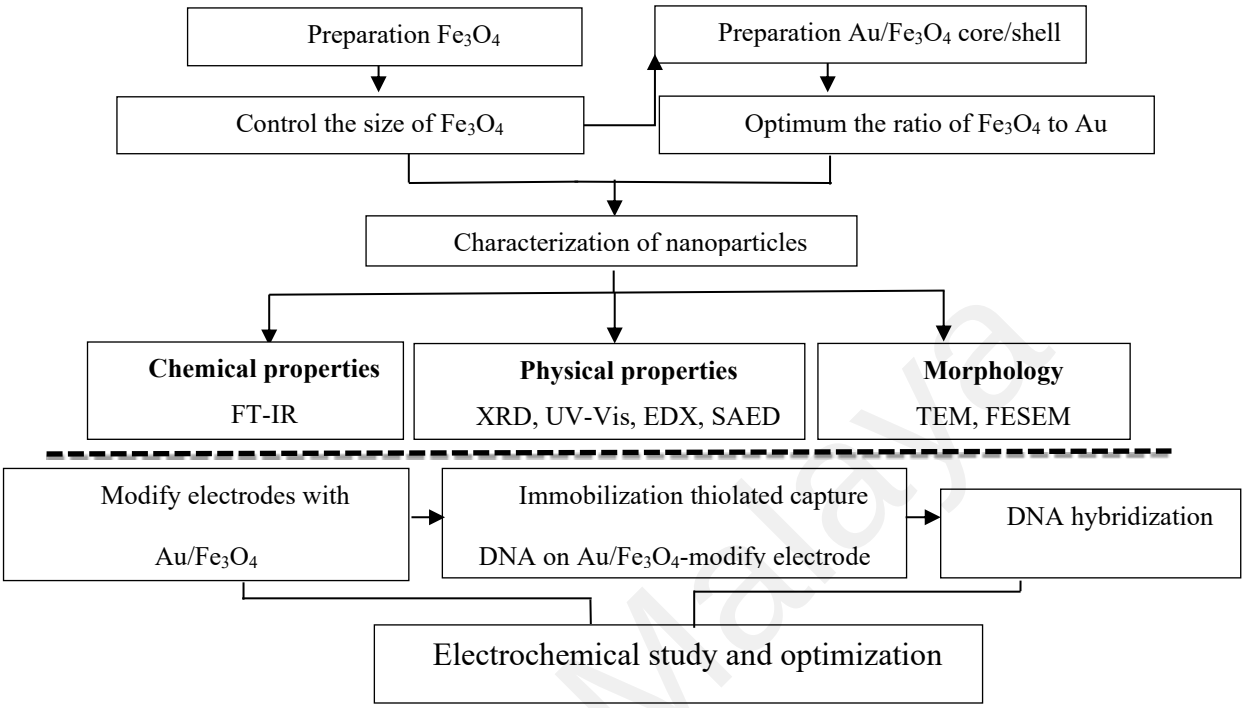

Figure 3.1: The overall methodology flowchart

Table 3.4: List of equipments used in this study

Apparatus/instrumentation	Model/Brands	Purposes
Ultrasonic bath	Model clean-02 JEIO TECH, (Korea)	For electrode cleaning, ensure the homogenous dispersion of NPs and for electrode modification
X-Ray Diffraction (XRD)	Bruker D8 (Bruker AXS, Billerica, MA)	To identify the phase structure of the NPs
Ultraviolet-visible spectrophotometer (UV-VIS)	Shimadzu UV-2600 UV-vis spectrophotometer (Japan)	To determine the absorbance of synthesized Fe_3O_4AuNPs suspension
Transmission electron microscopy (TEM)	JSM-6400, JEOL (Japan)	Characterize the size and shape of synthesis NPs
Field emission scanning electron microscopy (FESEM)	JSM-7600F, JEOL, (Japan)	Characterize the surface morphology of NPs
Energy dispersive x-ray (EDX)	Hitachi S-3400N	Determine the elemental composition of NPs
Fourier Transformed Infrared Spectroscopy (FTIR)	Perkin Elmer, Waltham, MA	Determine the functional group and types of bonds
Vibrating Sample Magnetometry (VSM)	Lake Shore Model 7400, Tokyo, Japan	To study the magnetic properties of the NPs
Selected area electron diffraction (SAED)	Tecnai G2 F20-FEI transmission electron microscope (Hillsboro, OR)	To identify the crystal structure of core-shell NPs
Hot plate stirrer	IKA 3581200, Clackson Laboratory (USA)	For stirring chemical solution
Centrifuge	USA scientific, USA	To separate solid from a solution
Vortex mixer	SciQuip VariMix, UK	To mix the solution
Auto lab Electrochemical workstation	PGSTAT-302N (Ecochemie, Netherlands)	For electrochemical measurements

3.3 Preparation of general solution

3.3.1 Preparation of phosphate buffer

0.1 M phosphate buffer solution (PBS) was prepared by mixing 1.0 M monosodium phosphate (NaH_2PO_4) and 1.0 M disodium phosphate (Na_2HPO_4) in DI water solution of approximately pH 7.4 which is the same with human blood pH.

3.3.2 Preparation of TE buffer

All the human papillomavirus lyophilized oligonucleotide was re-formed using TE buffer solution (10 mM Tris-(hydroxymethyl) aminomethane–HCl (Tris–HCl) and 1 mM EDTA (pH 8.0)) to prepare a stock solution of 100 µM and were storage at -20 °C. Later, the oligonucleotide stock solution was diluted with proper volume of TE buffer (pH 8) for the DNA hybridization studies. To remove excess of unbound oligonucleotide on the fabricated electrode surface during the immobilization and hybridization process, the TE buffer was also used as the washing buffer.

The prepared buffer of 50 mM Tris-HCl which contains 20 mM NaCl (pH 7.5) was used as the supporting electrolyte in electrochemical analysis and as the washing solution. 1.0 mM of $Fe(CN)_6^{3-/4-}$ solution containing supporting electrolyte was used for the characterization of the modified electrode.

To treat the Thiol-modified oligos before the reconstitution in the TE buffer solution, 200 µl 10 mM TCEP (solve 2.9 mg TCEP-HCL in 1 ml TE buffer, pH 8.0) was added and shaken for 60 min at room temperature. Then, the precipitate was added with 150 µl 3M NaAc [24.6g NaAc, 0.21 g MgAc in 100 ml distilled water] and filled with ethanol, shaken gently, incubated for 20 min at -20°C. Lastly, it was spun for 5 min at 13,000 rpm, the supernatant was discarded and pellet dried at room temperature.

3.4 Synthesis Process of Nanoparticles

3.4.1 Preparation of Fe_3O_4-NPs

In the synthesis of Fe_3O_4 -NPs, different amounts of natural honey 0.5, 1.0, 3.0, and 5.0 g were added to 100 mL of deionized water, as the co-precipitation agent and stabilizer to control the particle size. Then $FeCl_3 \cdot 6H_2O$ and $FeCl_2 \cdot 4H_2O$ (with a 2:1 molar ratio) were added under continuous stirring and nitrogen gas bubbling to inhibit oxidation. The mixture was titrated against a NaOH (2.0 M) solution under continuous stirring until the pH reached 10. The Fe_3O_4-NPs were formed instantly from this reaction. The resulting black suspension was centrifuged, washed three times with deionized water and ethanol mixture, and then dried in an oven at 60 °C.

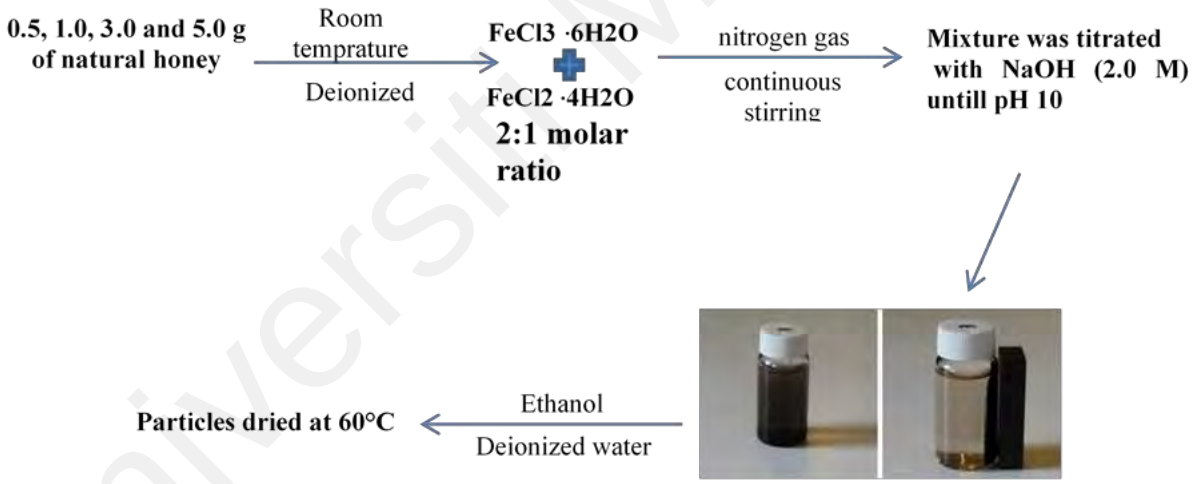

Figure 3.2: Synthesis flow chart of Fe_3O_4-NPs

3.4.2 Preparation of Core-Shell Nanoparticles

The gold-coated Fe_3O_4 nanoparticles were synthesized in high yields by the rapid and low-cost reduction of Au (III)-based precursors with honey under hydrothermal conditions for 20 minutes. For the creation of gold shell on magnetic nanoparticles, 5×10^{-2} g, 1×10^{-1}

g, and 15 × 10^{-2} g of iron oxide particles were dispersed in 50 mL ultra-pure water with ultrasonication for 2 minutes, separately. Then 25 mL 0.005 M $HAuCl_4$ was added to each aqueous solution and stirred for 15 minutes to ensure the complete adsorption of $[AuCl_4]^-$ ions on the Fe_3O_4-NPs surface. This was followed by the addition of 0.25 g of natural honey to the mixture, kept under hydrothermal conditions for 20 minutes at 120 °C, and then cooled to room temperature. Finally, the synthesized gold-coated iron oxide nanoparticles with different ratios of Fe_3O_4:Au, 1:1, 2:1 and 3:1, were isolated from the excess product with a strong magnet, washed three times with ultra-pure water and kept in the water for further usage.

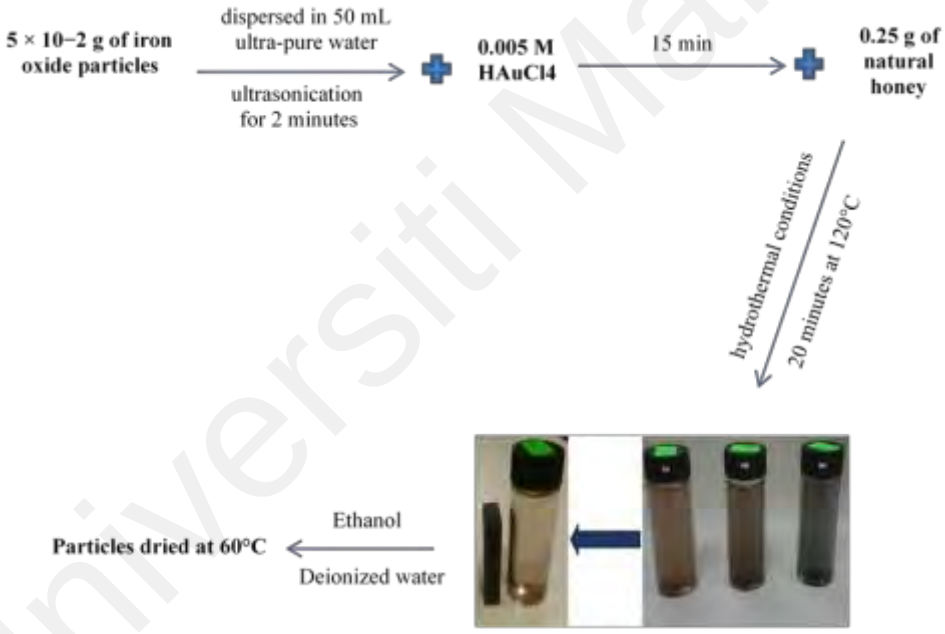

Figure 3.3: Synthesis flow chart of Fe_3O_4-Au NPs (1:1 Fe_3O_4-Au ratio)

3.5 Characterization of Synthesized Nanoparticles

3.5.1 Ultraviolet-Visible Spectrophotometry (UV-Vis)

UV-visible spectra were recorded using a Shimadzu UV-2600 UV-vis spectrophotometer (Japan) and quartz cuvette in a wavelength range of 400-800 nm. This instrument was used to analyze the absorbents peak of Fe_3O_4-Au core-shell NPs.

3.5.2 X-Ray Diffraction

The phase structure of the nanoparticles was analyzed using X-ray diffraction (Cu Kα 1.5406 Å radiation), with a Bruker D8 Advance diffractometer (Bruker AXS, Billerica, MA) at room temperature between 25 °C and 80 °C, in the 2q scale, with a scanning speed of 0.02 °/s and a step time of 3 seconds.

3.5.3 Fourier Transformed Infrared Spectroscopy

Fourier transformed infrared spectroscopy (FT-IR) was performed between 400 cm^{-1} and 4000 cm^{-1} at a resolution of 4 cm^{-1} to characterize possible biomolecules that are responsible for the capping and efficient stabilization of the Fe_3O_4Au-NPs. The FT-IR spectra were observed using a Spectrum 400 FT-IR/FT-FIR Spectrometer (Perkin Elmer, Waltham, MA).

3.5.4 Transmission Electron Microscopy

Transmission electron microscopy (TEM) was performed using a Tecnai G2 F20 from FEI transmission electron microscope (Hillsboro, OR), with an acceleration voltage of 200 kV. ImageJ version 1.46r program (National Institutes of Health, Bethesda, MD) were used to identify the size distributions of the nanoparticles. The samples were dispersed in DI water and a drop of the diluted sample was placed onto a 400-mesh carbon-coated copper grid. After that, the carbon-coated copper grid was dried at room temperature (27°C) before the imaging and loaded onto the microscope.

3.5.5 Scanning Electron Microscopy

The morphology of the Fe_3O_4-Au-NPs was determined through field emission scanning electron microscopy (FESEM). The FESEM and energy-dispersive X-ray spectroscopy (EDXS) were recorded using QuantaTM 450 FEG, Oxford instrument (Largo, FL). Each element has a special atomic structure, in which EDXS present information regarding the chemical composition of the compound. EDXS is an interaction between the X-ray and the compound being considered. Consequently, when this analysis is performed, X-rays are reflected from the compound and produce peaks. The peaks obtained in the spectrum represent the elements in the compound investigated.

3.5.6 Vibrating Sample Magnetometry

Vibration sample magnetometer (VSM) was used to study the magnetic properties of the samples by a VSM instrument (Lake Shore Model 7400, Tokyo, Japan) with magnetic fields up to 8 kOe on the dried samples at room temperature (27°C). The samples were measured in tablet form. The external magnetic field was swept from 10000 to -10000 Oe, and then back to 10000 Oe. The saturation magnetization values were normalized to the mass of NPs to yield the specific magnetization, Ms ($emug^{-1}$).

3.5.7 Selected Area Electron Diffraction (SAED)

Selected area electron diffraction (SAED) was performed using a Tecnai G2 F20 from FEI transmission electron microscope (Hillsboro, OR), with an acceleration voltage of 200 kV. The samples were dispersed in the distilled water and a drop of the diluted sample was placed onto a 400-mesh carbon-coated copper grid. After that, the carbon-coated copper grid was dried at room temperature (27°C) before the imaging and loaded onto the microscope.

3.5.8 Cytotoxicity Assay [MTT Test]

Cytotoxicity assay reveal the killing capacity of the test compound against a target cell. The cell viability of the synthesized Fe_3O_4-Au-NPs was evaluated by using 3-(4,5-dimethylthiazol-2-yl)-2,5-diphenyltetrazolium bromide (MTT) colorimetric technique. Briefly, in the 96 well plates, WEHI164 fibrosarcoma cells (1 × 104 cells/well) supplied from Institute Pastor, Iran, were seeded and incubated for 24 hours at 37 °C in 5% CO_2 incubator. This reaction was applied for the MTT reduction via the metabolically active cells by the action of dehydrogenase enzymes to produce the equivalents of NADPH and NADH. Then, the synthesized Fe_3O_4-Au- NPs with different concentrations from 0.54 to 140 ppm was added and incubated for another 24 hours. After this, 20 µL of 5 mg/mL MTT was added and the cells were incubated for 4 hours. After removing the medium, 100 µL of DMSO was added to the wells to dissolve the MTT crystals. The plates were placed on a shaker for another 15 minutes to complete dissolution of the formazan products. The quantity of formazan product was measured at 570 nm wavelength using a scanning Multiwell spectrophotometer (Epoch, BioTech instrument, Kimpton, UK). Each experiment was done in quadruplicate. The relative cell viability (%) related to nil nanoparticles as an untreated control cell was calculated by (A)test/ (A)control × 100 within (A)control and (A)test is the absorbance of the control and test samples, respectively. (Lahooti et al., 2017; Mokhodoeva et al., 2016; Sharkey et al., 2017)

$$Cell\ viability\ \% = \frac{(A)test\ sample}{(A)control} \times 100 \qquad \text{(Eq. 3.1)}$$

where (A) is the absorbance.

3.6 Preparation of Core-Shell Fe_3O_4-Au NPs modified electrodes (GCE and SPCE)

3.6.1 Fabrication of modified glassy carbon electrode

Prior to modify the bare glassy carbon electrode (3.0 mm diameter), the surface was polished to eliminate any traces which could affect the rate of electron transfer. The most common method is via mechanical polishing where GC electrode was polished with fine alumina powder (mean particle diameter of 0.3 and 0.05 μm) on a polishing pad. The electrode is held in a vertical position while making figure-8 motions on the polishing pad (Figure 3.4). To remove all traces of the polishing material, the electrode surface is rinsed with distilled water and then is sonicated in distilled water for a few minutes to ensure complete elimination of the alumina particles. The GC electrode was then dried under a pure nitrogen atmosphere at room temperature.

Then, synthesized Fe_3O_4-Au NPs (1 mg) were dispersed in ethanol (1 mL) by sonicating the mixture for 20 min in order to obtain a homogeneous suspension. Later, 5 μL of the resulting mixture was drop-casted onto the surface of a polished GCE (MF 2012, Electrical System, West Lafayette, IN) and dried at room temperature.

Figure 3.4: Glassy carbon electrode polishing process.

3.6.2 Fabrication of modified screen-printed carbon electrode

For this purpose, DI water was used for washing the bare SPCE and the electrode was electrochemical polished using cyclic voltammetry (CV) in 0.1 M sulfuric acid and 0.02 M

potassium chloride, ranging from (0.5 to 1.5 V) with a scan rate of 50 mVs^{-1} for 5 cycles. After that, the synthesized Fe_3O_4-Au NPs (1 mg) were dispersed in ethanol (1 mL) by sonicating the mixture for 20 min in order to obtain a homogeneous suspension. Then, 5 µL of the resulting mixture was drop-casted onto the surface of a polished screen-printed carbon electrode (SPCE) and dried at room temperature.

3.7 Electrochemical measurement

The electrochemical measurement and data analysis by cyclic voltammetry (CV), differential pulse voltammetry (DPV) and amperometric technique were performed using a potentiostat/galvanostat model PGSTAT-302N from Autolab (Ecochemie, Netherlands) connected to a computer and general-purpose electrochemical system (GPES) software version 4.9.

3.7.1 Experimental set-up

In this study, two types of electrodes; glassy carbon electrode (GCE) (Metrohm, Autolab) and not reusable screen-printed carbon electrode (SPCE) model DRP-C110 (DropSens, Spain) were combined into the potentiostat system based on the conventional three-electrode system. The electrochemical setup includes of the GCE (3 mm diameter) as the working electrode (WE), platinum as the counter electrode (CE, Metrohm, auto lab) and (Ag/AgCl 3M KCl) (Metrohm, auto lab) as the reference electrode (RE, Figure 3.5 a). For not reusable the SPCE, all three electrodes were printed on a ceramic substrate (L33 x W10 x H0.5 mm) consists of a carbon WE (4 mm diameter), a carbon CE, and Ag/AgCl RE as shown in Figure 3.5.

Figure 3.5: Image of the configuration of the electrochemical cell based on the three-electrode system; a) GCE; b) Screen-printed carbon electrode

3.7.2 Cyclic voltammetry (CV)

CV is one of the most common, significant, and sensitive electroanalytical method to study the redox processes, understanding reaction intermediates, and finding the stability of the reaction products. Cyclic voltammetry offers important information about the thermodynamics and kinetics of redox procedures based on polarization of the applied potential of the WE, in both the forward and reverse directions while monitoring the current. The peak potentials and peak currents of the redox peaks are two important parameters in a CV. If the electron transfer process is faster compared to the mass transport processes (such as diffusion) and faster than the chemical processes at the WE surface, the reaction is supposed to be electrochemically reversible and the peak separation is:

$$\Delta Ep = Epa - Epc = 2.303\ RT / nF \qquad \text{(Eq. 3.2)}$$

In this study, the CV technique was applied for the electrochemical performance of the fabricated electrodes.

3.7.3 Differential pulse voltammetry (DPV)

Differential pulse voltammetry is a controlled potential method of analysis at the working electrode, which involves a pulse of constant potential amplitude while increasing the potential with time. Figure 3.6 shows the pulse shape in DPV (Brett & Oliveira Brett, 1993). The DPV is a graph of differences between measured currents and applied potentials (Figure 3.7) (Brett & Oliveira Brett, 1993).

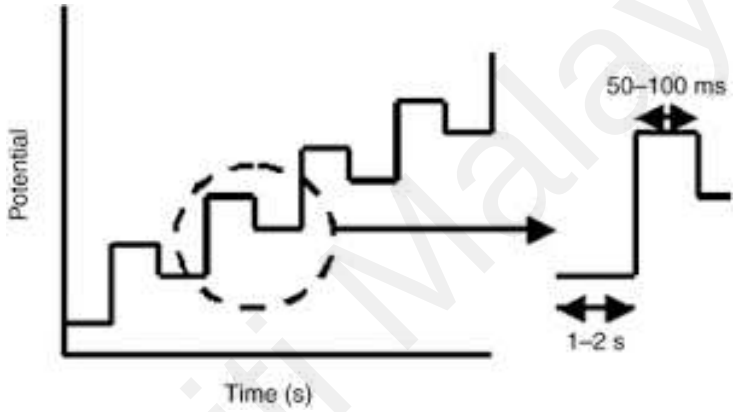

Figure 3.6: Diagram of the application of pulses in the differential pulse voltammetry (DPV) technique. Adapted from (Brett & Oliveira Brett, 1993)

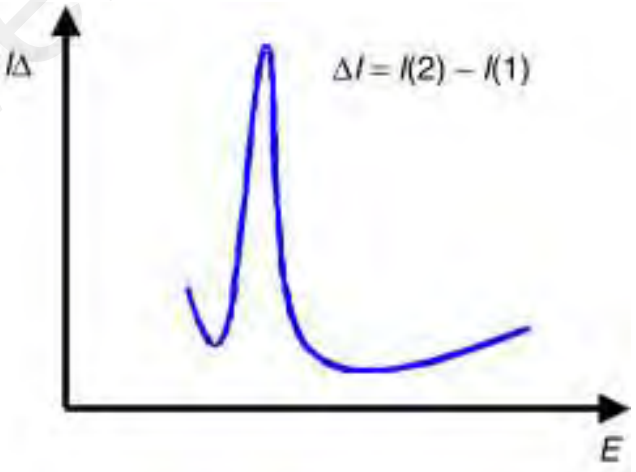

Figure 3.7: Typical response of a differential pulse voltammogram. Adapted from (Brett & Oliveira Brett, 1993)

Modified electrode's responses to the analyte concentration changes were studied with DPV. The DPV techniques possesses lower background current compared to CV and is used mainly for the calculation of the detection limit of the sensor electrode.

3.7.4 Chronoamperometry

In this method, the current is measured as a function of time while a constant potential is applied to the working electrode. The applied potential is normally chosen (based on the CV experiments) such that the resulting current is mass transport limited, therefore at the steady state current represents a concentration of the electroactive species, which is the analyte of interest or can be correlated to its concentration. The results are represented on a current versus time curve.

In this work, the effects of different kinds of interfering compounds on the analytical determination of dopamine by the amperometry response was investigated.

3.8 Human Papilloma Virus Electrochemical Detection Procedure

3.8.1 DNA probe immobilization and hybridization

The thiolated DNA probe (ssDNA) was immobilized on Fe_3O_4-Au-SPC electrode surface via the Au-S bond. Figure 3.8 shown the process of DNA immobilization and hybridization. The immobilization was achieved by drop-casting 10 µL of thiolated DNA probe on the surface of modified SPC electrode and incubated for 18 hours at 4 °C. The excess of unbound thiolated DNA probe on the modified electrode surface was washed carefully with TE buffer. The modified SPCE then was marked as ssDNA-Fe_3O_4-Au-SPCE. The hybridization process was performed by incubating ssDNA- Fe_3O_4-Au-SPCE with 10 µL of complementary DNA target (1 µM) for half an hour at 40 °C. TE buffer was used to wash the unbound complementary target DNA and prepared electrode dried with N_2 gas. The modified SPCE

was marked as dsDNA-Fe_3O_4-Au-SPCE. The Fe_3O_4-Au- modified SPCE (with and without of complementary DNA) was connected to the potentiostat for electrochemical measurements of the DNA probe immobilization and hybridization in 50 mM Tris-HCl, at pH 7.5 in 1.0 mM $[Fe(CN)_6]^{3-/4-}$ solution, in supporting electrolytes (0.1 M KCl and 0.02 M NaCl) at a potential range of -0.5 V-0.5 V, step potential of 0.005 V, modulation amplitude of 0.5 V with the interval time of 0.64 s at room temperature.

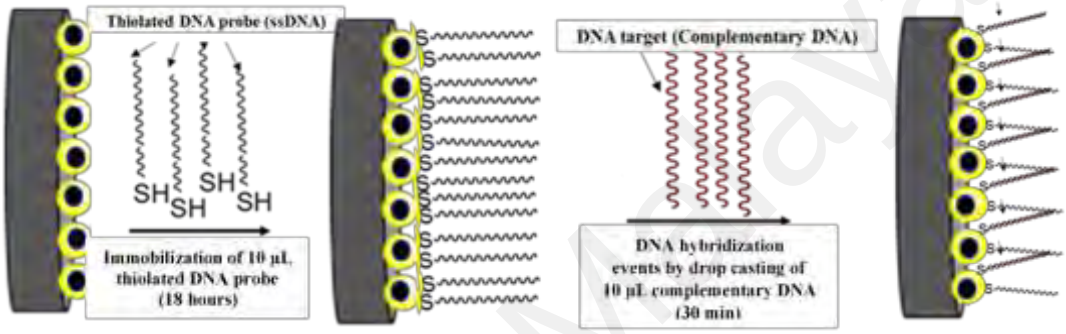

Figure 3.8: A Schematic representation of immobilization and hybridization of DNA

The one-factor-at-a-time (OFAT) method was carried out to optimize the fabrication of the modified Fe_3O_4-AuNPs-SPC electrode. The fabricated modified Fe_3O_4-AuNPs-SPC electrode was utilized to study the effect of DNA probe concentration (1 µM, 5µM, and 10 µM), the effect of DNA target concentration and the effect of the different synthetic targets. All the OFAT work was carried out in triplicate (n=3).

3.8.2 Electrochemical study

3.8.2.1 Cyclic voltammetry (CV)

CV characterization were performed at different modified SPC electrodes such as bare SPCE, Fe_3O_4-AuNPs-SPCE, ssDNA/Fe_3O_4-AuNPs-SPCE and hybridized DNA/Fe_3O_4-AuNPs-SPCE in 1.0 mM $[Fe(CN)_6]^{3-/4-}$ solution containing supporting electrolyte (0.1 M KCl), 50 mM Tris-HCl and 0.02 M NaCl, at pH 7.5 with a potential range of −0.5 to 0.5 V

and a scan rate of 50 mVs^{-1}. The GPES software version 4.9 (Eco Chemie, Netherlands) was used for the data analysis of different modified SPCE electrodes.

The effect of different scan rates (10 mVs^{-1}, 20 mV/s, 30 mV/s, 40 mV/s, 50 mV/s, 60 mV/s, 70 mV/s, 80 mV/s, 90 mV/s, 100 mV/s, 150 mV/s, 200 mV/s, 250 mV/s and 300 mV/s) of the modified SPC electrode was carried out in 1.0 mM $[Fe(CN)_6]^{3-/4-}$ solution containing supporting electrolyte (0.1 M KCl) and 50 mM Tris-HCl (pH 7.5).

The effect of different DNA Probe concentrations (1, 5, and 10 µM) hybridized with 1 µM target DNA was investigated in 1.0 mM $[Fe(CN)_6]^{3-/4-}$ solution containing supporting electrolyte (0.1 M KCl), 50 mM Tris-HCl and 0.02 M NaCl, pH 7.5.

3.8.2.2 Selectivity and sensitivity studies

Different kinds of human papillomavirus oligonucleotides such as the one-base mismatch, three base mismatch, and non-complementary at concentration of 100 nM were introduced to ssDNA/Fe3O4-AuNPs-SPCE, for selectivity studies. The DNA hybridization procedure of immobilized DNA and its target is reported in section 3.8.1. In order to study the sensitivity of fabricated electrode, the prepared ssDNA-Fe_3O_4-Au-SPCE was hybridized with complementary target DNA at different concentrations in the range of 10000 nM to 0.0001 nM. All the experiments were performed in triplicate (n=3).

3.9 Dopamine Electrochemical Detection Procedure

3.9.1 Electrochemical study

3.9.1.1 Cyclic voltammetry (CV)

CV characterization studies were performed at different modified GCE such as the bare GCE and Fe_3O_4-Au-NPs-GCE in 0.1 M phosphate buffer solution (pH7.4) and 100 µM of DA at a potential range of −0.3 to 0.8 V with a scan rate of 50 mVs^{-1}. The data analysis of

different modified GCE was performed using (GPES) software version 4.9 (Eco Chemie, Netherlands).

The effect of different scan rates (10 mVs^{-1}, 20 mV/s, 30 mV/s, 40 mV/s, 50 mV/s, 60 mV/s, 70 mV/s, 80 mV/s, 90 mV/s and 100 mV/s) of the modified GCE was carried out in 0.1 M phosphate buffer solution (pH7.4) and 100 µM of DA.

The effect of different solution pH with a pH range of 3−8 was investigated in 0.1 M phosphate buffer solution and100 µM of DA.

3.9.1.2 Selectivity and sensitivity studies

In selectivity studies, different concentration of DA (0.2, 1, 2, 5, 6, 10, 20, 40, 50, 60, 70, 85, 90, 100, 150, and 200 µM) in 0.1 M phosphate buffer solution, at pH 7.4 were introduced to Fe_3O_4-AuNPs-GCE.

In sensitivity studies, the fabricated Fe_3O_4-Au-GCE was studied in different compounds (50 µM $MgSO_4$, $NaSO_3$, KCl, glucose, AA, UA) in a phosphate buffer solution (pH 7.4). All the experiments were carried out in triplicate (n=3).

3.9.1.3 Stability studies

For stability studies, the fabricated Fe_3O_4-AuNPs-GCE was stored at 4 °C for a month. The fabricated electrode (n=3) were taken out and electrochemically measured in 0.1 M phosphate buffer solution (pH7.4) and 100 µM of DA at the potential range of −0.3 to 0.8 V with a scan rate of 50 mVs^{-1}.

CHAPTER 4: RESULTS AND DISCUSSION

Part 1:Synthesis and characterization of Fe_3O_4 NPs

4.1 Synthesis of Fe_3O_4 NPs

After adding NaOH and stirring the solution for 1 hour, the color of the iron chloride salts and honey mixture turned from pale yellow to black, which indicates the formation of Fe_3O_4 NPs. The separation of the Fe_3O_4 NPs from the solution was achieved using an external magnet. Figure 4.1 clearly displays that the synthesized Fe_3O_4 NPs can be attracted by an external permanent magnet, which evidenced that NPs possessed magnetic properties. Once the magnet was removed, the NPs could be dispersed readily by agitation.

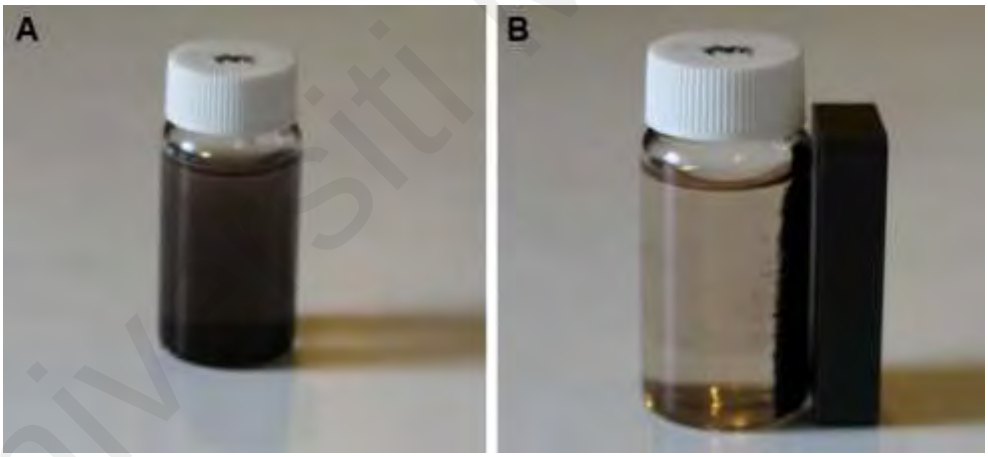

Figure 4.1: Suspension of synthesized Fe_3O_4 NPs by mixing Fe^{3+} and Fe^{2+} (2:1 M ratio) and honey (A), Separation of synthesized Fe_3O_4 NPs from media using an external magnet (B).

The Fe_3O_4 NPs are formed by adding a base to an aqueous mixture of Fe^{3+} and Fe^{2+} chloride at a 2:1 M ratio. The chemical reaction for the precipitation of Fe_3O_4 is as follows:

$$FeCl_2.4H_2O + 2FeCl_3.6H_2O + 8NaOH \rightarrow Fe_3O_4 + 8NaCl + 20H_2O \qquad \text{(Eq. 4.1)}$$

4.2 Characterization of Fe_3O_4 NPs

4.2.1 X-Ray Diffraction Analysis

The Fe_3O_4 -NPs were characterized by X-ray powder diffraction (XRD) and all peaks were analyzed and indexed using the ICDD database, by comparison with the magnetite standards (Figure 4.2)(Ayala-Valenzuela et al., 2005). The peaks were indexed to the (220, 311, 400, 422, 511, 440) and (533) planes, which is attributed to the 2θ of 30.46°, 35.76°, 43.51°, 53.24°, 56.88°, 63.32°, and 71.41°, respectively, with the standard diffraction spectrum (ref. code Fe_3O_4:01-088-0315)(Kalantari, Ahmad, Shameli, & Khandanlou, 2013).

Generally, the diffraction peaks with lower intensity in the XRD pattern represents a smaller size of the Fe_3O_4 -NPs. In this case, there is a decreased intensity of the peaks with increasing honey concentration, which also indicates a decrease in the particle size.

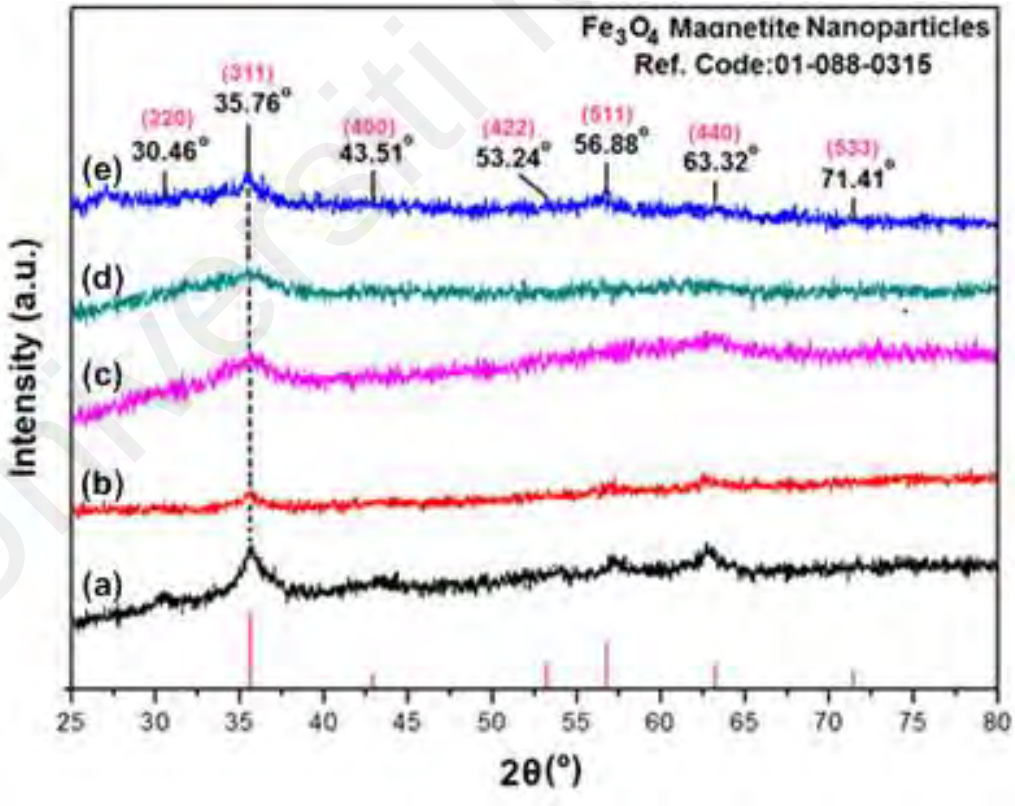

Figure 4.2: Powder X-ray diffraction patterns of Fe_3O_4 -NPs without (a) and with different concentrations of honey (0.5, 1, 3, and 5% [w/v]) (b–e), respectively.

4.2.2 Morphological Study

The TEM micrographs of the particle size and distribution of the Fe_3O_4 -NPs are presented in Figure 4.3. The images reveal significantly smaller nano magnetite particles with identical particle sizes which have a similar shape and are uniformly dispersed. Also, the Fe_3O_4 -NPs have a spherical morphology and a uniform distribution. From the TEM images, it is obvious that the particle size decreases from 3.21 to 1.92 nm for 0.5% and 5.0% (w/v) with the increase in the amount of honey. It is significant to mention that sucrose, glucose (a decomposition product of sucrose), and gluconic acid have hydroxyl groups, in addition to the carboxylic groups in gluconic acid, from the magnetite synthesis. These functional groups can be absorbed into define crystal planes or chelated with the Fe atoms as a covering material to create a steric block, like the common stabilizers and surfactants (Cushing, Kolesnichenko, & O'Connor, 2004).

The FESEM images show that the Fe_3O_4 -NPs synthesized using honey have a spherical structure (Figure 4.4). Significantly, no morphological differences were detected with the increase in the honey concentration, thus the structure of the nanoparticles remained unchanged.

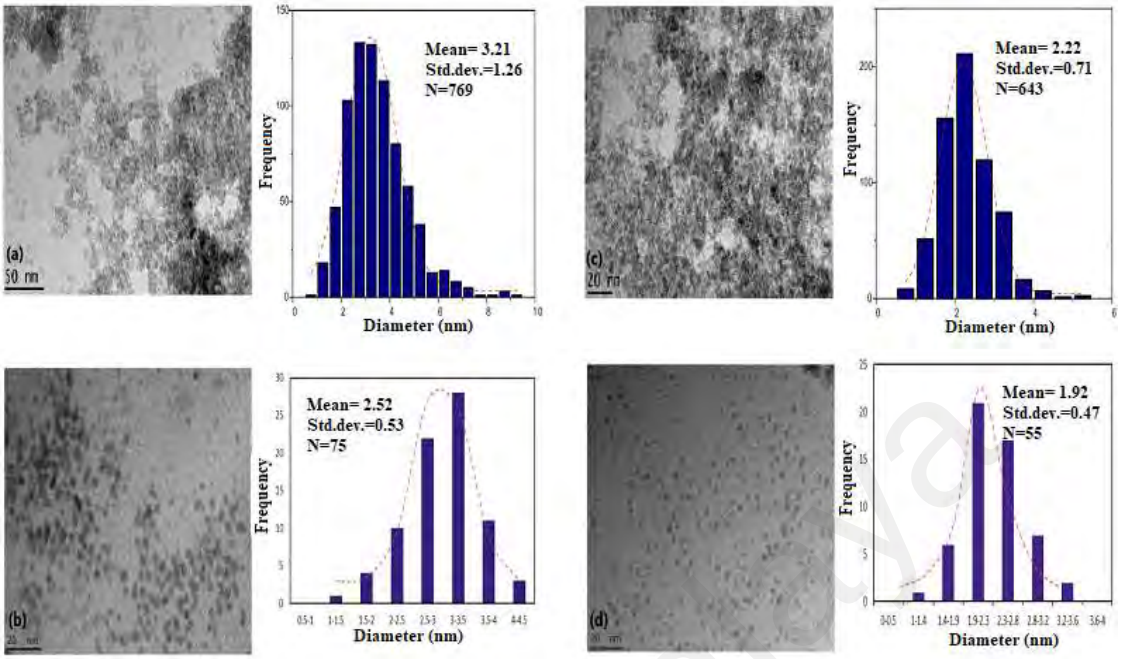

Figure 4.3: TEM images and histograms of particle size distribution for 0.5%, 1% 3% and 5% (w/v) honey/Fe_3O_4 -NPs. (a), (b), (c) and (d): 0.5% and 3% (w/v), respectively.

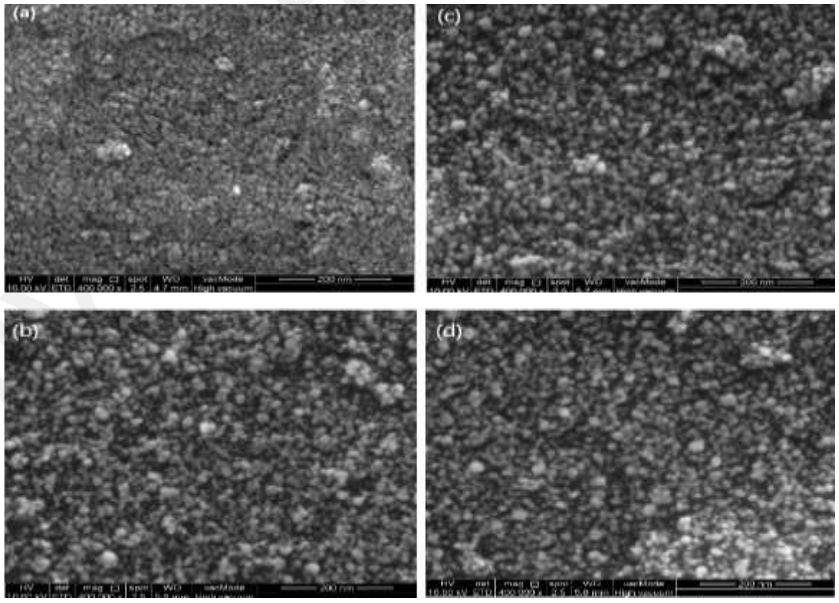

Figure 4.4: Surface morphology of magnetite nanoparticles with 0.5, 1, 3 and 5% (w/v) honey (a-d), respectively.

Figure 4.5 shows the chemical composition of the prepared nanoparticles. From the EDX spectrum, the oxygen and iron peaks reveal the presence of Fe_3O_4 -NPs; the peaks at around

0.7, 6.4, and 7 keV correspond to the Fe element(J. Chen, Wang, Huang, Liu, & Liu, 2009; Yougbaré et al., 2020). Besides, the EDX spectra of the Fe_3O_4 -NPs confirm the presence of elemental Fe without any impurity peaks.

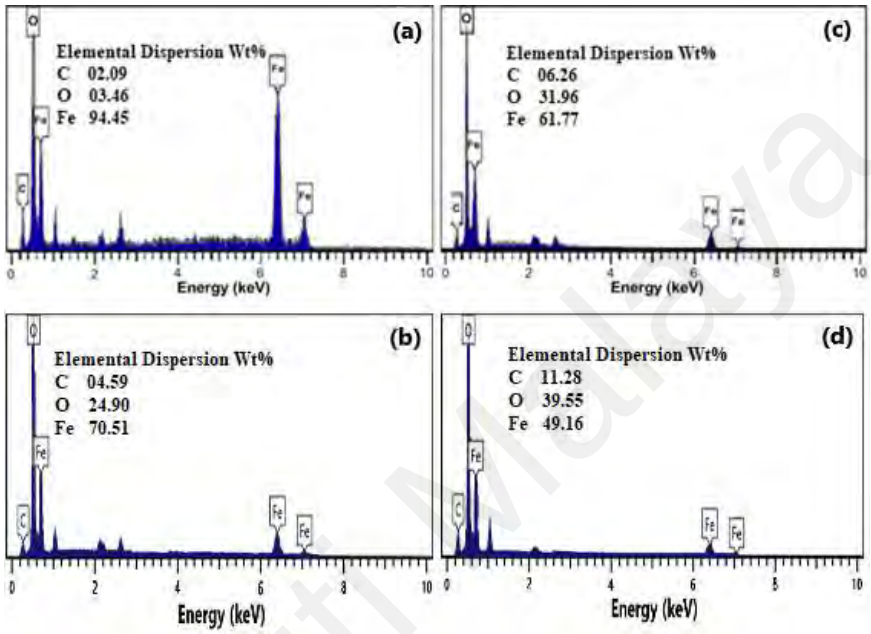

Figure 4.5: EDX spectroscopy of Fe_3O_4 -NPs with 0.5, 1, 3 and 5% (w/v) honey, (a-d), respectively.

4.2.3 Vibrating Sample Magnetometer

The magnetic characterization of the Fe_3O_4 -NPs was performed with VSM. Figure 4.6 shows the hysteresis loop of all samples at a magnetic field range of -8,000 to 8,000 Oe at room temperature. The samples (a), (b), (c), (d), and (e) display almost immensurable coercivity and remanence, indicating that the magnetic nanoparticles are superparamagnetic (Z. Li, Sun, & Gao, 2005).

The saturation magnetization (Ms) of Fe_3O_4 -NPs with 0.5, 1.0, 3.0, and 5.0% (w/v) honey are 19.91, 6.25, 3.75, and 2.19emu g^{-1}, respectively, which decrease with the decrease in the nanoparticles size. This is because of that the saturation magnetization Ms of NPs depends on their size, the saturation magnetization reducing along with the reduction of the size, as a

result of the spin disorder at the surface of the nanoparticles, which leads to a dominant effect at very small dimensions (Caizer, 2015). The VSM shows that the Ms of the Fe_3O_4 - NPs prepared using NaOH (without honey) as the reducing agent is 28.98 emu g^{-1} for sample (a). The presence of organic coating agents on the sample (b), (c), (d) and (e) decrease the saturation magnetization value compared to sample (a) which decreases the homogeneity due to the decrease of the surface moments (D. K. Kim, Mikhaylova, Zhang, & Muhammed, 2003). The result of the size decrease of nanoparticles also reflects upon the variation of the saturated magnetization of nanoparticles as a function of temperature, which is different from that of the corresponding bulk material, in the case of many nanostructures. Also, the Curie temperature of nanoparticles reduces along with the reduction of their size, the decrease being more noticeable when the nanoparticles are smaller, in the range of nanometers; consequently, a reasonable decrease in the saturation magnetization is anticipated (Caizer, 2015). Table 4.1 provides a comparison between the synthetic methods, particle sizes and saturation magnetization of the Fe_3O_4 NPs from the results of other researchers and this work.

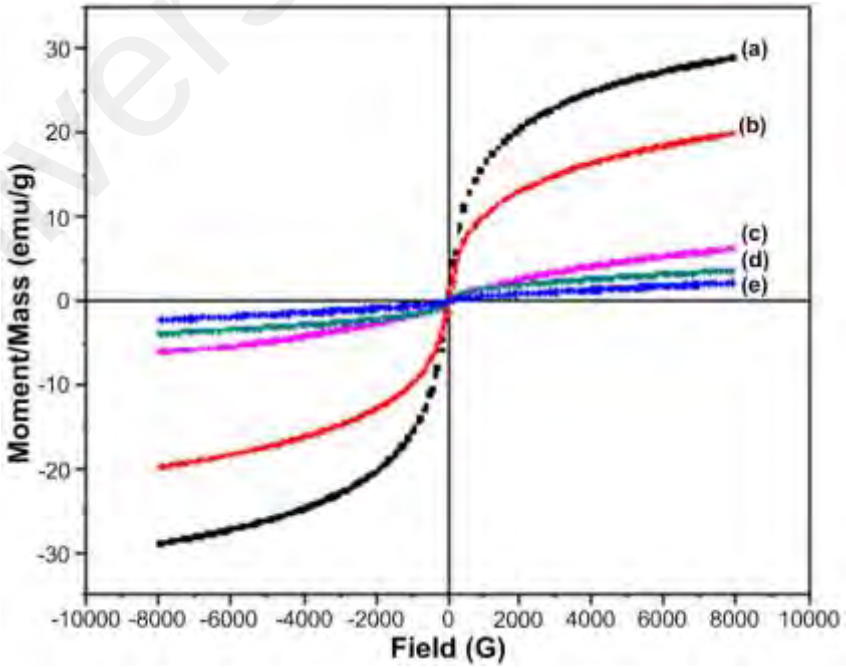

Figure 4.6: VSM of pure Fe_3O_4 (a) and Fe_3O_4 -NPs with 0.5, 1, 3 and 5% (w/v) honey (b–e, respectively).

Table 4.1 Comparison between the synthetic methods, particle sizes and saturation magnetization of Fe_3O_4 NPs from the results of other researchers and this work

Method of synthesis	Particle size (nm)	Saturation magnetization (Ms/ emu·g^{-1})	Reference
Co-precipitation method using NH_4 OH and chitosan	23	15	(Dung, Hai, Long, & Truc, 2009)
Quick precipitation using sodium hydroxide and rice straw	9.93	NA	(Khandanlou, Ahmad, Shameli, & Kalantari, 2013)
Co-precipitation method using NaOH and montmorillonite	8.24–12.88	12.10–32.40	(Kalantari et al., 2014)
Hydrothermal reduction route using sucrose	4–16	14.82–29.55	(X. Sun et al., 2009)
Co-precipitation method using NaOH and talc	2.27–8.13	NA	(Kalantari, Ahmad, Shameli, & Khandanlou, 2015)
A facile technique using diethyl amine	~25	35.76	(S. Ahmad, Riaz, Kaushik, & Alam, 2009)
Co-precipitation method using NaOH and carob leaf extract	4–8	NA	(Awwad & Salem, 2012)
Co-precipitation method using aqueous extract of brown seaweed (Sargassum muticum)	18	22.1	(Mahdavi, Namvar, Ahmad, & Mohamad, 2013)
Co-precipitation method using olive oil (magnetite (Fe_3O_4) and maghemite (γ-Fe_2O_3) nanoparticles)	20	40	(Palanisamy, Meenakshi Sundaram, Devabharathi, & Thangarasu, 2013)
Solvothermal synthesis	~200	78.03	(W. Zhang, Shen, & Hong, 2011)
Co-precipitation method	10	46.7	(El Ghandoor, Zidan, Khalil, & Ismail, 2012)
Colloidal method at room temperature	4–43	NA	(Martínez-Mera, Espinosa-Pesqueira, Pérez-Hernández, & Arenas-Alatorre, 2007)
Precipitation with forced mixing	~6.0	37.50	(Y. Zhu & Wu, 1999)
Co-precipitation method using NaOH and honey	3.21	19.91	Current study

4.2.4 Fourier Transform Infrared Spectroscopy Study

Honey contains proteins, minerals, vitamins and natural sugars (mostly fructose, sucrose, and glucose) (Devillers, Morlot, Pham-Delegue, & Dore, 2004; Nanda, Sarkar, Sharma, & Bawa, 2003; N. Singh & Bath, 1997; Terrab, Díez, & Heredia, 2002; White Jr, 1978). Fourier transformed infrared spectroscopy (FT-IR) was performed to determine the most probable biomolecules that are responsible for efficient stabilization and also the capping of Fe_3O_4 -NPs synthesized using honey. The FT-IR spectrum in Figure 4.7 shows a strong absorption band at 564.99 cm^{-1}, which is assigned to the Fe-O bond, demonstrates a high degree of crystallinity of the Fe_3O_4 -NPs (Karaoğlu, Baykal, Erdemi, Alpsoy, & Sozeri, 2011). The absorption band at 609.45 cm^{-1} in the FT-IR spectrum of the sample (Figure 4.7e) indicates the presence of some amount of oxidized maghemite on the surface of the magnetite. The characteristic band around 3,200 cm^{-1} is due to the presence of the O-H group (Xiaolang Chen, Yu, Zhang, & Lu, 2011).

The C-O stretching mode around 1073 cm^{-1} is due to the proteins in honey from the C-O-C symmetric stretching and C-O-H bending vibrations (S. Li et al., 2007). The amide I and II bands of proteins are expected to occur around 1660 and 1535 cm^{-1}, respectively (Basavaraja, Balaji, Lagashetty, Rajasab, & Venkataraman, 2008; V. Kumar, Guleria, Dasgupta, & Ranjan, 2020; Philip, 2009a, 2009b; Shankar et al., 2004; Solomun, Schimanski, Sturm, & Illenberger, 2004), in the current study, these bands occurred around 1600 and 1300 cm^{-1}. These bands occur as a result of the carboxyl stretching and N-H deformation vibrations in the amide linkages of protein. The proteins can be attached to the Fe_3O_4 -NPs via the free amine group or carboxylate ion of the amino acid residues (V. Kumar et al., 2020; Patra, Fraceto, Das, & Campos, 2020; J. Singh et al., 2018). The lack of C=O band is due to the presence of the C-O stretch and amide I and II bands in the FT-IR spectrum (Figure 4.7) of Fe_3O_4 -NPs which represent the stabilization of the system via the -COO−

(carboxylate ion) groups of amino acid, which remains with the free carboxylate groups in the proteins.

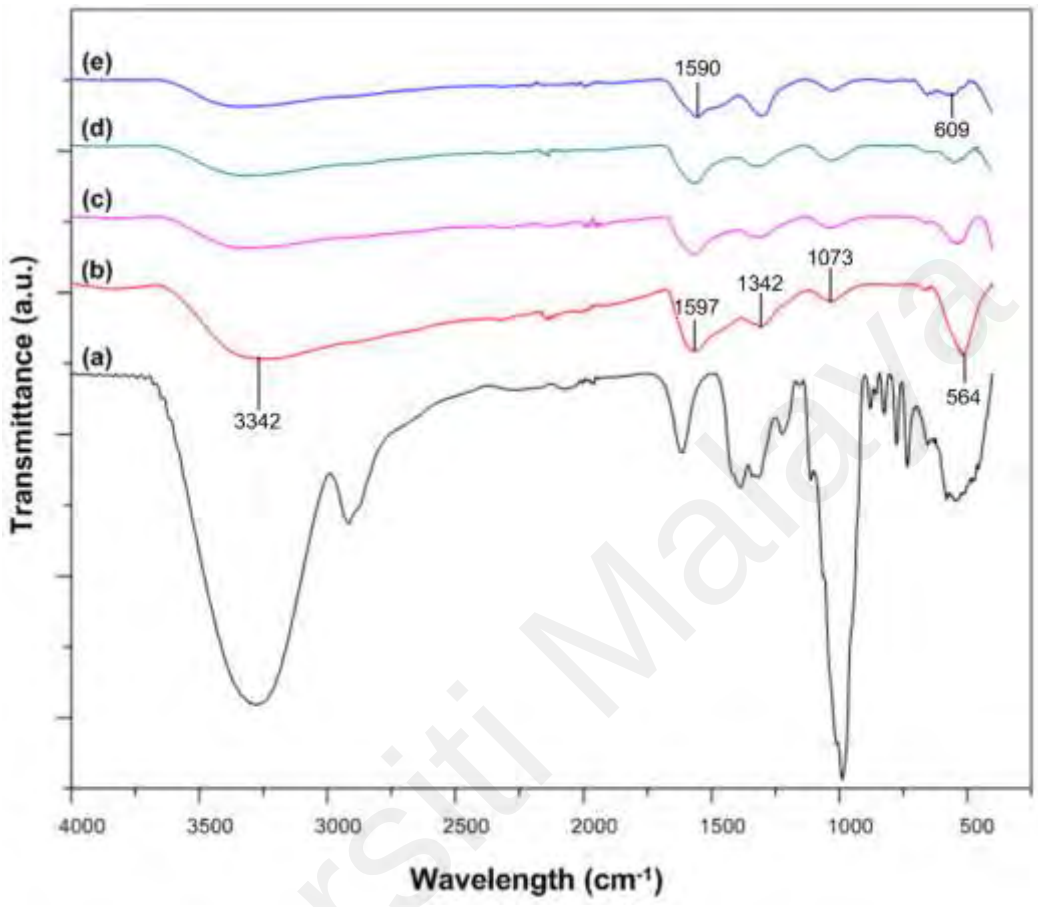

Figure 4.7: Fourier-transform infrared spectra of honey (a); magnetite nanoparticles with 0.5, 1, 3, and 5% (w/v) honey (b–e, respectively).

4.2.5 In Vitro Cytotoxicity Assay of Fe_3O_4 NPs

The in vitro cytotoxicity evaluation of Fe_3O_4 -NPs was performed by using 3-(4, 5-dimethylthiazol-2-yl)–2, 5-diphenyltetrazolium bromide (MTT) assay. As illustrated in Figure 4.8, the toxicity of the synthesized Fe_3O_4-NPs to the cells was found to be non-significant in higher concentrations until 140.0 ppm and they were well tolerated by the WEHI164 cells in the MTT assay.

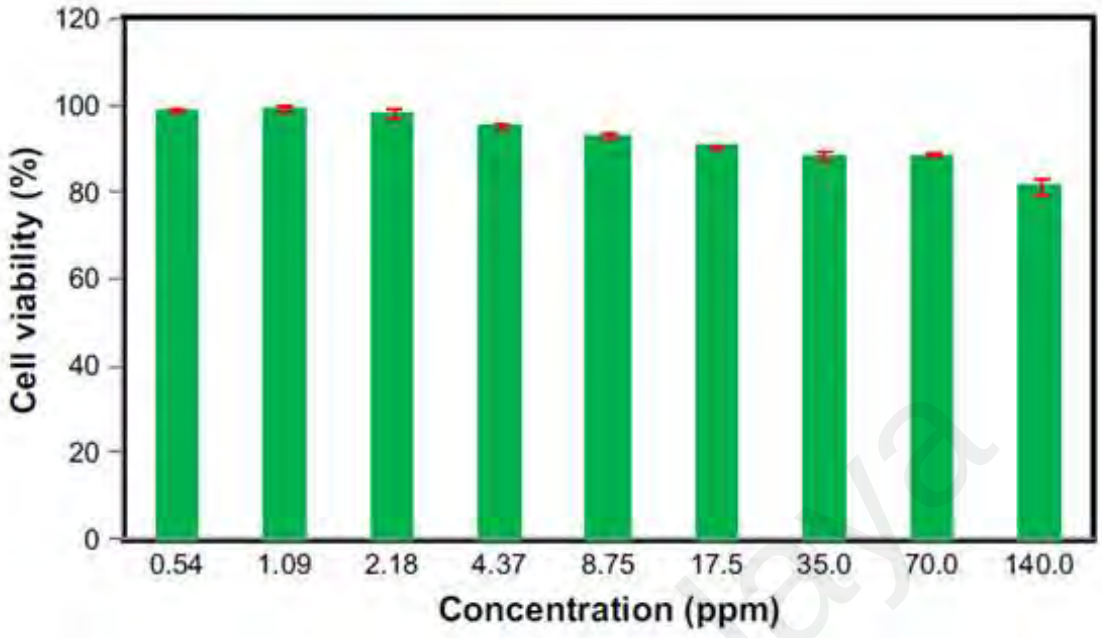

Figure 4.8: Cell viability of WEHI164 cells measured by the MTT assay (cells were incubated for 24 hours with the indicated concentrations of the magnetite nanoparticles).

Part 2: Synthesis and characterization of Core-Shell Fe_3O_4-Au NPs

4.3 Synthesis of Core-Shell Fe_3O_4-Au NPs

The iron oxide nanoparticles were coated with gold using honey under hydrothermal conditions which reduces the gold ions to metallic gold as the shell on the surface of the magnetic nanoparticles. Honey mostly consists of fructose and glucose, where glucose is oxidized to gluconic acid from the dilution in water, where the possible reducing agent might be fructose, sucrose and proteins/enzymes. As shown in Figure 4.9, once the synthesis of Fe_3O_4-Au core-shell NPs is completed, the core-shell nanoparticles can be separated by a magnet, while the color of the suspension turned clear, which is the proof for the high yield of gold coating on the surface of Fe_3O_4-NPs.

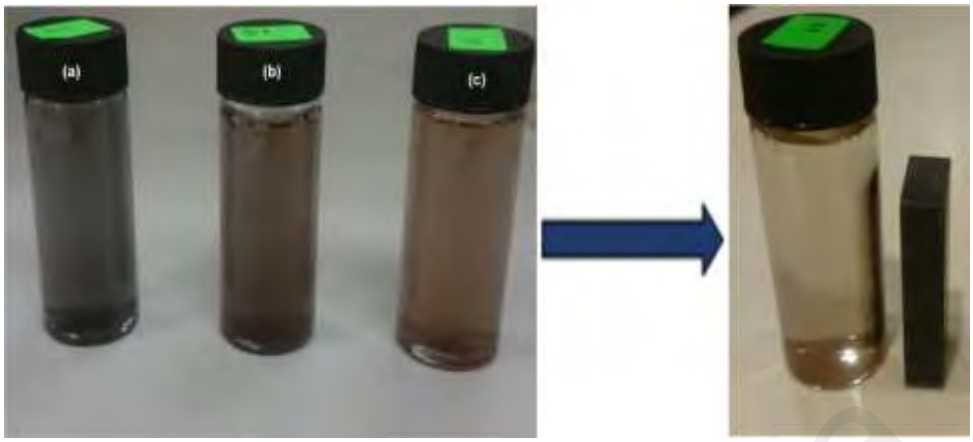

Figure 4.9: The Fe_3O_4/Au-NPs suspension with different ratios of 3:1, 2:1, and 1:1 (Fe_3O_4-NPs to Au), without (a-c) and with a magnetic field, respectively.

4.4 Characterization of Core-Shell Fe_3O_4-Au NPs

4.4.1 X-Ray Diffraction Analysis

The Fe_3O_4-Au core-shell NPs were characterized by powder X-ray diffraction (XRD) and all the peaks were analyzed and indexed with the JCPDS database (Figure 4.10) (Ayala-Valenzuela et al., 2005). In the XRD pattern of the magnetic nanoparticles, the peaks at 30.46° (220), 35.76° (311), 43.51° (400), 53.24° (422), 56.88° (511), 63.32° (440), and 71.41° (533) are attributed to the Fe_3O_4 (JCPDS ref. code: 01- 088-0315) (Kalantari et al., 2013). In the diffraction pattern of Fe_3O_4-Au core-shell NPs, the characteristic peaks of gold at 38.2°, 44.4°, 64.6°, and 77.6° can be indexed to the (111), (200), (220) and (311) planes of the fcc phase, respectively (JCPDS ref. code: 03-065-9857), beside a less intensive peak at 35.76° which is attributed to the magnetic core. The presence of the magnetite peaks in the Fe_3O_4-Au core-shell NPs could be due to the penetration of the X-rays through the magnetic core (Mandal et al., 2005). The decreased intensity of the diffraction peaks of the Fe_3O_4 phase in Fe_3O_4-Au core-shell NPs is a strong evidence of the full coverage of the magnetic core by the gold shell. Although, the complete invisibility of the magnetite peaks has been reported

in some of the synthesized core/ shell nanoparticles (Susmita Pal, Morales, Mukherjee, & Srikanth, 2009).

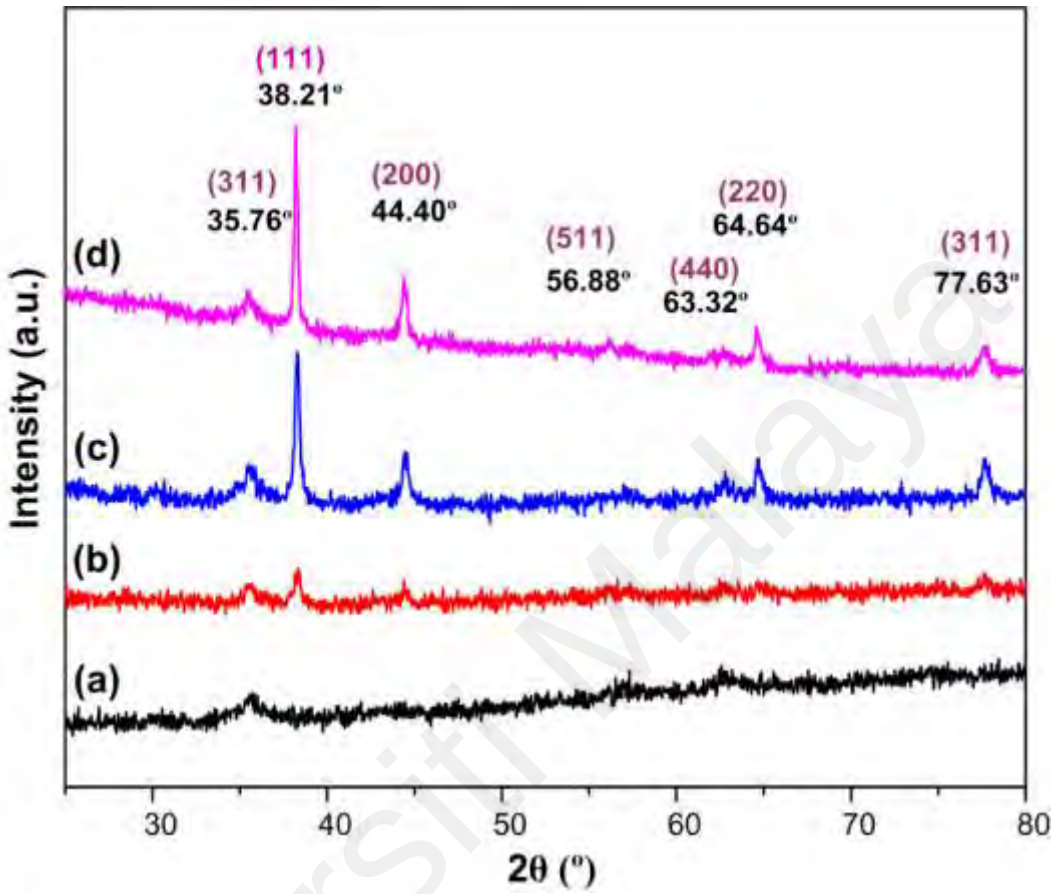

Figure 4.10: Powder X-ray diffraction patterns of Fe_3O_4-NPs (a) and Fe_3O_4-Au core-shell NPs with different molar ratio [3:1, 2:1, and 1:1 (b-d)], respectively.

4.4.2 UV-Vis Spectroscopy Analysis

The presence of the gold shell on the surface of Fe_3O_4-NPs was characterized via the UV-visible spectra (Figure 4.11). As revealed in Figure 4.11, the Fe_3O_4-NPs spectrum does not show absorption between 380 nm and 800 nm. In contrast, the UV-visible spectrum of gold nanoparticles shows a strong absorption band between 500 nm and 600 nm. The obtained Fe_3O_4-Au NPs were orange in color and shows absorption peaks at around 490 nm with considerable blue shift and broadening in the UV-visible spectrum. However, this peak was absent in the spectrum of iron oxide nanoparticles.

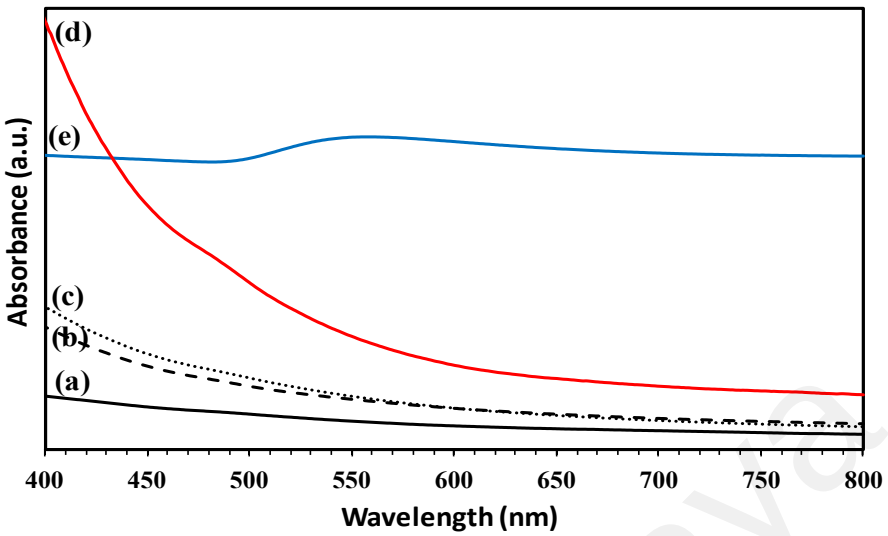

Figure 4.11: UV-visible absorption spectra of Fe_3O_4 NPs (a), Fe_3O_4-Au NPs with different molar ratio [3:1, 2:1, and 1:1 (b-d)] respectively and Au-NPs (e).

4.4.3 Morphological Study

Figure 4.12 shows the transmission electron microscopy (TEM) micrographs and the iron oxide nanoparticles size distribution histograms before and after the formation of the gold shell. The Fe_3O_4 NPs were synthesized via the co-precipitation method which produced nanometer sized particles with an average diameter of 3.21 ± 1.26 nm, from the TEM images. The TEM analysis shows that the average particle size of the Fe_3O_4 NPs increases from 3.21 nm to 3.49 nm and 4.11 nm for Fe_3O_4-Au NPs with a ratio of 2:1 and 1:1, respectively. The reduction of gold on the surface of the magnetic nanoparticles in this method produced uniform particles with an average Fe_3O_4-Au NPs size of 4.11 ± 1.26 nm with a ratio of 1:1.

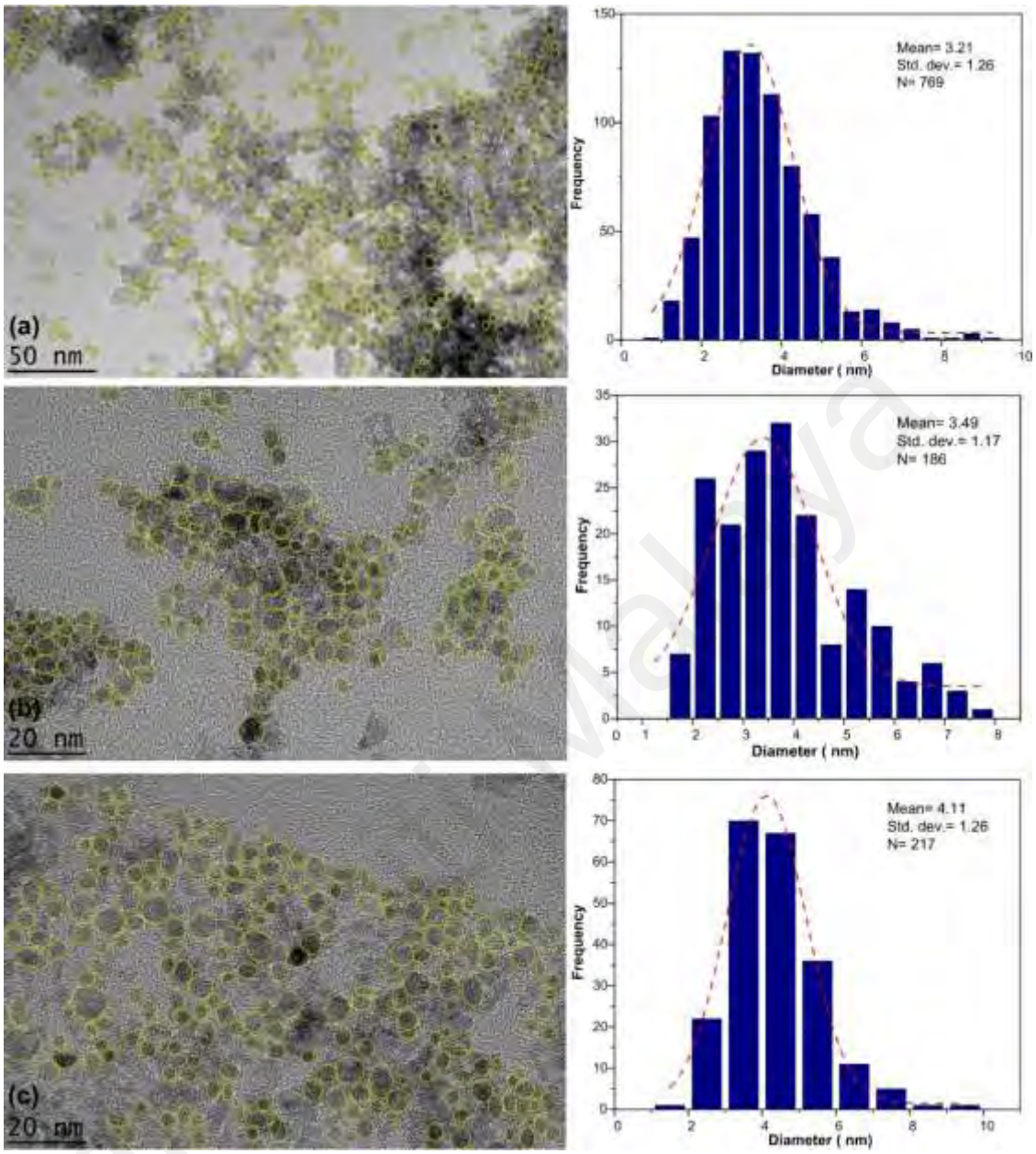

Figure 4.12: Transmission electron microscopy images and histograms of the particle size distribution for Fe_3O_4 NPs (a), Fe_3O_4-Au NPs with different molar ratio [2:1 and 1:1 (b and c)] respectively.

The selected area electron diffraction (SAED) pattern was also obtained for the Fe_3O_4-Au NPs. The bright circular spots clearly illustrate that the NPs are crystalline in nature (Figure 4.13). The SAED pattern displays the diffraction ring from the inner to the outer core, which can be indexed to the (1 1 1), (2 0 0), (2 2 0), and (3 1 1) reflections, respectively, of the fcc

gold. The two identifiable planes of (311) and (511) of the Fe_3O_4 NPs are shown in Figure 4.13, while the other Fe_3O_4 planes are overlaid with the Au planes.

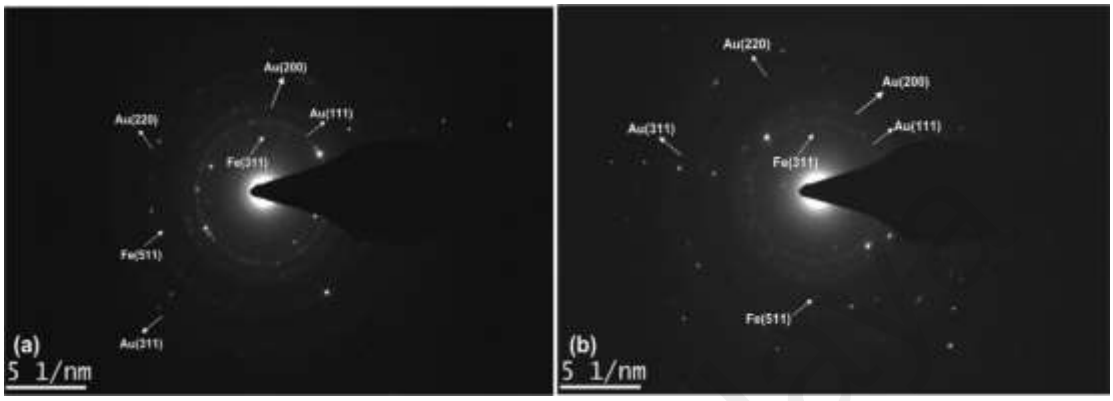

Figure 4.13: The selected area of electron diffraction (SAED) pattern for Fe_3O_4-Au NPs with different molar ratio [1:1 and 2:1 (a and b)], respectively.

The FESEM images of the Fe_3O_4-Au NPs change with the ratio of Fe_3O_4/Au (Figure 4.14). Significantly, the morphological changes are identified with the increase in the ratio of the gold to Fe_3O_4 NPs. This confirms the structural changes of the gold-NPs decorated on the surface of Fe_3O_4 NPs for particles with 3:1 ratio (Figure 4.14(c)), and the core-shell structure of Fe_3O_4-Au NPs with 1:1 ratio of gold/iron (Figure 4.14(a)).

Figure 4.15 shows the chemical composition of the prepared nanoparticles. From the EDX spectrum, the peak of oxygen, iron and gold are attributed to the presence of Fe_3O_4-Au NPs, while the peaks around 0.7, 6.4, and 7 keV correspond to the Fe element (J. Chen et al., 2009). The EDX spectra of Fe_3O_4-Au NPs confirm the presence of elemental Au and Fe without any impurity peaks, while the peaks at 2.1 and 8 to 14 keV are attributed to Au.

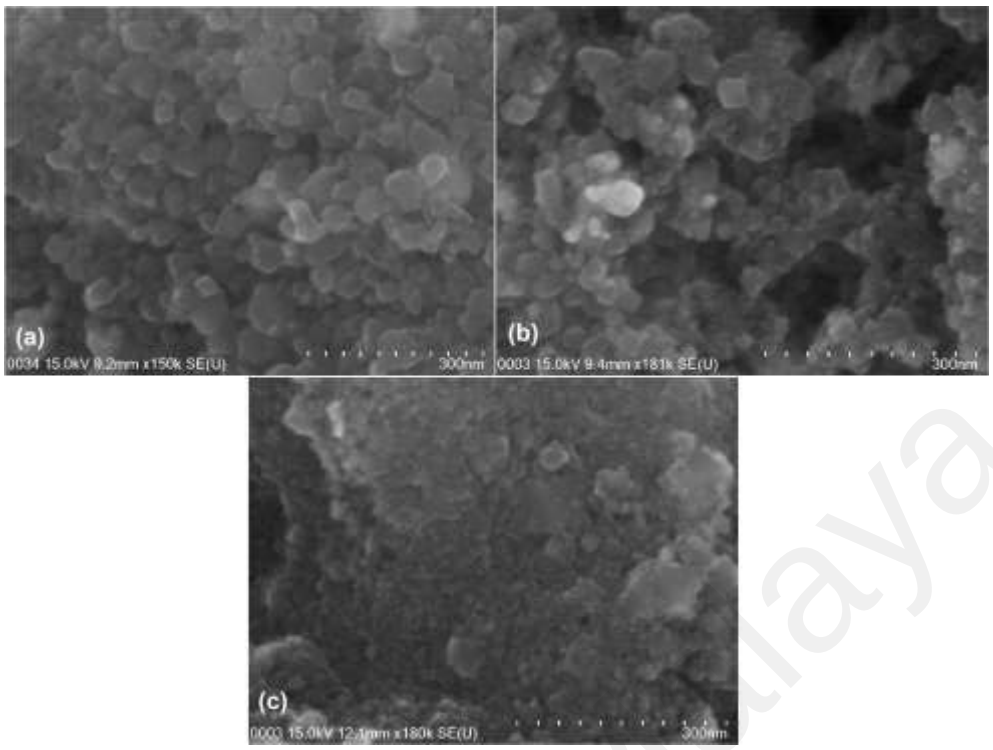

Figure 4.14: Surface morphology of Fe_3O_4-Au NPs with different molar ratio [1:1, 2:1, and 3:1 (a-c)] respectively

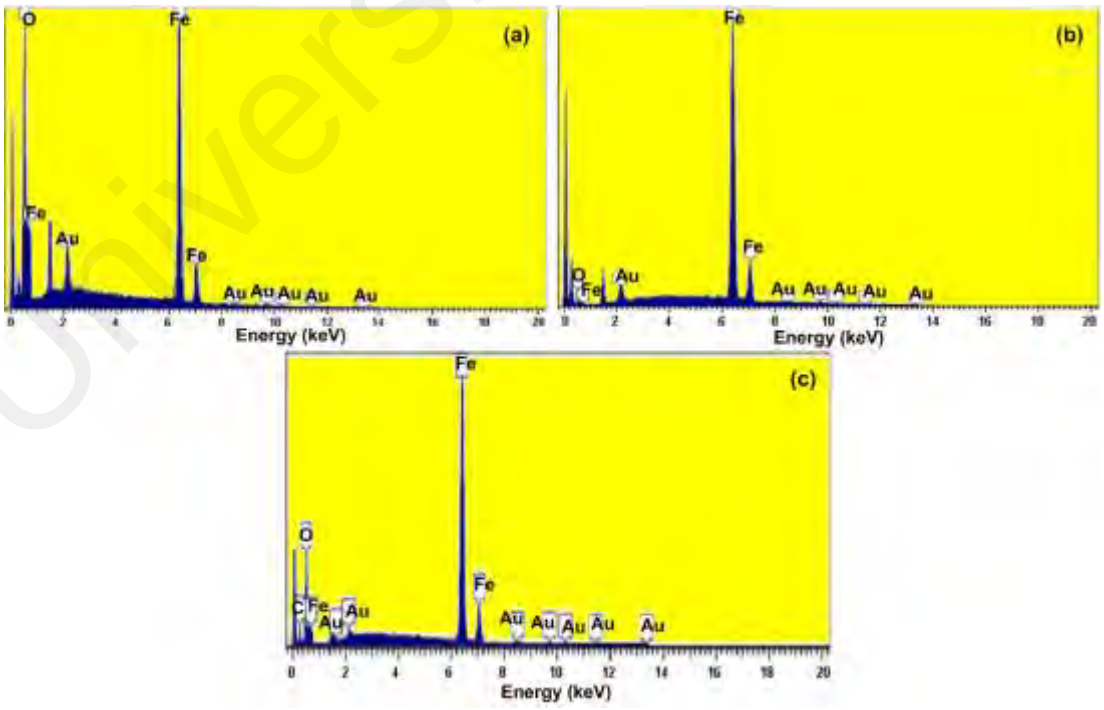

Figure 4.15: Energy-dispersive X-ray spectroscopy of Fe_3O_4-Au NPs with different molar ratios [1:1, 2:1, and 3:1 (a-c)] respectively.

4.4.4 Vibrating Sample Magnetometer

Figure 4.16 shows the magnetic properties of the Fe_3O_4 NPs and Fe_3O_4-Au NPs examined from a vibrating sample magnetometer (VSM). The hysteresis loop of the uncoated and gold-coated Fe_3O_4 NPs was measured with a magnetic field between −8 kOe and 8 kOe at room temperature. All samples display similar coercivity and remanence, indicating the retention of the superparamagnetism behavior of Fe_3O_4 NPs even after the shell formation (Z. Li et al., 2005). As shown in the magnetization curve, the saturation magnetization for the Fe_3O_4 NPs (a) and Fe_3O_4-Au NPs (b-d) are estimated as 23.78, 19.91, 18.90, and 16.98 emu g^{-1}, respectively. The decrease of saturated magnetization in the Fe_3O_4-Au NPs could be due to the presence of a non-magnetic gold layer.

In core-shell nanoparticles, core, where the magnetic moments are aligned, and shell, where the magnetic moments are in a disorder structure. Nonalignment of the spins from the surface of the nanoparticles is reflected in the reduction of the saturation magnetization of the nanoparticles, as compared to that of the corresponding bulk material, the effect being more strong when the nanoparticles are smaller (a few nm) (Caizer, 2015).

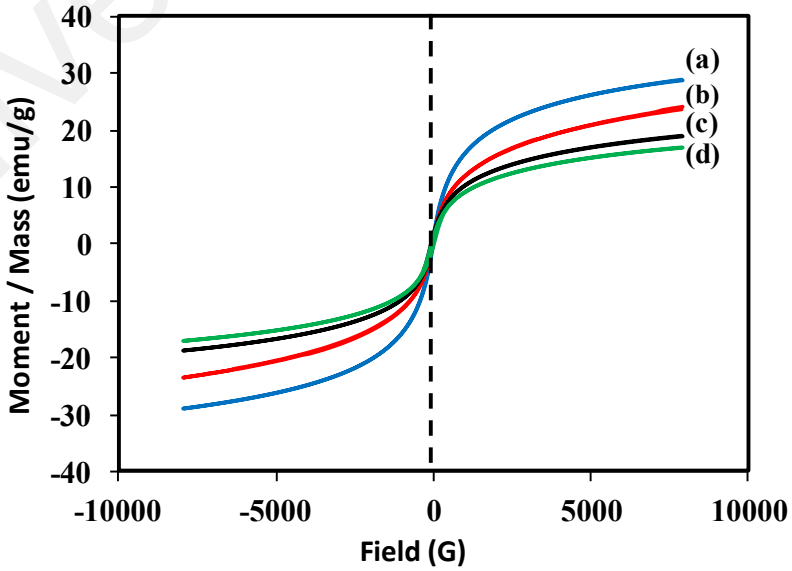

Figure 4.16: VSM of Fe_3O_4 NPs (a) and Fe_3O_4-Au NPs with different molar ratio [3:1, 2:1, and 1:1(b–d)] respectively.

4.4.5 Fourier Transformed Infrared Spectroscopy Study

Fourier transformed infrared spectroscopy (FT-IR) was performed to determine the biomolecules which stabilize and cover the synthesized Fe_3O_4-Au NPs. The FT-IR spectrum in Figure 4.17 shows a high absorption band at 564.99 cm^{-1} which is attributed to the Fe–O bond, which demonstrates a high level of crystallinity of the Fe_3O_4 NPs (Karaoğlu et al., 2011). The Fe_3O_4-Au NPs spectrum shows two absorption peaks, a medium intensity band at 2917 cm^{-1} and a weak band at 2839 cm^{-1}, are attributed to the stretching vibration of the C-H group. The characteristic band at around 3200 cm^{-1} is due to the presence of the O-H group (Xiaolang Chen et al., 2011). The C–O stretching band of protein in honey arises from the C–O–C symmetric stretching and C–O–H bending vibrations, expected to occur around 1073 cm^{-1} (S. Li et al., 2007). The amide I and II bands of proteins occur around 1597 and 1342 cm^{-1}, from the carboxyl stretching and N–H deformation vibrations in the amide linkages of protein. Proteins can be attached to the Fe_3O_4-Au NPs surface via the free amine group or carboxylate ion of the amino acid residues(V. Kumar et al., 2020; Patra et al., 2020; J. Singh et al., 2018). The lack of C = O band is due to the stretching mode, the presence of the C–O stretch, and the amide I and II bands in the FT-IR spectrum of Fe_3O_4-Au NPs which stabilize the system via the –COO− (carboxylate ion) groups from the remnant amino acids.

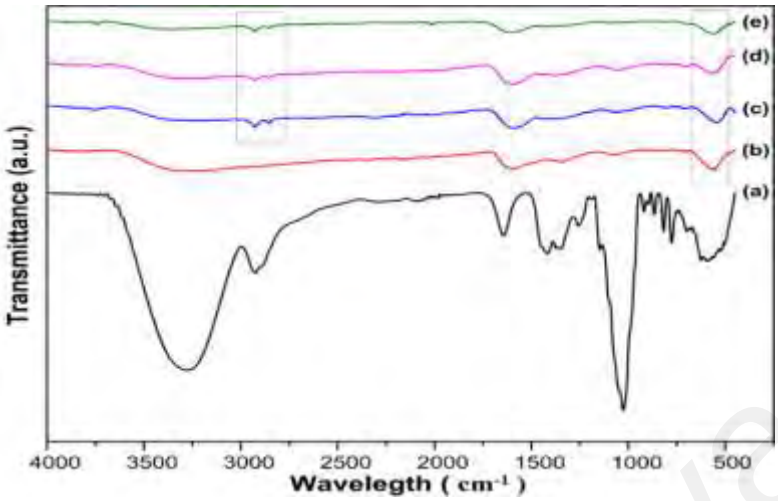

Figure 4.17: Fourier transformed infrared spectra of honey (a), Fe_3O_4 NPs (b), Fe_3O_4-Au NPs with different molar ratio [3:1, 2:1 & 1:1 (c-e)], respectively.

4.4.6 In Vitro Cytotoxicity Assay of Fe_3O_4 NPs

As shown in Figure 4.18, the synthesized Fe_3O_4-Au NPs are found non-toxic to the cells in higher concentration until 140.0 ppm which are used in biological applications, are well tolerated by the WEHI164 cells in the MTT assay.

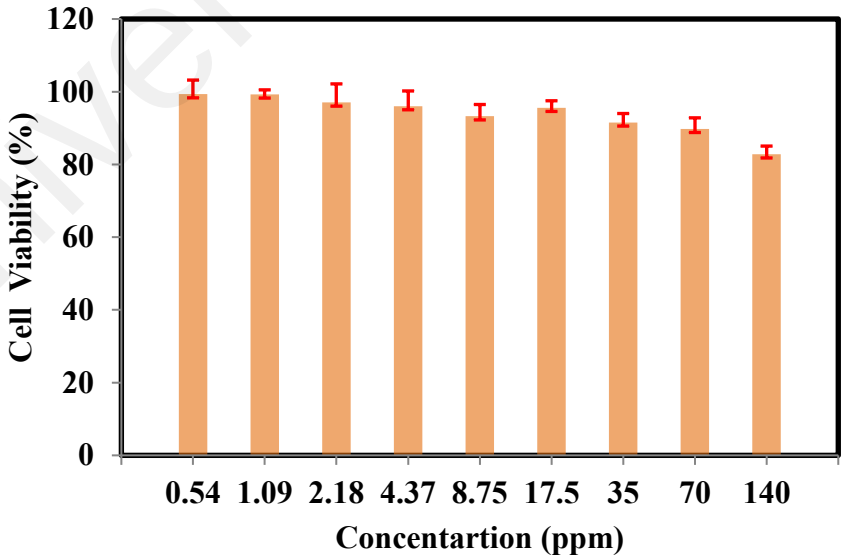

Figure 4.18: Cell viability of WEHI164 cells measured by the MTT assay (cells were incubated for 24 hours with the indicated concentrations of the Fe_3O_4-Au NPs).

Part 3: A novel electrochemical sensor based on Core-Shell Fe_3O_4-Au NPs signal amplification for the detection of dopamine

4.5 Electrochemical characterization of modified GC electrode

The electrocatalytic performance of the bare GC and Fe_3O_4-Au-GC electrodes was studied by CV. Figure 4.19 displays the CV current responses of the GC and Fe_3O_4-Au-GC in 0.1 M PBS (pH 7.0) containing 100 μM of DA at a scan rate of 50 mVs^{-1}. Compared with the bare GC electrode, the Fe_3O_4-Au-GC electrode strongly enhances the redox peak currents of dopamine. The notable increase in the redox peak currents of DA at the Fe_3O_4-Au-GC electrode can be attributed to the synergy between the Fe_3O_4 support and gold nanoparticles which increases the conductive area of the electrode surface. The presence of gold in the fabricated Fe_3O_4-Au-GCE is the ideal support material for DA adsorption and shuttles the electron between GCE and DA, as a result, the speed of electron transfer increases. As can be seen from Fig. 4.19, the CVs show an almost ideal reversible electron transfer processes (Nernstian) (O'Halloran, Pravda, & Guilbault, 2001). To understand the detecting mechanism engaged in the process, the electrochemical behavior of dopamine at the Fe_3O_4-Au-GCE was studied. When the applied potential is ramped between −0.3 V and 0.8 V, DA is electrochemically oxidized to form dopamine quinone (DAQ) from the exchange of two protons and two electrons. Then, these electrons are transferred to the GC electrode to produce faradaic current (Barnes, O'Mahony, Aldous, Hardacre, & Compton, 2010; D.-Q. Huang et al., 2012).

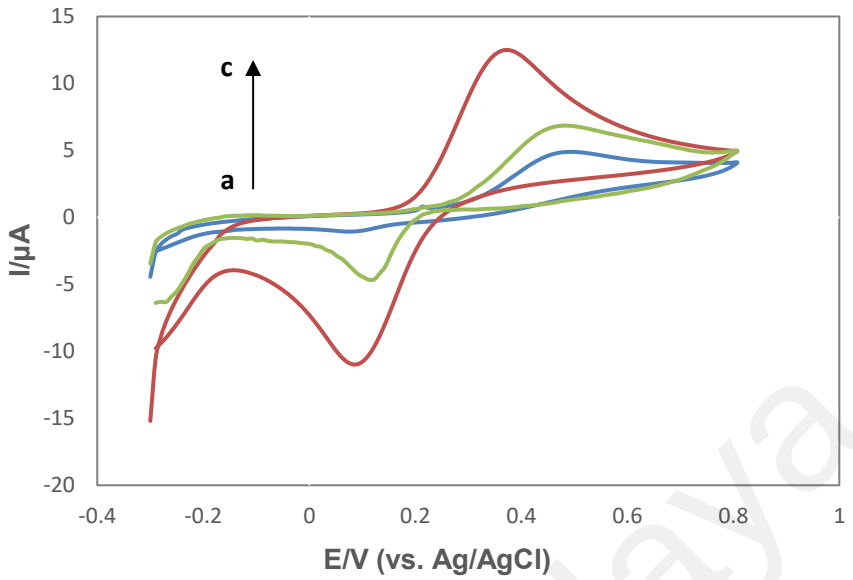

Figure 4.19: The cyclic voltammograms (CVs) of: (a) Bare GCE, b) Fe_3O_4-GCE and c) Fe_3O_4-Au-GCE in 0.1 M phosphate buffer solution (pH7.4) and 100 µM of DA.

Fig. 4.20a displays the effect of CV scan rates on the redox peak currents of 100 µM DA at Fe_3O_4-Au-GCE in 0.1 M PBS (pH 7.4). As can be seen in Fig. 4.20, the linear increase of the redox peak currents with the scan rate shows that the electrode reaction of the immobilized Fe_3O_4-Au is a surface-confined electrochemical process. The linear regression equation can be expressed as Ipa = 0.1059 (mV s^{-1}) + 6.3732 (R2 = 0.9463) and Ipc = -0.1356 (mV s^{-1}) − 2.8831 (R2 = 0.9204) (Figure 4.20b).

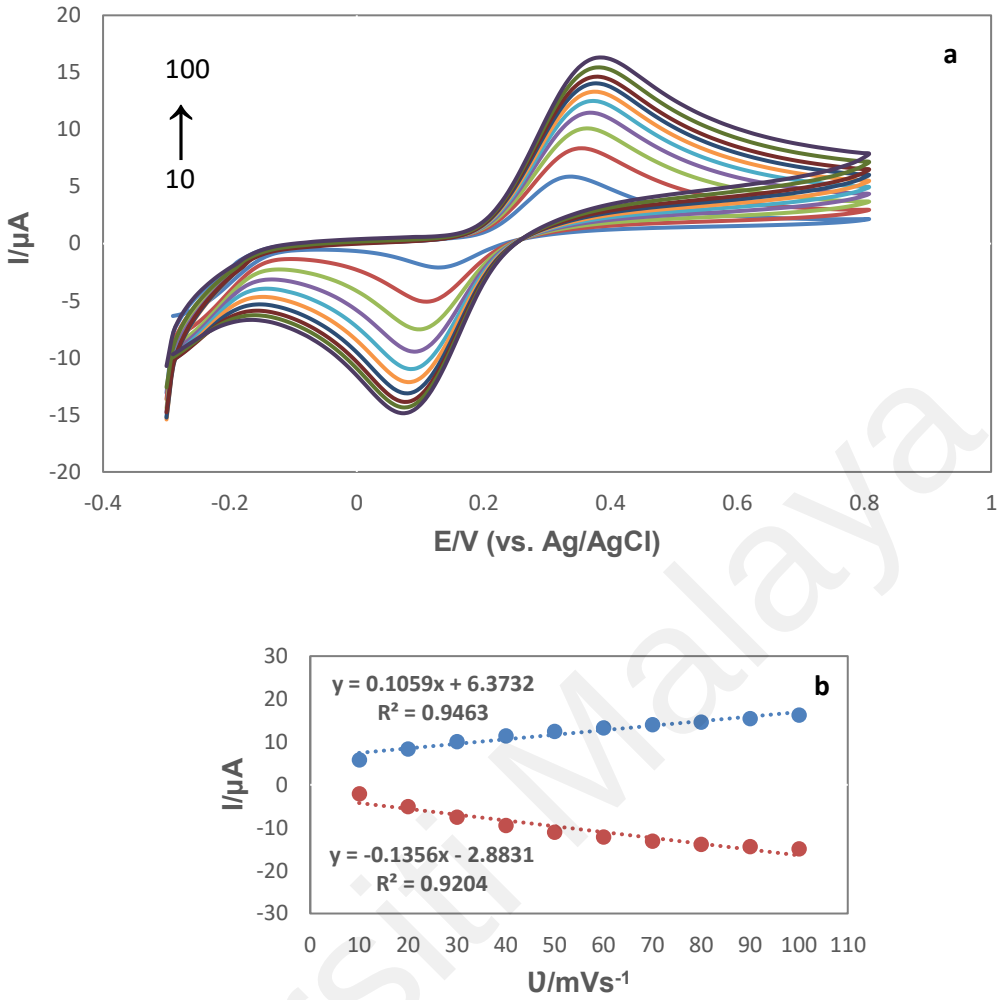

Figure 4.20: (a) The effect of scan rate on the peak current. (b) Plot of anodic peak current (µA) vs scan rate (mV s^{-1}): 10, 20, 30, 40, 50, 60, 70, 80, 90, 100 in 0.1 M phosphate buffer solution (pH7.4).

4.6 Electrochemical measurements of the sensor

4.6.1 Effect of PBS pH

The pH effect on the electrochemical response of the Fe_3O_4-Au-GCE upon the addition of 100 µM DA was studied using CVs. The change in the peak current with pH (pH range of 3−8) is shown in Figure 4.21. It can be observed that the anodic peak current increases with increasing pH until pH 6. Smaller currents are noticed when the pH of the solution was either

lower or higher than 6. However, the buffering at pH 7 shows the lower peak current compared to pH 6, nevertheless pH 7.4 was selected for the next experiments as it was close to the physiological pH.

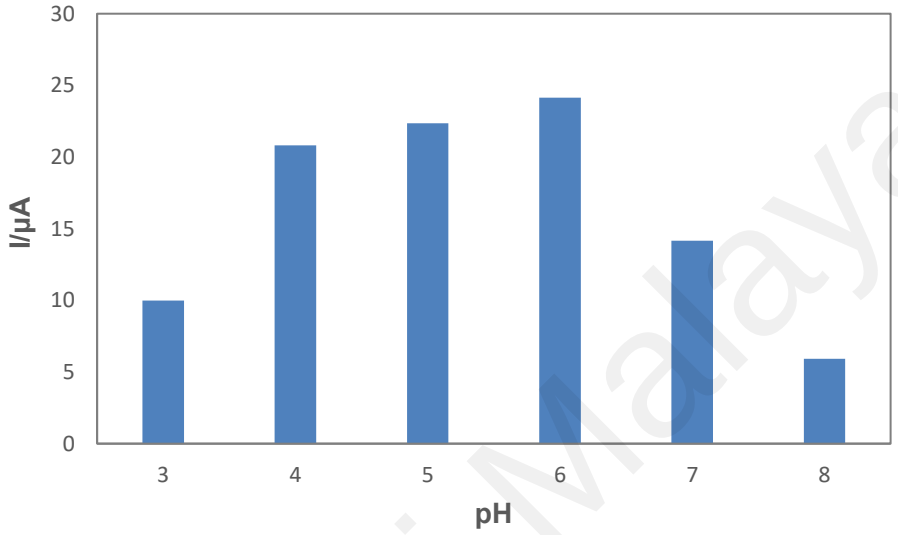

Figure 4.21: The effect of the pH of the PBS on the peak current, using 0.1 M phosphate buffer solution and 100 µM of DA in this research (n=3) at pH 3, 4, 5, 6, 7 and 8.

4.6.2 Sensitivity studies

To affirm the oxidation behavior of DA, amperometric responses of the Fe_3O_4-Au-GCE to successive DA concentration changes was investigated with DPV in 0.1 M phosphate buffer solution at pH 7.4. Figure 4.22a displays the dependence of the anodic peak current (Ipa) on the DA concentration. A continuous increase in the oxidation peak current was observed when the DA concentration was increased from 0.2 µM to 200 µM. The sensor was calibrated three times, and the standard deviations were calculated. The calibration curve for the Fe_3O_4-Au-GCE shows a linear segment from 0.2 to 200 µM with a linear regression equation of Ipa = 0.1226 (µA μM^{-1} cm^{-2}) - 0.9013 (R2 = 0.9897) (Figure 4.22b). The limit

of detection (LOD) and the limit of quantification (LOQ) of the Fe_3O_4-Au/GCE was calculated from the following equations (Lian et al., 2009):

$$LOD = 3S_B/b \qquad \text{(Eq. 4.2)}$$

$$LOQ = 10S_B/b \qquad \text{(Eq. 4.3)}$$

where S_B is the standard deviation of the blank solution and b is the slope of the analytical curve, as shown in Figure 4.22b. The calculated limit of detection (S/N = 3) and limit of quantification (S/N = 10) for the linear segment (0.2−200 µM of dopamine) are 0.041 and 0.139 µM, respectively. Also, the sensitivity for this linear segment is 0.1226 µA µM $^{-1}$ cm^{-2}.

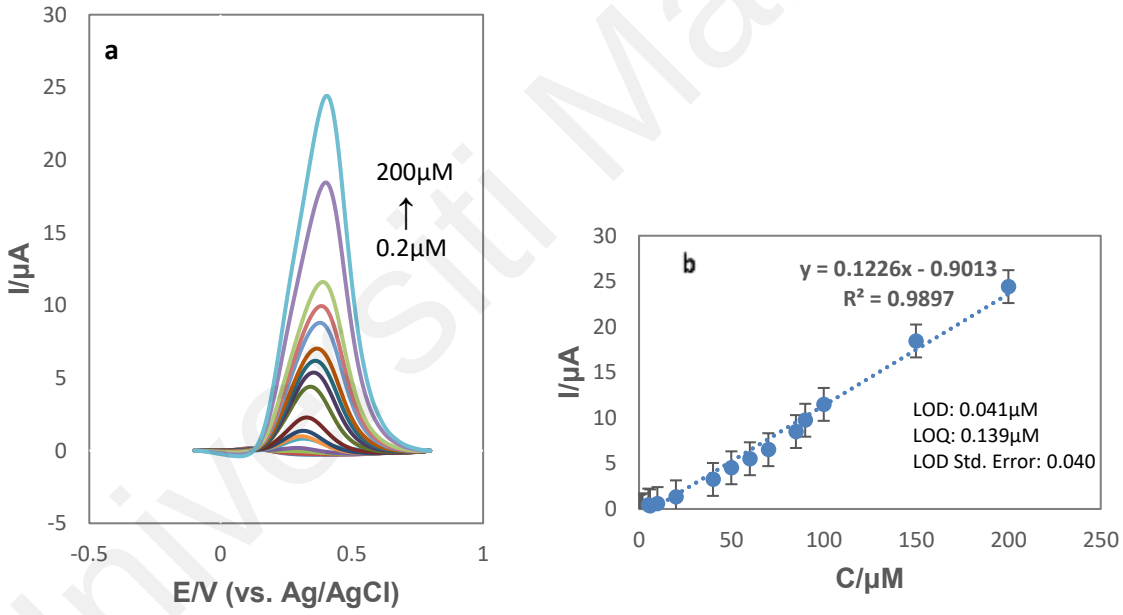

Figure 4.22: (a) DPV curves for different concentrations of DA in 0.1 M phosphate buffer solution (0.2, 1, 2, 5, 6, 10, 20, 40, 50,60, 70, 85, 90, 100, 150, and 200 µM, at pH 7.4 (b) Calibration curve at concentration range.

4.6.3 Selectivity and Stability studies

The selectivity and long-term stability are crucial factors for evaluating the sensing performance of the Fe_3O_4-Au-GCE. Ascorbic acid (AA) and uric acid (UA) are coexisting

interfering compounds with DA in human body fluids. Therefore, the selectivity of the Fe_3O_4-Au-GCE to DA was also studied by measuring the amperometric current-time response in the presence of different kinds of interfering compounds containing 50 µM of AA, UA, $NaSO_3$, $MgSO_4$, KCl, and glucose. When compared to the amperometric current response of the Fe_3O_4-Au-GCE in 5 and 3 µM DA in 0.1 M PBS solution (pH 7.4), the results in Fig. 4.23 didn't show any significant interference approving that the developed electrode exhibited good selectivity towards the detection of DA.

Furthermore, the stability of the Fe_3O_4-Au-GCE sensor is also a vital parameter that needs to be measured. It should be mentioned that the sensor was stored in PBS at 4 °C. The performance of the modified electrode was studied every seven days and the sensor retains approximately 96 % of initial response after two weeks, but decreased to approximately 84% after 4 weeks (I_0 and I are the current response of the fresh sensor and the current response after storage respectively). Therefore, the Fe_3O_4-Au-GCE sensor displayed good selectivity and stability for the electrocatalytic oxidation of DA. Moreover, the electrochemical activity of the fabricated sensor is comparable to other electrode materials for the detection of DA, as presented in Table 4.2.

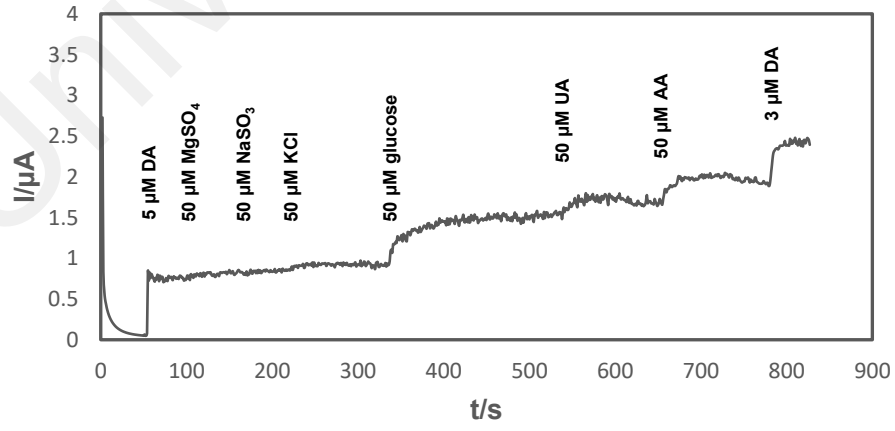

Figure 4.23: Amperometric response of successive additions of 5 & 3 µM DA and 50 µM $MgSO_4$, $NaSO_3$, KCl, glucose, AA, UA in a phosphate buffer solution (pH 7.4)

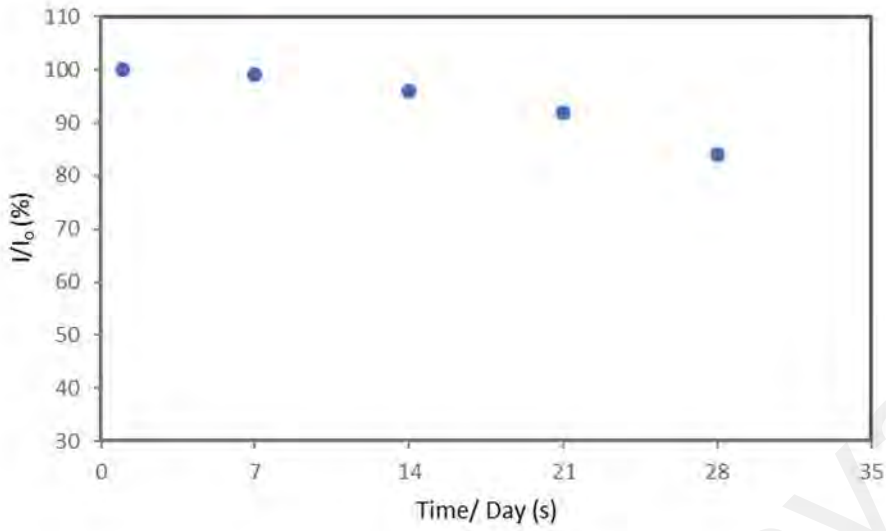

Figure 4.24: Stability studies of Fe_3O_4-Au-GCE.

Table 4.2: Summary and a comparison of the present work with previous reports in the literature regarding the performance of DA assays.

Electrode	Analytical technique	LOD (nM)	Reference
Nanostructured Au	Amperometry	26	(Hsu, Chen, Lee, & Chiu, 2012)
AuNPs@MIPs/Au	Amperometry	7.8	(Xue et al., 2013)
(patternable gold (Au) nanowire (NW)) NW/ glass	amperometry	400	(Tyagi et al., 2009)
Au@Fe3O4/GCE	Amperometry	2.7	(Thamilselvan, Manivel, Rajagopal, Nesakumar, & Suryanarayanan, 2019)
AuNPs/OPPy/ZnO	SWV	10	(Lin, 2015)
Au/RGO/GCE	DPV	1400	(C. Wang et al., 2014)
Au@Pd-RGO/GCE	DPV	24	(J. Jiang & Du, 2014)
AuNPs@MoS2/GCE	DPV	50	(H. Sun et al., 2014)
AuNPs@SiO2-MIPS/GCE	DPV	20	(D. Yu, Zeng, Qi, Zhou, & Shi, 2012)
PAMAM -AuNPs/RGO/GCE	DPV	20	(S. Liu et al., 2012)
RGO-AuNPs-CSHMs/GCE	DPV	300	(Xue Liu, Xie, & Li, 2012)
Au/ERGO/GCE	DPV	40	(S.-J. Li, Deng, Shi, & Liu, 2012)
ITO/(P2W16V2-AuPd/PEI)8	DPV	217	(C. Zhou, Li, Zhu, Pang, & Ma, 2013)
Au@Fe3O4/GCE	DPV	32	This work

4.6.4 Analysis of Real Samples

Analysis of Real Samples. The practical feasibility of the sensor has been evaluated in pharmaceutical samples. A commercially available dopamine hydrochloride injection of 4.22 mM concentration was acquired. The concentration of the injection sample was diluted to the final concentrations of 2, 40, and 90 μM by using 0.1 M phosphate buffer (pH 7.4). The recovery was obtained by using DPV to evaluate the accuracy of the method. On the basis of the replicates (n = 6), the relative standard deviation (RSD) of this method is presented in Table 4.3. The satisfactory recoveries of DA at the Fe_3O_4-Au-GCE in the range of 0.2−200 μM demonstrate the efficiency and reliability of this method.

Table 4.3: Detection of DA Concentration in Test Samples (Results Based on Six Replicate Determinations Per Sample)

Sample	Added/ μmol.l^{-1}	Found/ μmol l^{-1}	(RSD%) (n=6)	(Recovery%)
1	2	1.9060	0.1033	95.30
2	40	40.1252	2.7876	100.31
3	90	89.3917	1.4415	99.32

Part 4: Electrochemical sensing of HPV by Core-Shell Fe_3O_4-Au NPs

4.7 Electrochemical characterization of modified SPC electrode

The changes in electrochemical performance of the SPCE fabrication process were observed at each step by CV technique using potassium ferricyanide solution. Potassium ferricyanide $[Fe(CN)_6]^{3-/4-}$ is a good redox probe to validate the electron transfer behavior on the electrode surface during the fabrication process (A Benvidi et al., 2015; Peik-See, Pandikumar, Nay-Ming, Hong-Ngee, & Sulaiman, 2014). This is due to the $[Fe(CN)_6]^{3-/4-}$ ion which reveals good reversibility and fast electrochemical responses as stated in previous literature (Ahammad et al., 2011; Lyons & Keeley, 2006; Nascimento et al., 2011; Radhi, Al-Mulla, & Tan, 2014; Takahashi, Watahiki, Tomida, Wang, & Anzai, 2013; H.-B. Wang et al., 2014).

In this study, $[Fe(CN)_6]^{3-/4-}$ is used as the redox indicator based on the electrostatic repulsion principle where the current response of $[Fe(CN)_6]^{3-/4-}$ is higher at the bare electrode (without the presence of DNA strands) and become lower after hybridization (N.-y. Wu et al., 2013). This is attributed to the larger electrostatic repellence between the negatively charged phosphate in the DNA strands and the $[Fe(CN)_6]^{3-/4-}$ (N.-y. Wu et al., 2013).

Figure 4.25 shows the CV responses at the fabricated electrode in 1.0 mM $[Fe(CN)_6]^{3-/4-}$ and 50 mM Tris-HCl (pH 7.6) in the potential range of −0.5 V to 0.5 V at a scan rate of 100 mV/s. The bare SPCE showed a pair of well-defined redox peak due to the oxidation and reduction process of the $[Fe(CN)_6]^{3-/4-}$ (curve b).

The redox peak current (anodic and cathodic) are significantly improved after the modification of SPCE with Fe_3O_4-Au NPs due to the large surface area of NPs that enhances active surface area (curve a). However, a small peak-to-peak separation (anodic peak current potential–cathodic peak current potential) of the Fe_3O_4-AuNPs-SPCE confirms the role of AuNPs in improving the reversibility.

A significant decrease in redox peak current is detected when Fe_3O_4-AuNPs-SPCE is immobilized with thiolated ssDNA (DNA probe) (curve c). This is due to the introduction of the negative charge phosphate backbone of ssDNA which caused in the repulsion of the $[Fe(CN)_6^{3-/4-}]$ ion to the surface of modified electrodes (C. Wang et al., 2013) and indicates that the probe DNA was successfully immobilized on the Fe_3O_4-AuNPs-SPCE surface.

After the hybridization of the DNA target to the immobilized thiolated DNA probe, an additional decrease in the redox peak current is observed due to the greater electrostatic repulsion force between the $[Fe(CN)_6^{3-/4-}]$ ion and the hybridized DNA/Fe_3O_4-AuNPs-SPCE (curve d). In addition, the formation of hybridized DNA between the ssDNA probe and its complementary DNA could probably block the penetration of the $[Fe(CN)_6]^{3-/4-}$ ion to the surface of the modified electrode therefore lead to the suppression of the redox peak currents. The overall explanation indicates that the complementary DNA was successfully hybridized on the probe DNA immobilized on the Fe_3O_4-AuNPs-SPCE.

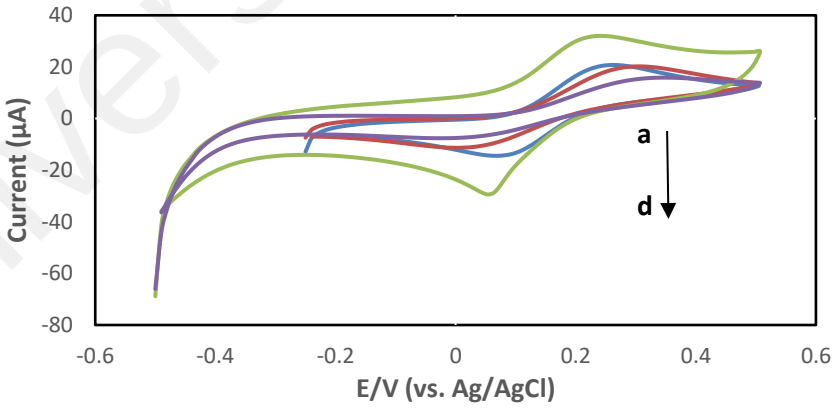

Figure 4.25: Cyclic voltammetry (CV) response at different modified SPCE; a) Fe_3O_4-AuNPs-SPCE; b) Bare SPCE; c) ssDNA/Fe_3O_4-AuNPs-SPCE d) Hybridized DNA/Fe_3O_4-AuNPs-SPCE; in 1.0 mM $[Fe(CN)_6]^{3-/4-}$ solution containing supporting electrolyte (0.1 M KCl), 50 mM Tris-HCl, NaCl 0.02 M, pH 7.5

The CVs for modified Fe_3O_4-Au-SPCE was investigated by varying the scan rate. The experiments were done using CV method in 1 mM $[Fe(CN)_6]^{3-/4-}$ containing 0.1 M KCl

solution at different scan rates (10 mV s^{-1} -300 mV s^{-1}) as shown in Figure 4.26 a. At higher scan rates, there is a slight shift of the anodic potential towards a positive direction while the cathodic potential shifts to the negative region. Figure 4.26 b shows that all anodic peak currents (I_{pa}) of $[Fe(CN)_6]^{3-/4-}$ shows a linear increase with the square root of scan rate in 1 mM $[Fe(CN)_6]^{3-/4-}$ which proposes that the electrochemical reaction of $[Fe(CN)_6]^{3-/4-}$ is controlled by a diffusion process (Dai Tran, Nguyen, Van Hieu, et al., 2011; Nascimento et al., 2011). This finding reveals that the modification of bare SPCE with Fe_3O_4-Au-NPs shows good electrochemical properties, which are the advantages in DNA signal detection.

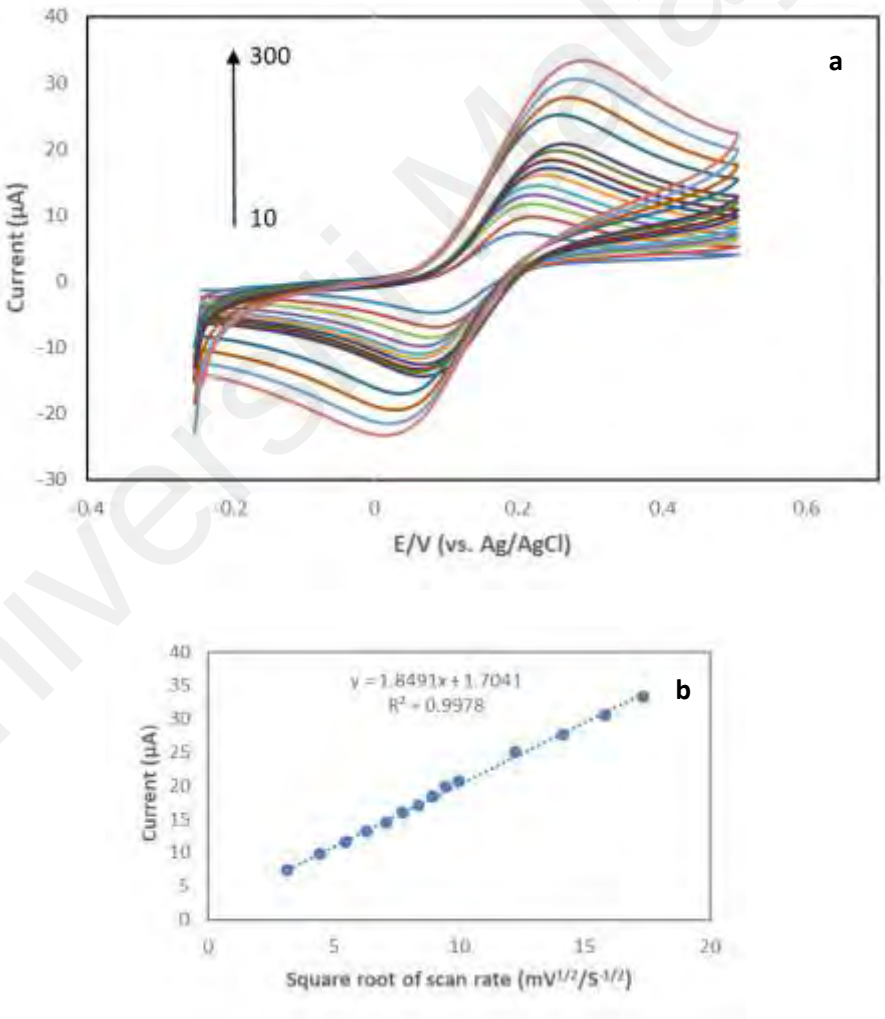

Figure 4.26: CV responses of a) Fe_3O_4-AuNPs-SPCE in 1.0 mM $[Fe(CN)_6]^{3-/4-}$ solution containing supporting electrolyte (0.1 M KCl), at pH 7.5, at different scan rates (10 mV-300 mV), b) The plot of oxidation peak current of $Fe(CN)_6]^{3-/4-}$ for Fe_3O_4-AuNPs-SPCE against square roots of scan rate.

4.8 Electrochemical measurements of the biosensor

4.8.1 Effect of DNA probe concentration

The immobilization of DNA probe (ssDNA) on the working electrode surface is a very important stage in the DNA electrochemical sensor construction, as this influences the DNA probe characterization, hybridization signal, sensitivity and sensor performance (F. Li, Chen, & Zhang, 2008). A suitable amount of DNA probe loaded on the electrode surface is greatly important to improve the DNA hybridization events, simultaneously avoids the steric hindrance and repulsive electrostatic interaction between the DNA probe and the target DNA (Bettazzi et al., 2008; Glazer, Fidanza, McGall, & Frank, 2001).

The loading of a high amount of probe DNA on the modified Fe_3O_4-AuNPs-SPCE is possible due to the high surface area and could provide better resolution than the bare electrode.

Figure 4.27 displays that the peak current of the fabricated electrode decreases linearly when the DNA probe concentration increases from 1 μM to 5 μM. It can be expected that at 5 μM of DNA probe concentration, the electrode surface is completely saturated with the available binding sites of Fe_3O_4-Au NPs on the fabricated electrode surface. From Figure 4.27, a slight increase in the peak current of the fabricated electrode is observed when the DNA probe concentration is above 5.0 μM. A larger amount of immobilized DNA probe on the fabricated electrode surface will cause difficulties in the binding of the target DNA to the DNA probe which slightly blocks the hybridization process. Thus, there is a smaller hybridization event on the DNA probe surface at higher concentrations, hence the current response does not decrease further. Therefore, the effective range of DNA probe concentration for Fe_3O_4-AuNPs-SPCE is 5 μM.

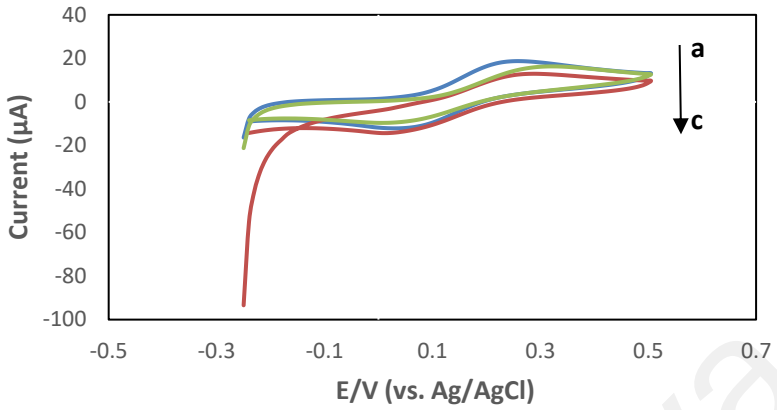

Figure 4.27: Cyclic voltammetry (CV) response at different DNA Probe concentration; a) 1 µM; b) 10 µM; c) 5 µM Hybridized with1 µM target DNA; in 1.0 mM $[Fe(CN)_6]^{3-/4-}$ solution containing supporting electrolyte (0.1 M KCl), 50 mM Tris-HCl, NaCl 0.02 M, pH 7.5

4.8.2 Sensitivity studies

With the optimized probe DNA concentration, the sensitivity of the Fe_3O_4-Au-SPCE DNA sensor was evaluated by the hybridization of probe DNA with varied concentrations ranging of complementary DNA target from 0.0001 nM to 1000 nM using DPV (Figure 4.28a). As seen from the figure, the peak current of Fe_3O_4-Au-SPCE is reduced linearly with the increase in the concentration of the synthetic complementary target until 1000 nM, indicating a larger duplex structure formation on the electrode surface (Zheng et al., 2014).

Figure 4.28a and 4.28b conclude that the developed DNA sensor (Fe_3O_4-Au-SPCE) can detect 0.0001 nM (100 fM) of human papillomavirus complementary oligonucleotide as the lowest concentration. The peak current values vary linearly with different complementary DNA concentration which obeys a linear regression equation of Ipa = -2.4006 (µA μM^{-1} cm^{-2}) + 22.787 with a regression coefficient of 0.9669 (Figure 4.28b).

Table 2.5 shows an evaluation of the linear range and detection limit of a different DNA sensors for HPV detection. The fabricated DNA sensor shows acceptable sensitivity compared to another previously developed DNA sensor in HPV detection.

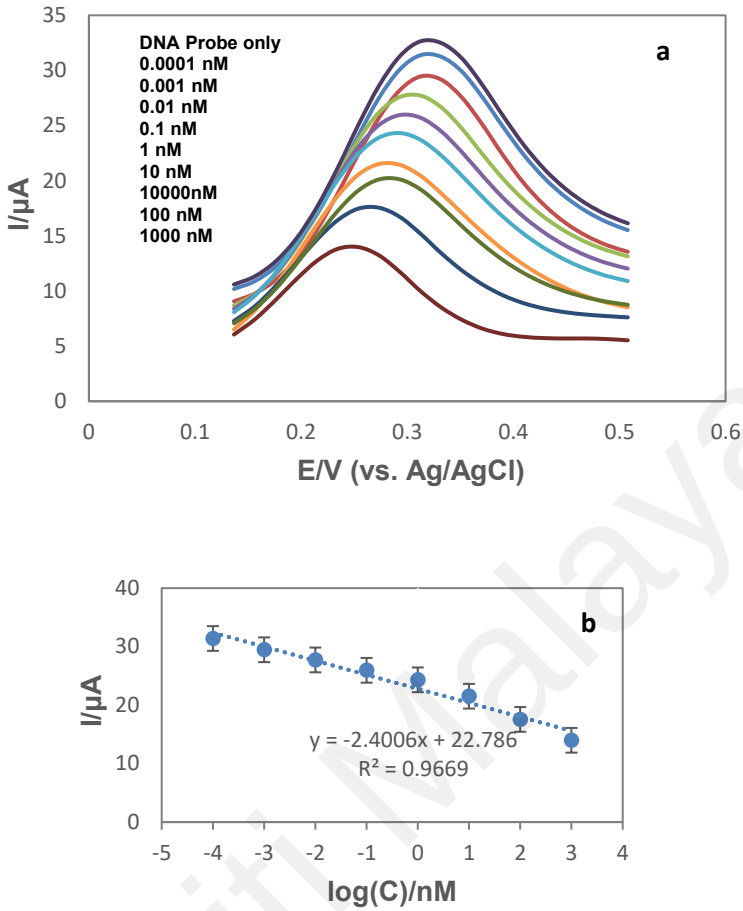

Figure 4.28: a) DPV response of Fe_3O_4-AuNPs-SPCE at different concentration of target DNA; b) calibration curve of Fe_3O_4-AuNPs-SPCE

4.8.3 Selectivity studies

The selectivity studies for the fabricated DNA sensors (Fe_3O_4-Au-SPCE) are considered via the hybridization of DNA probe ssDNA/Fe_3O_4-Au-SPCE with different types of synthetic DNA target sequences such as non-complementary, single-base mismatch, three-base mismatch and complementary DNA sequences at the concentration of 10 nM (Figure 4.29). Figure 4.29 shows that the peak current of non-complementary sequences (Figure 4.29b) is almost equal to the current of the background signal using the DNA probe (Figure 4.29a) without the DNA hybridization. Figure 4.29 shows the decrease of peak current upon the hybridization of three base mismatch sequences (Figure 4.29c), single-base mismatch

(Figure 4.29d) and complementary DNA target (Figure 4.29 e), due to creation of more duplex on the electrode surface.

Generally, the peak current of the fabricated DNA increases after hybridization in the order of DNA probe: without the target > non-complementary DNA > three bases-Mismatch > one base-mismatch > complementary sequences. This outcome concludes that the newly developed DNA sensor shows good selectivity, which was able to differentiate between complementary, three base-mismatch, and non-complementary sequences detection.

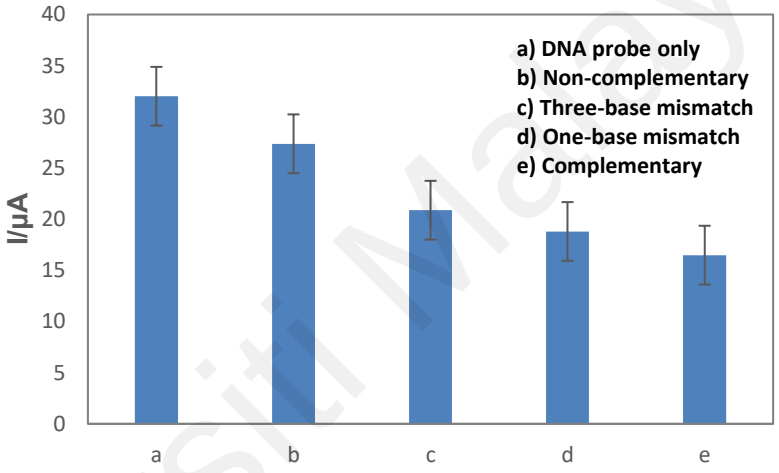

Figure 4.29: Selectivity studies of Fe_3O_4-AuNPs-SPCE in 1.0 mM $[Fe(CN)_6]^{3-/4-}$ a solution containing supporting electrolyte (0.1 M KCl), pH 7.5, scan rates 100 mV s^{-1}.

CHAPTER 5: CONCLUSION AND FUTURE WORK

Fe_3O_4 NPs and core-shell Fe_3O_4-Au NPs have been successfully synthesized using natural honey with green synthesis methods. It was also found that honey works as a reducing and stabilizer agent in producing NPs. The most possible co-reducing agent is fructose and the presence of proteins in natural honey as the capping agent is responsible for the stabilization. The particle size of the synthesized material can be controlled with the change in the concentration of the natural honey.

A series of characterization technique including FESEM, EDX, TEM, SAED, XRD, UV-Vis spectroscopy, FTIR spectroscopy, VSM, and cytotoxicity assay have been accomplish to investigate the surface morphology, chemical composition, functional groups, magnetic properties and toxicity of both Fe_3O_4 NPs and core-shell Fe_3O_4-Au NPs. The TEM images of Fe_3O_4 NPs showed that the particle size decreases from 3.21 to 2.22 nm with the increase in the amount of honey from 0.5% to 3.0% (w/v), respectively. The TEM images of core-shell Fe_3O_4-Au NPs show that the particle size increases from 3.21 to 4.11 nm in the Fe_3O_4 NPs and Fe_3O_4-Au NPs (with a molar ratio of 1:1), respectively. The VSM results reveal a superparamagnetic behavior of both Fe_3O_4 NPs and Fe_3O_4-Au NPs, with a decrease in saturation magnetization from 23.78 emu g^{-1} for Fe_3O_4 NPs to 16.98 emu g^{-1} for Fe_3O_4-Au NPs (with a ratio of 1:1), which is attributed to the formation of the gold shell. The FESEM images demonstrated that the surface morphology of synthesized NPs is spherical in appearance, which increases the surface area and provides an ideal situation for DNA probe immobilization and hybridization process in the HPV sensor and also for dopamine sensor. The presence of gold by EDX spectrum, SAED, and UV-Vis spectrum indicate the successful incorporation of gold shell on the surface of Fe_3O_4-NPs.

In this work, the core-shell Fe_3O_4-Au NPs were modified onto GCE and SPCE electrodes for the electrochemical detection of dopamine and human papillomavirus, respectively. At the first stage, both electrodes are modified via the chemical modification process, Fe_3O_4-AuNPs-GCE and Fe_3O_4-AuNPs-SPCE. The CV analysis confirmed that both fabricated electrodes, Fe_3O_4-Au-GCE, and Fe_3O_4-AuNPs-SPCE exhibited good electron transfer properties. In fact, the modification of the bare electrodes with core-Shell Fe_3O_4-Au NPs improves the electron transfer properties and the conductivity compared to the bare electrodes.

The enhanced electrocatalytic performance of Fe_3O_4-AuNPs-GCE modified electrode compared to the bare electrode is due to the larger surface area and high conductivity, as well as the fast electron transfer rate by the Fe_3O_4-AuNPs, confirming the important role of NPs. This modified electrode was stable enough in the electrochemical measurements and showed good sensitivity and selectivity towards dopamine detection. There were no significant changes in the current response in the detection of 5 and 3 μM dopamine in the presence of interfering compounds such as AA, UA, $NaSO_3$, $MgSO_4$, KCl, and glucose. The Fe_3O_4-AuNPs gave good dopamine sensing performance with a low detection limit of 0.0321 μM and excellent sensitivity value of 0.1186 μA μM^{-1} cm^{-2} with a linear concentration range of 0.2−200 μM.

A 14-base thiolated DNA probe was immobilized onto the fabricated Fe_3O_4-AuNPs-SPCE surface to allow the hybridization with its complementary 14-base DNA target (pure synthetic oligonucleotide). Using $[Fe(CN)_6]^{3-/4-}$ as the redox indicator, the fabricated electrode was able to discriminate the redox $[Fe(CN)_6]^{3-/4-}$ current signal with and without the presence of its complementary DNA target. A significant reduction in the $[Fe(CN)_6]^{3-/4-}$

current signal is detected for the fabricated electrode after the hybridization with the complementary DNA target. This result assumes that a larger amount of $[Fe(CN)_6]^{3-/4-}$ was accumulated on the surface of the DNA probe (ssDNA) compared to the hybridize DNA (dsDNA) as $[Fe(CN)_6]^{3-/4-}$ exhibits strong attraction to the free guanine bases in the ssDNA sequences. In the following work, the focus towards the optimization improves the performance of the developed DNA electrochemical sensor (Fe_3O_4-AuNPs-SPCE). The enhancement of DNA probe loading onto the fabricated electrode was an important stage in this study, where the OFAT approach was employed. The OFAT method was used to find the effective range of the tested parameters. In this study, the amount of immobilized DNA probe is directly associated to the available surface area of the fabricated Fe_3O_4-AuNPs-SPCE. A larger amount of DNA probe immobilized onto the fabricated electrode surface leads to the larger decrease in the peak current until the optimum amount of immobilized DNA on the surface of the electrode is reached.

Based on this study, future developments should focus on the further applications of these nanoparticles for other diagnostic purposes. The conjugation of prepared core-shell nanoparticles with electrochemical sensing systems enhances the performance in the electro-analysis method.

REFERENCES

Abi, A., & Ferapontova, E. E. (2012). Unmediated by DNA electron transfer in redox-labeled DNA duplexes end-tethered to gold electrodes. *Journal of the American Chemical Society, 134*(35), 14499-14507.

Abreu, A. L., Souza, R. P., Gimenes, F., & Consolaro, M. E. (2012a). A review of methods for detect human Papillomavirus infection. *Virology journal, 9*(1), 262.

Abreu, A. L., Souza, R. P., Gimenes, F., & Consolaro, M. E. (2012b). A review of methods for detect human Papillomavirus infection. *Virology journal, 9*(1), 1-9.

Absalan, G., Akhond, M., Bananejad, A., & Ershadifar, H. (2015). Highly sensitive determination of nitrite using a carbon ionic liquid electrode modified with Fe 3 O 4 magnetic nanoparticle. *Journal of the Iranian Chemical Society, 12*(7), 1293-1301.

Abu-Salah, K. M., Zourob, M. M., Mouffouk, F., Alrokayan, S. A., Alaamery, M. A., & Ansari, A. A. (2015). DNA-based nanobiosensors as an emerging platform for detection of disease. *Sensors, 15*(6), 14539-14568.

Adamiano, A., Iafisco, M., & Tampieri, A. (2018). Magnetic core-shell nanoparticles: Remote driving, hyperthermia, and controlled drug release. In *Core-shell nanostructures for drug delivery and theranostics* (pp. 259-296): Elsevier.

Adarakatti, P. S., & Kempahanumakkagari, S. K. (2018). Modified electrodes for sensing. In *Electrochemistry* (pp. 58-95).

Adekunle, A. S., Agboola, B. O., Pillay, J., & Ozoemena, K. I. (2010). Electrocatalytic detection of dopamine at single-walled carbon nanotubes–iron (III) oxide nanoparticles platform. *Sensors and Actuators B: Chemical, 148*(1), 93-102.

Ahammad, A. S., Choi, Y.-H., Koh, K., Kim, J.-H., Lee, J.-J., & Lee, M. (2011). Electrochemical detection of cardiac biomarker troponin I at gold nanoparticle-modified ITO electrode by using open circuit potential. *Int. J. Electrochem. Sci, 6*(6), 1906-1916.

Ahmad, S., Riaz, U., Kaushik, A., & Alam, J. (2009). Soft template synthesis of super paramagnetic Fe 3 O 4 nanoparticles a novel technique. *Journal of Inorganic and Organometallic Polymers and Materials, 19*(3), 355-360.

Ahmad, T., Bae, H., Rhee, I., Chang, Y., Jin, S.-U., & Hong, S. (2012). Gold-coated iron oxide nanoparticles as a T 2 contrast agent in magnetic resonance imaging. *Journal of nanoscience and nanotechnology, 12*(7), 5132-5137.

Alkasir, R. S., Ganesana, M., Won, Y.-H., Stanciu, L., & Andreescu, S. (2010). Enzyme functionalized nanoparticles for electrochemical biosensors: a comparative study with applications for the detection of bisphenol A. *Biosensors and Bioelectronics, 26*(1), 43-49.

Amina, S. J., & Guo, B. (2020). A Review on the Synthesis and Functionalization of Gold Nanoparticles as a Drug Delivery Vehicle. *International journal of nanomedicine, 15*, 9823.

Arif, R., & Khan, S. (2020). Nanosensors Based on DNA as an Emerging Technology for the Detection of Disease. In *Nanobiosensors for Agricultural, Medical and Environmental Applications* (pp. 91-120): Springer.

Armistead, P. M., & Thorp, H. H. (2002). Electrochemical detection of gene expression in tumor samples: overexpression of Rak nuclear tyrosine kinase. *Bioconjugate chemistry, 13*(2), 172-176.

Arvand, M., Orangpour, S., & Ghodsi, N. (2015). Differential pulse stripping voltammetric determination of the antipsychotic medication olanzapine at a magnetic nano-composite with a core/shell structure. *RSC Advances, 5*(57), 46095-46103.

Atar, N., Eren, T., Yola, M. L., Karimi-Maleh, H., & Demirdögen, B. (2015). Magnetic iron oxide and iron oxide@ gold nanoparticle anchored nitrogen and sulfur-functionalized reduced graphene oxide electrocatalyst for methanol oxidation. *RSC Advances, 5*(33), 26402-26409.

Atta, N. F., & El-Kady, M. F. (2010). Novel poly (3-methylthiophene)/Pd, Pt nanoparticle sensor: Synthesis, characterization and its application to the simultaneous analysis of dopamine and ascorbic acid in biological fluids. *Sensors and Actuators B: Chemical, 145*(1), 299-310.

Avasthi, A., Caro, C., Pozo-Torres, E., Leal, M. P., & García-Martín, M. L. (2020). Magnetic nanoparticles as MRI contrast agents. *Topics in Current Chemistry, 378*, 1-43.

Awwad, A. M., & Salem, N. M. (2012). A green and facile approach for synthesis of magnetite nanoparticles. *Nanoscience and Nanotechnology, 2*(6), 208-213.

Ayala-Valenzuela, O., Matutes-Aquino, J., Betancourt-Galindo, R., Garcia-Cerda, L., Fernandez, O. R., Fannin, P., & Giannitsis, A. (2005). Magnetite-cobalt ferrite nanoparticles for kerosene-based magnetic fluids. *Journal of Magnetism and Magnetic Materials, 294*(2), e37-e41.

Bachhuka, A., Christo, S. N., Cavallaro, A., Diener, K. R., Mierczynska, A., Smith, L. E., . . . Vasilev, K. (2015). Hybrid core/shell microparticles and their use for understanding biological processes. *Journal of colloid and interface science, 457*, 9-17.

Baig, N., Kammakakam, I., & Falath, W. (2021). Nanomaterials: A review of synthesis, properties, recent progress, and challenges. *Materials Advances*.

Baldrich, E., Gómez, R., Gabriel, G., & Muñoz, F. X. (2011). Magnetic entrapment for fast, simple and reversible electrode modification with carbon nanotubes: application to dopamine detection. *Biosensors and Bioelectronics, 26*(5), 1876-1882.

Ban, Z., Barnakov, Y. A., Li, F., Golub, V. O., & O'Connor, C. J. (2005). The synthesis of core–shell iron@ gold nanoparticles and their characterization. *Journal of Materials Chemistry, 15*(43), 4660-4662.

Barnes, E. O., O'Mahony, A. M., Aldous, L., Hardacre, C., & Compton, R. G. (2010). The electrochemical oxidation of catechol and dopamine on platinum in 1-Ethyl-3-methylimidazolium bis (trifluoromethylsulfonyl) imide ([C2mim][NTf2]) and 1-Butyl-3-methylimidazolium tetrafluoroborate ([C4mim][BF4]): Adsorption effects in ionic liquid voltammetry. *Journal of Electroanalytical Chemistry, 646*(1-2), 11-17.

Bartholomew, D. A., Luff, R. D., Quigley, N. B., Curtis, M., & Olson, M. C. (2011). Analytical performance of Cervista® HPV 16/18 genotyping test for cervical cytology samples. *Journal of Clinical Virology, 51*(1), 38-43.

Bartolome, J. P., Echegoyen, L., & Fragoso, A. (2015). Reactive carbon nano-onion modified glassy carbon surfaces as DNA sensors for human papillomavirus oncogene detection with enhanced sensitivity. *Analytical chemistry, 87*(13), 6744-6751.

Bartosik, M., Durikova, H., Vojtesek, B., Anton, M., Jandakova, E., & Hrstka, R. (2016). Electrochemical chip-based genomagnetic assay for detection of high-risk human papillomavirus DNA. *Biosensors and Bioelectronics, 83*, 300-305.

Baruwati, B., & Varma, R. S. (2009). High value products from waste: grape pomace extract—a three-in-one package for the synthesis of metal nanoparticles. *ChemSusChem: Chemistry & Sustainability Energy & Materials, 2*(11), 1041-1044.

Basavaraja, S., Balaji, S., Lagashetty, A., Rajasab, A., & Venkataraman, A. (2008). Extracellular biosynthesis of silver nanoparticles using the fungus Fusarium semitectum. *Materials Research Bulletin, 43*(5), 1164-1170.

Bayda, S., Adeel, M., Tuccinardi, T., Cordani, M., & Rizzolio, F. (2020). The history of nanoscience and nanotechnology: From chemical–physical applications to nanomedicine. *Molecules, 25*(1), 112.

Baydar, D. E., Kulac, I., Ozagari, A., & Tezel, G. G. (2013). Occurrence of dysplasia and human papilloma virus typing in penile condylomas. *Urology, 81*(1), 211. e219-211. e215.

Beattie, W. G., Meng, L., Turner, S. L., Varma, R. S., Dao, D. D., & Beattie, K. L. (1995). Hybridization of DNA targets to glass-tethered oligonucleotide probes. *Molecular biotechnology, 4*(3), 213-225.

Benvidi, A., Firouzabadi, A. D., Tezerjani, M. D., Moshtaghiun, S., Mazloum-Ardakani, M., & Ansarin, A. (2015). A highly sensitive and selective electrochemical DNA biosensor to diagnose breast cancer. *Journal of Electroanalytical Chemistry, 750*, 57-64.

Benvidi, A., Jahanbani, S., Mirjalili, B.-F., & Zare, R. (2016). Electrocatalytic oxidation of hydrazine on magnetic bar carbon paste electrode modified with benzothiazole and iron oxide nanoparticles: Simultaneous determination of hydrazine and phenol. *Chinese Journal of Catalysis, 37*(4), 549-560.

Bettazzi, F., Lucarelli, F., Palchetti, I., Berti, F., Marrazza, G., & Mascini, M. (2008). Disposable electrochemical DNA-array for PCR amplified detection of hazelnut allergens in foodstuffs. *Analytica chimica acta, 614*(1), 93-102.

Bezinge, L., Suea-Ngam, A., deMello, A. J., & Shih, C.-J. (2020). Nanomaterials for molecular signal amplification in electrochemical nucleic acid biosensing: recent advances and future prospects for point-of-care diagnostics. *Molecular Systems Design & Engineering, 5*(1), 49-66.

Bodulev, O., & Sakharov, I. Y. (2020). Isothermal nucleic acid amplification techniques and their use in bioanalysis. *Biochemistry (Moscow), 85*(2), 147-166.

Bonyani, M., Mirzaei, A., Leonardi, S. G., Bonavita, A., & Neri, G. (2015). Electrochemical properties of Ag@ iron oxide nanocomposite for application as nitrate sensor. *Electroanalysis, 27*(11), 2654-2662.

Brett, C., & Oliveira Brett, A. M. (1993). *Electrochemistry: principles, methods, and applications*.

Bulychev, N. (2021). Application of optical spectroscopy for investigation of synthesis of hydrogen and nanoparticles in electric discharge in liquid-phase media. *International Journal of Hydrogen Energy, 46*(1), 61-65.

Burd, E. M. (2016). Human papillomavirus laboratory testing: the changing paradigm. *Clinical microbiology reviews, 29*(2), 291-319.

Cagnin, S., Caraballo, M., Guiducci, C., Martini, P., Ross, M., SantaAna, M., . . . Lanfranchi, G. (2009). Overview of electrochemical DNA biosensors: new approaches to detect the expression of life. *Sensors, 9*(4), 3122-3148.

Caizer, C. (2015). Nanoparticle size effect on some magnetic properties. *Handbook of Nanoparticles (Springer, 2015)*.

Campos-Ferreira, D. S., Nascimento, G. A., Souza, E. V., Souto-Maior, M. A., Arruda, M. S., Zanforlin, D. M., . . . Lima-Filho, J. L. (2013). Electrochemical DNA biosensor for human papillomavirus 16 detection in real samples. *Analytica chimica acta, 804*, 258-263.

Campos-Ferreira, D. S., Souza, E. V., Nascimento, G. A., Zanforlin, D. M., Arruda, M. S., Beltrao, M. F., . . . Lima-Filho, J. L. (2016). Electrochemical DNA biosensor for the detection of human papillomavirus E6 gene inserted in recombinant plasmid. *Arabian Journal of Chemistry, 9*(3), 443-450.

Catalano, E., Miola, M., Ferraris, S., Novak, S., Oltolina, F., Cochis, A., . . . Follenzi, A. (2017). Magnetite and silica-coated magnetite nanoparticles are highly biocompatible on endothelial cells in vitro. *Biomedical Physics & Engineering Express, 3*(2), 025015.

Chalklen, T., Jing, Q., & Kar-Narayan, S. (2020). Biosensors Based on Mechanical and Electrical Detection Techniques. *Sensors, 20*(19), 5605.

Chandra, S., Lang, H., & Bahadur, D. (2013). Polyaniline-iron oxide nanohybrid film as multi-functional label-free electrochemical and biomagnetic sensor for catechol. *Analytica chimica acta, 795*, 8-14.

Chaturvedi, S., & Dave, P. N. (2014). *Emerging applications of nanoscience.* Paper presented at the Materials Science Forum.

Chaturvedi, V. K., Singh, A., Singh, V. K., & Singh, M. P. (2019). Cancer nanotechnology: a new revolution for cancer diagnosis and therapy. *Current drug metabolism, 20*(6), 416-429.

Chauhan, N., & Pundir, C. S. (2011). An amperometric biosensor based on acetylcholinesterase immobilized onto iron oxide nanoparticles/multi-walled carbon nanotubes modified gold electrode for measurement of organophosphorus insecticides. *Analytica chimica acta, 701*(1), 66-74.

Chen, J., Wang, F., Huang, K., Liu, Y., & Liu, S. (2009). Preparation of Fe3O4 nanoparticles with adjustable morphology. *Journal of alloys and compounds, 475*(1-2), 898-902.

Chen, X., Hong, C.-Y., Lin, Y.-H., Chen, J.-H., Chen, G.-N., & Yang, H.-H. (2012). Enzyme-free and label-free ultrasensitive electrochemical detection of human immunodeficiency virus DNA in biological samples based on long-range self-assembled DNA nanostructures. *Analytical chemistry, 84*(19), 8277-8283.

Chen, X., Yu, J., Zhang, Z., & Lu, C. (2011). Study on structure and thermal stability properties of cellulose fibers from rice straw. *Carbohydrate polymers, 85*(1), 245-250.

Cheng, J., Wang, X., Nie, T., Yin, L., Wang, S., Zhao, Y., . . . Mei, H. (2020). A novel electrochemical sensing platform for detection of dopamine based on gold nanobipyramid/multi-walled carbon nanotube hybrids. *Analytical and bioanalytical chemistry*, 1-9.

Cheng, L., Fan, Y., Shen, X., & Liang, H. (2019). Highly sensitive detection of dopamine at ionic liquid functionalized RGO/ZIF-8 nanocomposite-modified electrode. *Journal of Nanomaterials, 2019*.

Chin, S. F., Pang, S. C., & Tan, C. H. (2011). Green synthesis of magnetite nanoparticles (via thermal decomposition method) with controllable size and shape.

Cho, I.-H., Kim, D. H., & Park, S. (2020). Electrochemical biosensors: Perspective on functional nanomaterials for on-site analysis. *Biomaterials research, 24*(1), 1-12.

Cho, S.-J., Jarrett, B. R., Louie, A. Y., & Kauzlarich, S. M. (2006). Gold-coated iron nanoparticles: a novel magnetic resonance agent for T1 and T2 weighted imaging. *Nanotechnology, 17*(3), 640.

Chu, T., Tran, L. T., Tran, H. V., Tran, T., Nguyen, N. T., Bui, D., & Tran, P. Q. (2021). Multi-walled Carbon Nanotubes/Manganese Dioxide Nano-flowers-like/Polyaniline Nanowires Nanocomposite Modified Electrode: A New Platform for a Highly Sensitive Electrochemical Impedance DNA Sensor.

Civit, L., Fragoso, A., Hölters, S., Dürst, M., & O'Sullivan, C. K. (2012). Electrochemical genosensor array for the simultaneous detection of multiple high-risk human papillomavirus sequences in clinical samples. *Analytica chimica acta, 715*, 93-98.

Civit, L., Fragoso, A., & O'Sullivan, C. (2010). Electrochemical biosensor for the multiplexed detection of human papillomavirus genes. *Biosensors and Bioelectronics, 26*(4), 1684-1687.

Clark Jr, L. C., & Lyons, C. (1962). Electrode systems for continuous monitoring in cardiovascular surgery. *Annals of the New York Academy of sciences, 102*(1), 29-45.

Cobos, C., Figueroa, J. A., Mirandola, L., Colombo, M., Summers, G., Figueroa, A., . . . Riaz, J. (2014). The role of human papilloma virus (HPV) infection in non-anogenital cancer and the promise of immunotherapy: a review. *International reviews of immunology, 33*(5), 383-401.

Cubie, H. A. (2013). Diseases associated with human papillomavirus infection. *Virology, 445*(1-2), 21-34.

Cushing, B. L., Kolesnichenko, V. L., & O'Connor, C. J. (2004). Recent advances in the liquid-phase syntheses of inorganic nanoparticles. *Chemical reviews, 104*(9), 3893-3946.

Dai Tran, L., Nguyen, B. H., Van Hieu, N., Tran, H. V., Le Nguyen, H., & Nguyen, P. X. (2011). Electrochemical detection of short HIV sequences on chitosan/Fe3O4 nanoparticle based screen printed electrodes. *Materials Science and Engineering: C, 31*(2), 477-485.

Dai Tran, L., Nguyen, D. T., Nguyen, B. H., Do, Q. P., & Le Nguyen, H. (2011). Development of interdigitated arrays coated with functional polyaniline/MWCNT for electrochemical biodetection: Application for human papilloma virus. *Talanta, 85*(3), 1560-1565.

Das, R. K., Pachapur, V. L., Lonappan, L., Naghdi, M., Pulicharla, R., Maiti, S., . . . Brar, S. K. (2017). Biological synthesis of metallic nanoparticles: plants, animals and microbial aspects. *Nanotechnology for Environmental Engineering, 2*(1), 1-21.

Dastjerdi, R., & Montazer, M. (2010). A review on the application of inorganic nano-structured materials in the modification of textiles: focus on anti-microbial properties. *Colloids and Surfaces B: Biointerfaces, 79*(1), 5-18.

De Souza, C. D., Nogueira, B. R., & Rostelato, M. E. C. (2019). Review of the methodologies used in the synthesis gold nanoparticles by chemical reduction. *Journal of alloys and compounds, 798*, 714-740.

Delport, F., Pollet, J., Janssen, K., Verbruggen, B., Knez, K., Spasic, D., & Lammertyn, J. (2012). Real-time monitoring of DNA hybridization and melting processes using a fiber optic sensor. *Nanotechnology, 23*(6), 065503.

Deng, K., Li, C., Huang, H., & Li, X. (2017). Rolling circle amplification based on signal-enhanced electrochemical DNA sensor for ultrasensitive transcription factor detection. *Sensors and Actuators B: Chemical, 238*, 1302-1308.

Devillers, J., Morlot, M., Pham-Delegue, M., & Dore, J. (2004). Classification of monofloral honeys based on their quality control data. *Food Chemistry, 86*(2), 305-312.

Dheyab, M. A., Aziz, A. A., & Jameel, M. S. (2020). Synthesis and optimization of the sonochemical method for functionalizing gold shell on Fe3O4 core nanoparticles using response surface methodology. *Surfaces and Interfaces, 21*, 100647.

Dheyab, M. A., Aziz, A. A., Jameel, M. S., Noqta, O. A., & Mehrdel, B. (2020). Synthesis and coating methods of biocompatible iron oxide/gold nanoparticle and nanocomposite for biomedical applications. *Chinese Journal of Physics, 64*, 305-325.

Duan, H., Wang, D., & Li, Y. (2015). Green chemistry for nanoparticle synthesis. *Chemical Society Reviews, 44*(16), 5778-5792.

Dung, D. T. K., Hai, T. H., Long, B. D., & Truc, P. N. (2009). *Preparation and characterization of magnetic nanoparticles with chitosan coating.* Paper presented at the Journal of Physics: Conference Series.

Dwivedi, S., Purohit, P., Misra, R., Pareek, P., Goel, A., Khattri, S., . . . Sharma, P. (2017). Diseases and molecular diagnostics: a step closer to precision medicine. *Indian Journal of Clinical Biochemistry, 32*(4), 374-398.

Eddin, F. B. K., & Fen, Y. W. (2020). Recent advances in electrochemical and optical sensing of dopamine. *Sensors (Basel, Switzerland), 20*(4).

Einstein, M. H., Martens, M. G., Garcia, F. A., Ferris, D. G., Mitchell, A. L., Day, S. P., & Olson, M. C. (2010). Clinical validation of the Cervista® HPV HR and 16/18 genotyping tests for use in women with ASC-US cytology. *Gynecologic oncology, 118*(2), 116-122.

El-Sherbiny, I. M., & Salih, E. (2018). Green synthesis of metallic nanoparticles using biopolymers and plant extracts. *Green Metal Nanoparticles: Synthesis, Characterization and Their Applications*, 293-319.

El Ghandoor, H., Zidan, H., Khalil, M. M., & Ismail, M. (2012). Synthesis and some physical properties of magnetite (Fe3O4) nanoparticles. *Int. J. Electrochem. Sci, 7*(6), 5734-5745.

Elbaz, J., Tel-Vered, R., Freeman, R., Yildiz, H. B., & Willner, I. (2009). Switchable motion of DNA on solid supports. *Angewandte Chemie International Edition, 48*(1), 133-137.

Elbialy, N. S., Fathy, M. M., & Khalil, W. M. (2014). Preparation and characterization of magnetic gold nanoparticles to be used as doxorubicin nanocarriers. *Physica Medica, 30*(7), 843-848.

Eom, G., Oh, C., Moon, J., Kim, H., Kim, M. K., Kim, K., . . . Lee, H. J. (2019). Highly sensitive and selective detection of dopamine using overoxidized polypyrrole/sodium dodecyl sulfate-modified carbon nanotube electrodes. *Journal of Electroanalytical Chemistry, 848*, 113295.

Erogul, S., Bas, S. Z., Ozmen, M., & Yildiz, S. (2015). A new electrochemical sensor based on Fe3O4 functionalized graphene oxide-gold nanoparticle composite film for simultaneous determination of catechol and hydroquinone. *Electrochimica Acta, 186*, 302-313.

Espinosa, J. R., Galván, M., Quiñones, A. S., Ayala, J. L., & Durón, S. M. (2019). DNA biosensor based on double-layer discharge for the detection of HPV type 16. *Sensors, 19*(18), 3956.

Fan, F., Feng, Y., Tang, P., & Li, D. (2015). Facile synthesis and photocatalytic performance of ZnO nanoparticles self-assembled spherical aggregates. *Materials Letters, 158*, 290-294.

Fang, C.-L., Qian, K., Zhu, J., Wang, S., Lv, X., & Yu, S.-H. (2008). Monodisperse α-Fe2O3@ SiO2@ Au core/shell nanocomposite spheres: synthesis, characterization and properties. *Nanotechnology, 19*(12), 125601.

Fernandes, D. M., Costa, M., Pereira, C., Bachiller-Baeza, B., Rodríguez-Ramos, I., Guerrero-Ruiz, A., & Freire, C. (2014). Novel electrochemical sensor based on N-doped carbon nanotubes and Fe3O4 nanoparticles: Simultaneous voltammetric determination of ascorbic acid, dopamine and uric acid. *Journal of colloid and interface science, 432*, 207-213.

Filik, H., Avan, A. A., Aydar, S., & Arpacı, R. B. (2014). Simultaneous electrochemical preconcentration and determination of dopamine and uric acid by square-wave adsorptive stripping voltammetry using a poly (Safranine O)-modified glassy carbon electrode. *Int. J. Electrochem. Sci, 9*, 2775-2789.

Forcier, M., & Musacchio, N. (2010). An overview of human papillomavirus infection for the dermatologist: disease, diagnosis, management, and prevention. *Dermatologic Therapy, 23*(5), 458-476.

Fouad, D. M., El-Said, W. A., & Mohamed, M. B. (2015). Spectroscopic characterization of magnetic Fe3O4@ Au core shell nanoparticles. *Spectrochimica Acta Part A: Molecular and Biomolecular Spectroscopy, 140*, 392-397.

Frías, I. A., Avelino, K. Y., Silva, R. R., Andrade, C. A., & Oliveira, M. D. (2015). Trends in biosensors for HPV: identification and diagnosis. *Journal of Sensors, 2015*.

Fuku, X., Baker, P., & Iwuoha, E. (2020). Influence of quantum dot surface on electrochemical DNA sensing mechanism.

Gao, F., Zhu, Z., Lei, J., Geng, Y., & Ju, H. (2013). Sub-femtomolar electrochemical detection of DNA using surface circular strand-replacement polymerization and gold nanoparticle catalyzed silver deposition for signal amplification. *Biosensors and Bioelectronics, 39*(1), 199-203.

Gao, X., Cai, Q., Li, H., & Jie, G. (2020). Supersandwich nanowire/quantum dots sensitization structure-based photoelectrochemical "signal-on" platform for ultrasensitive detection of thrombin. *Analytical chemistry, 92*(9), 6734-6740.

Gao, Y., Xu, S., He, T., Li, J., Liu, L., Zhang, Y., . . . Yu, J. (2020). Ultrasensitive and specific microRNA detection via dynamic light scattering of DNA network based on rolling circle amplification. *Sensors and Actuators B: Chemical, 324*, 128693.

García-Merino, B., Bringas, E., & Ortiz, I. (2021). Synthesis and applications of surface-modified magnetic nanoparticles: progress and future prospects. *Reviews in Chemical Engineering*.

Gawande, M. B., Goswami, A., Asefa, T., Guo, H., Biradar, A. V., Peng, D.-L., . . . Varma, R. S. (2015). Core–shell nanoparticles: synthesis and applications in catalysis and electrocatalysis. *Chemical Society Reviews, 44*(21), 7540-7590.

Ge, J., & Yin, Y. (2008). Magnetically tunable colloidal photonic structures in alkanol solutions. *Advanced Materials, 20*(18), 3485-3491.

George, J. M., Antony, A., & Mathew, B. (2018). Metal oxide nanoparticles in electrochemical sensing and biosensing: a review. *Microchimica Acta, 185*(7), 1-26.

Ghoreishian, S. M., Kang, S.-M., Raju, G. S. R., Norouzi, M., Jang, S.-C., Yun, H. J., . . . Huh, Y. S. (2019). γ-Radiolysis as a highly efficient green approach to the synthesis of metal nanoclusters: a review of mechanisms and applications. *Chemical Engineering Journal, 360*, 1390-1406.

Ghosh Chaudhuri, R., & Paria, S. (2011). Core/shell nanoparticles: classes, properties, synthesis mechanisms, characterization, and applications. *Chemical reviews, 112*(4), 2373-2433.

Girousi, S., & Kinigopoulou, V. (2010). Detection of short oligonucleotide sequences using an electrochemical DNA hybridization biosensor. *Central European Journal of Chemistry, 8*(4), 732-736.

Glazer, M., Fidanza, J., McGall, G., & Frank, C. (2001). Colloidal silica films for high-capacity DNA probe arrays. *Chemistry of materials, 13*(12), 4773-4782.

Goon, I. Y., Lai, L. M., Lim, M., Munroe, P., Gooding, J. J., & Amal, R. (2009). Fabrication and dispersion of gold-shell-protected magnetite nanoparticles: systematic control using polyethyleneimine. *Chemistry of materials, 21*(4), 673-681.

Gravitt, P. E., & Jamshidi, R. (2005). Diagnosis and management of oncogenic cervical human papillomavirus infection. *Infectious Disease Clinics, 19*(2), 439-458.

Guo, T., Lin, M., Huang, J., Zhou, C., Tian, W., Yu, H., . . . Xiao, Y. (2018). The recent advances of magnetic nanoparticles in medicine. *Journal of Nanomaterials, 2018*.

Han, G., Cai, J., Liu, C., Ren, J., Wang, X., Yang, J., & Wang, X. (2021). Highly sensitive electrochemical sensor based on xylan-based Ag@ CQDs-rGO nanocomposite for dopamine detection. *Applied Surface Science, 541*, 148566.

Han, S., Liu, W., Zheng, M., & Wang, R. (2020). Label-free and ultrasensitive electrochemical DNA biosensor based on urchinlike carbon nanotube-gold nanoparticle nanoclusters. *Analytical chemistry, 92*(7), 4780-4787.

Handler, M. Z., Handler, N. S., Majewski, S., & Schwartz, R. A. (2015). Human papillomavirus vaccine trials and tribulations: Clinical perspectives. *Journal of the American Academy of Dermatology, 73*(5), 743-756.

Handler, N. S., Handler, M. Z., Majewski, S., & Schwartz, R. A. (2015). Human papillomavirus vaccine trials and tribulations: vaccine efficacy. *Journal of the American Academy of Dermatology, 73*(5), 759-767.

Hatefi-Mehrjardi, A., Karimi, M. A., Soleymanzadeh, M., & Barani, A. (2020). Highly sensitive detection of dopamine, ascorbic and uric acid with a nanostructure of dianix yellow/multi-walled carbon nanotubes modified electrode. *Measurement, 163*, 107893.

Hayat, A., Catanante, G., & Marty, J. L. (2014). Current trends in nanomaterial-based amperometric biosensors. *Sensors, 14*(12), 23439-23461.

Heydarzadeh, S., Roshanfekr, H., Peyman, H., & Kashanian, S. (2020). Modeling of ultrasensitive DNA hybridization detection based on gold nanoparticles/carbon-nanotubes/chitosan-modified electrodes. *Colloids and Surfaces A: Physicochemical and Engineering Aspects, 587*, 124219.

Hoskins, C., Min, Y., Gueorguieva, M., McDougall, C., Volovick, A., Prentice, P., . . . Wang, L. (2012). Hybrid gold-iron oxide nanoparticles as a multifunctional platform for biomedical application. *Journal of nanobiotechnology, 10*(1), 27.

Hou, C., Tang, W., Zhang, C., Wang, Y., & Zhu, N. (2014). A novel and sensitive electrochemical sensor for bisphenol A determination based on carbon black supporting ferroferric oxide nanoparticles. *Electrochimica Acta, 144*, 324-331.

Hsu, M.-S., Chen, Y.-L., Lee, C.-Y., & Chiu, H.-T. (2012). Gold nanostructures on flexible substrates as electrochemical dopamine sensors. *ACS applied materials & interfaces, 4*(10), 5570-5575.

Huang, D.-Q., Chen, C., Wu, Y.-M., Zhang, H., Sheng, L.-Q., Xu, H.-J., & Liu, Z.-D. (2012). The determination of dopamine using glassy carbon electrode pretreated by a simple electrochemical method. *Int. J. Electrochem. Sci, 7*, 5510-5520.

Huang, H., Bai, W., Dong, C., Guo, R., & Liu, Z. (2015). An ultrasensitive electrochemical DNA biosensor based on graphene/Au nanorod/polythionine for human papillomavirus DNA detection. *Biosensors and Bioelectronics, 68*, 442-446.

Huang, Y., Han, Y., Gao, Y., Gao, J., Ji, H., He, Q., . . . Han, L. (2021). Electrochemical sensor array with nanoporous gold nanolayer and ceria@ gold corona-nanocomposites enhancer integrated into microfluidic for simultaneous ultrasensitive lead ion detection. *Electrochimica Acta, 373*, 137921.

Huang, Y., Miao, Y.-E., Ji, S., Tjiu, W. W., & Liu, T. (2014). Electrospun carbon nanofibers decorated with Ag–Pt bimetallic nanoparticles for selective detection of dopamine. *ACS applied materials & interfaces, 6*(15), 12449-12456.

Hwang, S. J., & Shroyer, K. R. (2012). Biomarkers of cervical dysplasia and carcinoma. *Journal of oncology, 2012*.

Jampasa, S., Siangproh, W., Laocharoensuk, R., Yanatatsaneejit, P., Vilaivan, T., & Chailapakul, O. (2018). A new DNA sensor design for the simultaneous detection of HPV type 16 and 18 DNA. *Sensors and Actuators B: Chemical, 265*, 514-521.

Jampasa, S., Wonsawat, W., Rodthongkum, N., Siangproh, W., Yanatatsaneejit, P., Vilaivan, T., & Chailapakul, O. (2014). Electrochemical detection of human papillomavirus DNA type 16 using a pyrrolidinyl peptide nucleic acid probe immobilized on screen-printed carbon electrodes. *Biosensors and Bioelectronics, 54*, 428-434.

Jeevanandam, J., Barhoum, A., Chan, Y. S., Dufresne, A., & Danquah, M. K. (2018). Review on nanoparticles and nanostructured materials: history, sources, toxicity and regulations. *Beilstein journal of nanotechnology, 9*(1), 1050-1074.

Jiang, B., Lian, L., Xing, Y., Zhang, N., Chen, Y., Lu, P., & Zhang, D. (2018). Advances of magnetic nanoparticles in environmental application: environmental remediation and (bio) sensors as case studies. *Environmental Science and Pollution Research, 25*(31), 30863-30879.

Jiang, J., & Du, X. (2014). Sensitive electrochemical sensors for simultaneous determination of ascorbic acid, dopamine, and uric acid based on Au@ Pd-reduced graphene oxide nanocomposites. *Nanoscale, 6*(19), 11303-11309.

Jiang, K., Wang, Y., Thakur, G., Kotsuchibashi, Y., Naicker, S., Narain, R., & Thundat, T. (2017). Rapid and highly sensitive detection of dopamine using conjugated oxaborole-based polymer and glycopolymer systems. *ACS applied materials & interfaces, 9*(18), 15225-15231.

Johnson, L. R., Starkey, C. R., Palmer, J., Taylor, J., Stout, S., Holt, S., . . . Tyree, G. (2008). A comparison of two methods to determine the presence of high-risk HPV cervical infections. *American journal of clinical pathology, 130*(3), 401-408.

Kalantari, K., Ahmad, M. B., Shameli, K., Hussein, M. Z. B., Khandanlou, R., & Khanehzaei, H. (2014). Size-controlled synthesis of Fe3O4 magnetic nanoparticles in the layers of montmorillonite. *Journal of Nanomaterials, 2014*.

Kalantari, K., Ahmad, M. B., Shameli, K., & Khandanlou, R. (2013). Synthesis of talc/Fe3O4 magnetic nanocomposites using chemical co-precipitation method. *International journal of nanomedicine, 8*, 1817.

Kalantari, K., Ahmad, M. B., Shameli, K., & Khandanlou, R. (2015). Size-controlled synthesis of Fe 3 O 4 magnetite nanoparticles on the exterior of talc layers. *Research on Chemical Intermediates, 41*(4), 2139-2151.

Kang, D., White, R. J., Xia, F., Zuo, X., Vallée-Bélisle, A., & Plaxco, K. W. (2012). DNA biomolecular-electronic encoder and decoder devices constructed by multiplex biosensors. *NPG Asia Materials, 4*(1), e1.

Karaoğlu, E., Baykal, A., Erdemi, H., Alpsoy, L., & Sozeri, H. (2011). Synthesis and characterization of dl-thioctic acid (DLTA)–Fe3O4 nanocomposite. *Journal of alloys and compounds, 509*(37), 9218-9225.

Karimizefreh, A., Mahyari, F. A., VaezJalali, M., Mohammadpour, R., & Sasanpour, P. (2017). Impedimetic biosensor for the DNA of the human papilloma virus based on the use of gold nanosheets. *Microchimica Acta, 184*(6), 1729-1737.

Karunakaran, C., Rajkumar, R., & Bhargava, K. (2015). Introduction to biosensors. In *Biosensors and Bioelectronics* (pp. 1-68): Elsevier.

Katanga, J., Kjaer, S. K., Manongi, R., Wu, C. S., Iftner, T., Waldstrom, M., . . . Rasch, V. (2019). Performance of care HPV, hybrid capture 2 and visual inspection with acetic

acid for detection of high-grade cervical lesion in Tanzania: A cross-sectional study. *PloS one, 14*(6), e0218559.
Khan, I., Saeed, K., & Khan, I. (2019). Nanoparticles: Properties, applications and toxicities. *Arabian Journal of Chemistry, 12*(7), 908-931.
Khandanlou, R., Ahmad, M. B., Shameli, K., & Kalantari, K. (2013). Synthesis and characterization of rice straw/Fe3O4 nanocomposites by a quick precipitation method. *Molecules, 18*(6), 6597-6607.
Kim, D. K., Mikhaylova, M., Zhang, Y., & Muhammed, M. (2003). Protective coating of superparamagnetic iron oxide nanoparticles. *Chemistry of materials, 15*(8), 1617-1627.
Kim, Y. S., Lee, S. M., Govindaiah, P., Lee, S. J., Lee, S. H., Kim, J. H., & Cheong, I. W. (2013). Multifunctional Fe3O4 nanoparticles-embedded poly (styrene)/poly (thiophene) core/shell composite particles. *Synthetic Metals, 175*, 56-61.
Knopp, D., Tang, D., & Niessner, R. (2009). Bioanalytical applications of biomolecule-functionalized nanometer-sized doped silica particles. *Analytica chimica acta, 647*(1), 14-30.
Kouassi, G. K., & Irudayaraj, J. (2006). Magnetic and gold-coated magnetic nanoparticles as a DNA sensor. *Analytical chemistry, 78*(10), 3234-3241.
Kowalczyk, A., & Nowicka, A. M. (2016). Application of mercury–mediated thymine–base pairs for successful voltammetric detection of HPV 18. *Sensors and Actuators B: Chemical, 237*, 810-816.
Kumar, H., & Neelam, R. (2016). Enzyme-based electrochemical biosensors for food safety: A review. *Nanobiosensors in Disease Diagnosis, 5*, 29-39.
Kumar, S., Bhushan, P., & Bhattacharya, S. (2018). Fabrication of nanostructures with bottom-up approach and their utility in diagnostics, therapeutics, and others. In *Environmental, Chemical and Medical Sensors* (pp. 167-198): Springer.
Kumar, V., Guleria, P., Dasgupta, N., & Ranjan, S. (2020). *Functionalized Nanomaterials I: Fabrications*: CRC Press.
Labuda, J., Brett, A. M. O., Evtugyn, G., Fojta, M., Mascini, M., Ozsoz, M., . . . Wang, J. (2010). Electrochemical nucleic acid-based biosensors: Concepts, terms, and methodology (IUPAC Technical Report). *Pure and Applied Chemistry, 82*(5), 1161-1187.
Lahooti, A., Sarkar, S., Rad, H. S., Gholami, A., Nosrati, S., Muller, R. N., . . . Yousefnia, H. (2017). PEGylated superparamagnetic iron oxide nanoparticles labeled with 68 Ga as a PET/MRI contrast agent: a biodistribution study. *Journal of Radioanalytical and Nuclear Chemistry, 311*(1), 769-774.
Lai, S. L., Tan, W. L., & Yang, K.-L. (2011). Detection of DNA targets hybridized to solid surfaces using optical images of liquid crystals. *ACS applied materials & interfaces, 3*(9), 3389-3395.
Lancaster, M. (2020). *Green chemistry: an introductory text*: Royal society of chemistry.
Lata, S., Batra, B., Karwasra, N., & Pundir, C. S. (2012). An amperometric H2O2 biosensor based on cytochrome c immobilized onto nickel oxide nanoparticles/carboxylated multiwalled carbon nanotubes/polyaniline modified gold electrode. *Process Biochemistry, 47*(6), 992-998.
Lee, J., Yang, J., Ko, H., Oh, S., Kang, J., Son, J., . . . Suh, J. S. (2008). Multifunctional magnetic gold nanocomposites: human epithelial cancer detection via magnetic resonance imaging and localized synchronous therapy. *Advanced Functional Materials, 18*(2), 258-264.

Lee, S., Oh, J., Kim, D., & Piao, Y. (2016). A sensitive electrochemical sensor using an iron oxide/graphene composite for the simultaneous detection of heavy metal ions. *Talanta, 160*, 528-536.

Li, B.-Q., Nie, F., Sheng, Q.-L., & Zheng, J.-B. (2015). An electrochemical sensor for sensitive determination of nitrites based on Ag-Fe 3 O 4-graphene oxide magnetic nanocomposites. *Chemical Papers, 69*(7), 911-920.

Li, F., Chen, W., & Zhang, S. (2008). Development of DNA electrochemical biosensor based on covalent immobilization of probe DNA by direct coupling of sol–gel and self-assembly technologies. *Biosensors and Bioelectronics, 24*(4), 781-786.

Li, G., Zhong, P., Ye, Y., Wan, X., Cai, Z., Yang, S., . . . He, Q. (2019). A Highly Sensitive and Stable Dopamine Sensor Using Shuttle-Like α-Fe2O3 Nanoparticles/Electro-Reduced Graphene Oxide Composites. *Journal of the Electrochemical Society, 166*(15), B1552.

Li, J., Wang, Y., Sun, Y., Ding, C., Lin, Y., Sun, W., & Luo, C. (2017). A novel ionic liquid functionalized graphene oxide supported gold nanoparticle composite film for sensitive electrochemical detection of dopamine. *RSC Advances, 7*(4), 2315-2322.

Li, J., Xu, Q., Wei, X., & Hao, Z. (2013). Electrogenerated chemiluminescence immunosensor for Bacillus thuringiensis Cry1Ac based on Fe3O4@ Au nanoparticles. *Journal of agricultural and food chemistry, 61*(7), 1435-1440.

Li, L., Wang, S., Yang, T., Huang, S., & Wang, J. (2012). Electrochemical growth of gold nanoparticles on horizontally aligned carbon nanotubes: a new platform for ultrasensitive DNA sensing. *Biosensors and Bioelectronics, 33*(1), 279-283.

Li, N.-N., Kang, T.-F., Zhang, J.-J., Lu, L.-P., & Cheng, S.-Y. (2015). Fe 3 O 4@ ZrO 2 magnetic nanoparticles as a new electrode material for sensitive determination of organophosphorus agents. *Analytical Methods, 7*(12), 5053-5059.

Li, S.-J., Deng, D.-H., Shi, Q., & Liu, S.-R. (2012). Electrochemical synthesis of a graphene sheet and gold nanoparticle-based nanocomposite, and its application to amperometric sensing of dopamine. *Microchimica Acta, 177*(3-4), 325-331.

Li, S., Shen, Y., Xie, A., Yu, X., Zhang, X., Yang, L., & Li, C. (2007). Rapid, room-temperature synthesis of amorphous selenium/protein composites using Capsicum annuum L extract. *Nanotechnology, 18*(40), 405101.

Li, X., Xu, H., Chen, Z.-S., & Chen, G. (2011). Biosynthesis of nanoparticles by microorganisms and their applications. *Journal of Nanomaterials, 2011*.

Li, Z., Sun, Q., & Gao, M. (2005). Preparation of water-soluble magnetite nanocrystals from hydrated ferric salts in 2-pyrrolidone: mechanism leading to Fe3O4. *Angewandte Chemie International Edition, 44*(1), 123-126.

Lian, W., Wang, L., Song, Y., Yuan, H., Zhao, S., Li, P., & Chen, L. (2009). A hydrogen peroxide sensor based on electrochemically roughened silver electrodes. *Electrochimica Acta, 54*(18), 4334-4339.

Liang, C.-H., Wang, C.-C., Lin, Y.-C., Chen, C.-H., Wong, C.-H., & Wu, C.-Y. (2009). Iron oxide/gold core/shell nanoparticles for ultrasensitive detection of carbohydrate− protein interactions. *Analytical chemistry, 81*(18), 7750-7756.

Liepold, P., Kratzmüller, T., Persike, N., Bandilla, M., Hinz, M., Wieder, H., . . . Hartwich, G. (2008). Electrically detected displacement assay (EDDA): a practical approach to nucleic acid testing in clinical or medical diagnosis. *Analytical and bioanalytical chemistry, 391*(5), 1759.

Lim, I.-I. S., Njoki, P. N., Park, H.-Y., Wang, X., Wang, L., Mott, D., & Zhong, C.-J. (2008). Gold and magnetic oxide/gold core/shell nanoparticles as bio-functional nanoprobes. *Nanotechnology, 19*(30), 305102.

Lin, M. (2015). A dopamine electrochemical sensor based on gold nanoparticles/over-oxidized polypyrrole nanotube composite arrays. *RSC Advances, 5*(13), 9848-9851.
Linthorst, J. A. (2010). An overview: origins and development of green chemistry. *Foundations of chemistry, 12*(1), 55-68.
Liu, H., Hou, P., Zhang, W., & Wu, J. (2010). Synthesis of monosized core–shell Fe3O4/Au multifunctional nanoparticles by PVP-assisted nanoemulsion process. *Colloids and Surfaces A: Physicochemical and Engineering Aspects, 356*(1-3), 21-27.
Liu, L.-s., Wu, C., & Zhang, S. (2017). Ultrasensitive detection of DNA and ramos cell using in situ selective crystallization based quartz crystal microbalance. *Analytical chemistry, 89*(7), 4309-4313.
Liu, Q., Xu, Z., Finch, J., & Egerton, R. (1998). A novel two-step silica-coating process for engineering magnetic nanocomposites. *Chemistry of materials, 10*(12), 3936-3940.
Liu, S., Yan, J., He, G., Zhong, D., Chen, J., Shi, L., . . . Jiang, H. (2012). Layer-by-layer assembled multilayer films of reduced graphene oxide/gold nanoparticles for the electrochemical detection of dopamine. *Journal of Electroanalytical Chemistry, 672*, 40-44.
Liu, X., Ou, X., Lu, Q., Zhang, J., Chen, S., & Wei, S. (2014). Electrochemical sensor based on overoxidized dopamine polymer and 3, 4, 9, 10-perylenetetracarboxylic acid for simultaneous determination of ascorbic acid, dopamine, uric acid, xanthine and hypoxanthine. *RSC Advances, 4*(80), 42632-42637.
Liu, X., Xie, L., & Li, H. (2012). Electrochemical biosensor based on reduced graphene oxide and Au nanoparticles entrapped in chitosan/silica sol–gel hybrid membranes for determination of dopamine and uric acid. *Journal of Electroanalytical Chemistry, 682*, 158-163.
Liu, Y., Liu, J., Liu, J., Gan, W., Ye, B.-c., & Li, Y. (2017). Highly sensitive and selective voltammetric determination of dopamine using a gold electrode modified with a molecularly imprinted polymeric film immobilized on flaked hollow nickel nanospheres. *Microchimica Acta, 184*(5), 1285-1294.
Lo, C. K., Xiao, D., & Choi, M. M. (2007). Homocysteine-protected gold-coated magnetic nanoparticles: synthesis and characterisation. *Journal of materials chemistry, 17*(23), 2418-2427.
LOPEZ, L. C. O. (2016). Enhancement of electrochemical glucose sensing by using multiwall carbon nanotubes decorated with iron oxide nanoparticles. *International Journal of Electrochemical Science, 11*, 6356-6369.
Lu, Q., Yao, K., Xi, D., Liu, Z., Luo, X., & Ning, Q. (2006). Synthesis and characterization of composite nanoparticles comprised of gold shell and magnetic core/cores. *Journal of Magnetism and Magnetic Materials, 301*(1), 44-49.
Lugani, Y., Sooch, B. S., Singh, P., & Kumar, S. (2021). Nanobiotechnology applications in food sector and future innovations. In *Microbial Biotechnology in Food and Health* (pp. 197-225): Elsevier.
Lunn, G., & Sansone, E. B. (2012). *Destruction of hazardous chemicals in the laboratory*: John Wiley & Sons.
Luo, X., Lee, T. M.-H., & Hsing, I.-M. (2008). Immobilization-free sequence-specific electrochemical detection of DNA using ferrocene-labeled peptide nucleic acid. *Analytical chemistry, 80*(19), 7341-7346.
Lv, M.-M., Fan, S.-F., Wang, Q.-L., Lv, Q.-Y., Song, X., & Cui, H.-F. (2020). An enzyme-free electrochemical sandwich DNA assay based on the use of hybridization chain reaction and gold nanoparticles: application to the determination of the DNA of Helicobacter pylori. *Microchimica Acta, 187*(1), 1-10.

Lyons, M. E., & Keeley, G. P. (2006). The redox behaviour of randomly dispersed single walled carbon nanotubes both in the absence and in the presence of adsorbed glucose oxidase. *Sensors, 6*(12), 1791-1826.

Madrakian, T., Maleki, S., Heidari, M., & Afkhami, A. (2016). An electrochemical sensor for rizatriptan benzoate determination using Fe3O4 nanoparticle/multiwall carbon nanotube-modified glassy carbon electrode in real samples. *Materials Science and Engineering: C, 63*, 637-643.

Magro, M., & Vianello, F. (2019). Bare iron oxide nanoparticles: Surface tunability for biomedical, sensing and environmental applications. *Nanomaterials, 9*(11), 1608.

Mahato, K., Nagpal, S., Shah, M. A., Srivastava, A., Maurya, P. K., Roy, S., . . . Chandra, P. (2019). Gold nanoparticle surface engineering strategies and their applications in biomedicine and diagnostics. *3 Biotech, 9*(2), 57.

Mahdavi, M., Namvar, F., Ahmad, M. B., & Mohamad, R. (2013). Green biosynthesis and characterization of magnetic iron oxide (Fe3O4) nanoparticles using seaweed (Sargassum muticum) aqueous extract. *Molecules, 18*(5), 5954-5964.

Mahmoodi, P., Fani, M., Rezayi, M., Avan, A., Pasdar, Z., Karimi, E., . . . Ghayour-Mobarhan, M. (2019). Early detection of cervical cancer based on high-risk HPV DNA-based genosensors: A systematic review. *Biofactors, 45*(2), 101-117.

Majidi, S., Zeinali Sehrig, F., Farkhani, S. M., Soleymani Goloujeh, M., & Akbarzadeh, A. (2016). Current methods for synthesis of magnetic nanoparticles. *Artificial cells, nanomedicine, and biotechnology, 44*(2), 722-734.

Maleki, H., Simchi, A., Imani, M., & Costa, B. (2012). Size-controlled synthesis of superparamagnetic iron oxide nanoparticles and their surface coating by gold for biomedical applications. *Journal of Magnetism and Magnetic Materials, 324*(23), 3997-4005.

Malekzad, H., Zangabad, P. S., Mirshekari, H., Karimi, M., & Hamblin, M. R. (2017). Noble metal nanoparticles in biosensors: recent studies and applications. *Nanotechnology reviews, 6*(3), 301-329.

Mandal, M., Kundu, S., Ghosh, S. K., Panigrahi, S., Sau, T. K., Yusuf, S., & Pal, T. (2005). Magnetite nanoparticles with tunable gold or silver shell. *Journal of colloid and interface science, 286*(1), 187-194.

Mani, G. K., & Rayappan, J. B. B. (2015). Facile synthesis of ZnO nanostructures by spray pyrolysis technique and its application as highly selective H2S sensor. *Materials Letters, 158*, 373-376.

Manisekaran, R. (2018). Literature Survey on Magnetic, Gold, and Core-Shell Nanoparticles. In *Design and Evaluation of Plasmonic/Magnetic Au-MFe2O4 (M-Fe/Co/Mn) Core-Shell Nanoparticles Functionalized with Doxorubicin for Cancer Therapeutics* (pp. 37-72): Springer.

Martínez-Mera, I., Espinosa-Pesqueira, M., Pérez-Hernández, R., & Arenas-Alatorre, J. (2007). Synthesis of magnetite (Fe3O4) nanoparticles without surfactants at room temperature. *Materials Letters, 61*(23-24), 4447-4451.

Melo, I. M., Ribeiro, E. A., & Canevari, R. A. (2018). Potential Diagnostic Techniques for Cervical Cancer Prevention-Review. *Journal of Cancer Treatment and Diagnosis, 2*(4).

Menazea, A. (2020). Femtosecond laser ablation-assisted synthesis of silver nanoparticles in organic and inorganic liquids medium and their antibacterial efficiency. *Radiation Physics and Chemistry, 168*, 108616.

Mitsudome, T., & Kaneda, K. (2013). Advanced core–shell nanoparticle catalysts for efficient organic transformations. *ChemCatChem, 5*(7), 1681-1691.

Mokhodoeva, O., Vlk, M., Málková, E., Kukleva, E., Mičolová, P., Štamberg, K., . . . Kozempel, J. (2016). Study of 223 Ra uptake mechanism by Fe 3 O 4 nanoparticles: towards new prospective theranostic SPIONs. *Journal of Nanoparticle Research, 18*(10), 301.

Mondal, S., Roy, N., Laskar, R. A., Sk, I., Basu, S., Mandal, D., & Begum, N. A. (2011). Biogenic synthesis of Ag, Au and bimetallic Au/Ag alloy nanoparticles using aqueous extract of mahogany (Swietenia mahogani JACQ.) leaves. *Colloids and Surfaces B: Biointerfaces, 82*(2), 497-504.

Mukherjee, S., Liang, L., & Veiseh, O. (2020). Recent advancements of magnetic nanomaterials in cancer therapy. *Pharmaceutics, 12*(2), 147.

Mukhopadhyay, S., & Sharma, S. (2013). Nanoscience and nanotechnology: cracking prodigal farming. *Journal of Bionanoscience, 7*(5), 497-502.

Musza, K., Szabados, M., Ádám, A. A., Kónya, Z., Kukovecz, Á., Sipos, P., & Pálinkó, I. (2019). Mechanochemically modified hydrazine reduction method for the synthesis of nickel nanoparticles and their catalytic activities in the Suzuki–Miyaura cross-coupling reaction. *Reaction Kinetics, Mechanisms and Catalysis, 126*(2), 857-868.

Nadagouda, M. N., & Varma, R. S. (2008). Green synthesis of silver and palladium nanoparticles at room temperature using coffee and tea extract. *Green Chemistry, 10*(8), 859-862.

Nanda, V., Sarkar, B., Sharma, H., & Bawa, A. (2003). Physico-chemical properties and estimation of mineral content in honey produced from different plants in Northern India. *Journal of Food Composition and Analysis, 16*(5), 613-619.

Nascimento, H. P., Oliveira, M. D., de Melo, C. P., Silva, G. J., Cordeiro, M. T., & Andrade, C. A. (2011). An impedimetric biosensor for detection of dengue serotype at picomolar concentration based on gold nanoparticles-polyaniline hybrid composites. *Colloids and Surfaces B: Biointerfaces, 86*(2), 414-419.

Nasirizadeh, N., & Zare, H. R. (2009). Differential pulse voltammetric simultaneous determination of noradrenalin and acetaminophen using a hematoxylin biosensor. *Talanta, 80*(2), 656-663.

Nasirizadeh, N., Zare, H. R., Pournaghi-Azar, M. H., & Hejazi, M. S. (2011). Introduction of hematoxylin as an electroactive label for DNA biosensors and its employment in detection of target DNA sequence and single-base mismatch in human papilloma virus corresponding to oligonucleotide. *Biosensors and Bioelectronics, 26*(5), 2638-2644.

Ngo, D. B., Chaibun, T., Yin, L. S., Lertanantawong, B., & Surareungchai, W. (2021). Electrochemical DNA detection of hepatitis E virus genotype 3 using PbS quantum dot labelling. *Analytical and bioanalytical chemistry, 413*(4), 1027-1037.

Nikabadi, H. R., Shahtahmasebi, N., Rokn-Abadi, M. R., Mohagheghi, M. B., & Goharshadi, E. (2013). Gradual growth of gold nanoseeds on silica for SiO2@ gold homogeneous nano core/shell applications by the chemical reduction method. *Physica Scripta, 87*(2), 025802.

Nikam, A., Prasad, B., & Kulkarni, A. (2018). Wet chemical synthesis of metal oxide nanoparticles: a review. *CrystEngComm, 20*(35), 5091-5107.

Niu, X., Zheng, W., Yin, C., Weng, W., Li, G., Sun, W., & Men, Y. (2017). Electrochemical DNA biosensor based on gold nanoparticles and partially reduced graphene oxide modified electrode for the detection of Listeria monocytogenes hly gene sequence. *Journal of Electroanalytical Chemistry, 806*, 116-122.

Norouz Dizaji, A., Yilmaz, M., & Piskin, E. (2016). Silver or gold deposition onto magnetite nanoparticles by using plant extracts as reducing and stabilizing agents. *Artificial cells, nanomedicine, and biotechnology, 44*(4), 1109-1115.

O'Halloran, M. P., Pravda, M., & Guilbault, G. G. (2001). Prussian Blue bulk modified screen-printed electrodes for H2O2 detection and for biosensors. *Talanta, 55*(3), 605-611.

Pal, S., Morales, M., Mukherjee, P., & Srikanth, H. (2009). Synthesis and magnetic properties of gold coated iron oxide nanoparticles. *Journal of applied physics, 105*(7), 07B504.

Pal, S., Verma, A., Raikwar, S., Prajapati, Y., & Saini, J. (2018). Detection of DNA hybridization using graphene-coated black phosphorus surface plasmon resonance sensor. *Applied Physics A, 124*(5), 1-11.

Palanisamy, K., Meenakshi Sundaram, N., Devabharathi, V., & Thangarasu, P. (2013). Synthesis and characterization of olive oil mediated iron oxide nanoparticles. *Digest Journal of Nanomaterials & Biostructures (DJNB), 8*(2).

Palecek, E., & Bartosik, M. (2012). Electrochemistry of nucleic acids. *Chemical reviews, 112*(6), 3427-3481.

Pan, M., Gu, Y., Yun, Y., Li, M., Jin, X., & Wang, S. (2017). Nanomaterials for electrochemical immunosensing. *Sensors, 17*(5), 1041.

Pan, M., Yang, J., Liu, K., Yin, Z., Ma, T., Liu, S., . . . Wang, S. (2020). Noble metal nanostructured materials for chemical and biosensing systems. *Nanomaterials, 10*(2), 209.

Pang, L.-L., Li, J.-S., Jiang, J.-H., Le, Y., Shen, G. L., & Yu, R.-Q. (2007). A novel detection method for DNA point mutation using QCM based on Fe3O4/Au core/shell nanoparticle and DNA ligase reaction. *Sensors and Actuators B: Chemical, 127*(2), 311-316.

Papaphilippou, P., Loizou, L., Popa, N. C., Han, A., Vekas, L., Odysseos, A., & Krasia-Christoforou, T. (2009). Superparamagnetic hybrid micelles, based on iron oxide nanoparticles and well-defined diblock copolymers possessing β-ketoester functionalities. *Biomacromolecules, 10*(9), 2662-2671.

Parveen, K., Banse, V., & Ledwani, L. (2016). *Green synthesis of nanoparticles: their advantages and disadvantages.* Paper presented at the AIP conference proceedings.

Patra, J. K., & Baek, K.-H. (2014). Green nanobiotechnology: factors affecting synthesis and characterization techniques. *Journal of Nanomaterials, 2014*, 219.

Patra, J. K., Fraceto, L. F., Das, G., & Campos, E. V. R. (2020). *Green Nanoparticles*: Springer.

Peik-See, T., Pandikumar, A., Nay-Ming, H., Hong-Ngee, L., & Sulaiman, Y. (2014). Simultaneous electrochemical detection of dopamine and ascorbic acid using an iron oxide/reduced graphene oxide modified glassy carbon electrode. *Sensors, 14*(8), 15227-15243.

Pham, T. T. H., Cao, C., & Sim, S. J. (2008). Application of citrate-stabilized gold-coated ferric oxide composite nanoparticles for biological separations. *Journal of Magnetism and Magnetic Materials, 320*(15), 2049-2055.

Philip, D. (2009a). Biosynthesis of Au, Ag and Au–Ag nanoparticles using edible mushroom extract. *Spectrochimica Acta Part A: Molecular and Biomolecular Spectroscopy, 73*(2), 374-381.

Philip, D. (2009b). Honey mediated green synthesis of gold nanoparticles. *Spectrochimica Acta Part A: Molecular and Biomolecular Spectroscopy, 73*(4), 650-653.

Piro, B., Kapella, A., Le, V., Anquetin, G., Zhang, Q., Reisberg, S., . . . Pham, M. (2011). Towards the detection of human papillomavirus infection by a reagentless electrochemical peptide biosensor. *Electrochimica Acta, 56*(28), 10688-10693.

Pustovalov, V., Astafyeva, L., & Fritzsche, W. (2012). Optical properties of core–shell gold–silver and silver–gold nanoparticles for near UV and visible radiation wavelengths. *Plasmonics, 7*(3), 469-474.

Radhakrishnan, S., Krishnamoorthy, K., Sekar, C., Wilson, J., & Kim, S. J. (2014). A highly sensitive electrochemical sensor for nitrite detection based on Fe2O3 nanoparticles decorated reduced graphene oxide nanosheets. *Applied Catalysis B: Environmental, 148*, 22-28.

Radhi, M., Al-Mulla, E. A. J., & Tan, W. (2014). Electrochemical characterization of the redox couple of Fe (III)/Fe (II) mediated by grafted polymer electrode. *Research on Chemical Intermediates, 40*(1), 179-192.

Ramos, A., Santos, M., Godoi, C., de Queiroz, L., Nandenha, J., Fontes, E., . . . de Souza, R. (2020). High CO tolerance of Pt nanoparticles synthesized by sodium borohydride in a time-domain NMR spectrometer. *International Journal of Hydrogen Energy, 45*(43), 22973-22978.

Ran, G., Chen, X., & Xia, Y. (2017). Electrochemical detection of serotonin based on a poly (bromocresol green) film and Fe 3 O 4 nanoparticles in a chitosan matrix. *RSC Advances, 7*(4), 1847-1851.

Rao, X., Tatoulian, M., Guyon, C., Ognier, S., Chu, C., & Abou Hassan, A. (2019). A comparison study of functional groups (amine vs. thiol) for immobilizing AuNPs on zeolite surface. *Nanomaterials, 9*(7), 1034.

Rasheed, P. A., & Sandhyarani, N. (2017). Electrochemical DNA sensors based on the use of gold nanoparticles: a review on recent developments. *Microchimica Acta, 184*(4), 981-1000.

Rashid, J. I. A., & Yusof, N. A. (2017). The strategies of DNA immobilization and hybridization detection mechanism in the construction of electrochemical DNA sensor: A review. *Sensing and bio-sensing research, 16*, 19-31.

Ratnam, K. V., Manjunatha, H., Janardan, S., Naidu, K. C. B., & Ramesh, S. (2020). Nonenzymatic electrochemical sensor based on metal oxide, MO (M= Cu, Ni, Zn, and Fe) nanomaterials for neurotransmitters: An abridged review. *Sensors International*, 100047.

Razzaque, S., Hussain, S. Z., Hussain, I., & Tan, B. (2016). Design and utility of metal/metal oxide nanoparticles mediated by thioether end-functionalized polymeric ligands. *Polymers, 8*(4), 156.

Riedel, R., Mahr, N., Yao, C., Wu, A., Yang, F., & Hampp, N. (2020). Synthesis of gold–silica core–shell nanoparticles by pulsed laser ablation in liquid and their physico-chemical properties towards photothermal cancer therapy. *Nanoscale, 12*(5), 3007-3018.

Robinson, I., Tung, L. D., Maenosono, S., Wälti, C., & Thanh, N. T. (2010). Synthesis of core-shell gold coated magnetic nanoparticles and their interaction with thiolated DNA. *Nanoscale, 2*(12), 2624-2630.

Rodaree, K., Maturos, T., Chaotheing, S., Pogfay, T., Suwanakitti, N., Wongsombat, C., . . . Lomas, T. (2011). DNA hybridization enhancement using piezoelectric microagitation through a liquid coupling medium. *Lab on a Chip, 11*(6), 1059-1064.

Ronkainen, N. J., Halsall, H. B., & Heineman, W. R. (2010). Electrochemical biosensors. *Chemical Society Reviews, 39*(5), 1747-1763.

Rosario, R., & Mutharasan, R. (2014). Nucleic acid electrochemical and electromechanical biosensors: a review of techniques and developments. *Reviews in analytical chemistry, 33*(4), 213-230.

Rossi, P. G., Benevolo, M., Vocaturo, A., Caraceni, D., Ciccocioppo, L., Frega, A., . . . Rosini, S. (2013). Prognostic value of HPV E6/E7 mRNA assay in women with negative colposcopy or CIN1 histology result: a follow-up study. *PloS one, 8*(2), e57600.

Rudakovskaya, P. G., Beloglazkina, E. K., Majouga, A. G., & Zyk, N. V. (2010). Synthesis and characterization of terpyridine-type ligand-protected gold-coated Fe3O4 nanoparticles. *Mendeleev Communications, 3*(20), 158-160.

Sabzi, R., Sehatnia, B., Pournaghi-Azar, M., & Hejazi, M. (2008). Electrochemical detection of human papilloma virus (HPV) target DNA using MB on pencil graphite electrode. *Journal of the Iranian Chemical Society, 5*(3), 476-483.

Sajid, M., Nazal, M. K., Mansha, M., Alsharaa, A., Jillani, S. M. S., & Basheer, C. (2016). Chemically modified electrodes for electrochemical detection of dopamine in the presence of uric acid and ascorbic acid: a review. *TrAC Trends in Analytical Chemistry, 76*, 15-29.

Salgueirino-Maceira, V., Correa-Duarte, M. A., Farle, M., López-Quintela, A., Sieradzki, K., & Diaz, R. (2006). Bifunctional gold-coated magnetic silica spheres. *Chemistry of materials, 18*(11), 2701-2706.

Salihov, S. V., Ivanenkov, Y. A., Krechetov, S. P., Veselov, M. S., Sviridenkova, N. V., Savchenko, A. G., . . . Beloglazkina, E. K. (2015). Recent advances in the synthesis of Fe3O4@ AU core/shell nanoparticles. *Journal of Magnetism and Magnetic Materials, 394*, 173-178.

Salimović-Bešić, I., Tomić-Čiča, A., Smailji, A., & Hukić, M. (2013). Comparison of the detection of HPV-16, 18, 31, 33, and 45 by type-specific DNA-and E6/E7 mRNA-based assays of HPV DNA positive women with abnormal Pap smears. *Journal of virological methods, 194*(1-2), 222-228.

Salvador, M., Gutiérrez, G., Noriega, S., Moyano, A., Blanco-López, M. C., & Matos, M. (2021). Microemulsion Synthesis of Superparamagnetic Nanoparticles for Bioapplications. *International Journal of Molecular Sciences, 22*(1), 427.

Samson, R., Navale, G. R., & Dharne, M. S. (2020). Biosensors: frontiers in rapid detection of COVID-19. *3 Biotech, 10*(9), 1-9.

Shabatina, T. I., Vernaya, O. I., Shabatin, V. P., & Melnikov, M. Y. (2020). Magnetic Nanoparticles for Biomedical Purposes: Modern Trends and Prospects. *Magnetochemistry, 6*(3), 30.

Shah, M., Badwaik, V., Kherde, Y., Waghwani, H. K., Modi, T., Aguilar, Z. P., . . . Webb, C. (2014). Gold nanoparticles: various methods of synthesis and antibacterial applications. *Front Biosci, 19*(8), 1320-1344.

Shankar, S. S., Ahmad, A., Pasricha, R., Khan, M. I., Kumar, R., & Sastry, M. (2004). Immobilization of biogenic gold nanoparticles in thermally evaporated fatty acid and amine thin films. *Journal of colloid and interface science, 274*(1), 69-75.

Sharkey, J., Lewis, P. J. S., Barrow, M., Alwahsh, S. M., Noble, J., Livingstone, E., . . . Liptrott, N. (2017). Functionalized superparamagnetic iron oxide nanoparticles provide highly efficient iron-labeling in macrophages for magnetic resonance–based detection in vivo. *Cytotherapy, 19*(4), 555-569.

Shen, L., Li, B., & Qiao, Y. (2018). Fe3O4 nanoparticles in targeted drug/gene delivery systems. *Materials, 11*(2), 324.

Shen, L., Qiao, Y., Guo, Y., Meng, S., Yang, G., Wu, M., & Zhao, J. (2014). Facile co-precipitation synthesis of shape-controlled magnetite nanoparticles. *Ceramics International, 40*(1), 1519-1524.

Shi, W., & Ma, Z. (2010). Amperometric glucose biosensor based on a triangular silver nanoprisms/chitosan composite film as immobilization matrix. *Biosensors and Bioelectronics, 26*(3), 1098-1103.

Shifrina, Z. B., & Bronstein, L. M. (2018). Magnetically recoverable catalysts: beyond magnetic separation. *Frontiers in chemistry, 6*, 298.

Shukla, S., Govender, P., & Tiwari, A. (2016). Polymeric micellar structures for biosensor technology. In *Advances in Biomembranes and Lipid Self-Assembly* (Vol. 24, pp. 143-161): Elsevier.

Singh, J., Dutta, T., Kim, K.-H., Rawat, M., Samddar, P., & Kumar, P. (2018). 'Green'synthesis of metals and their oxide nanoparticles: applications for environmental remediation. *Journal of nanobiotechnology, 16*(1), 1-24.

Singh, N., & Bath, P. K. (1997). Quality evaluation of different types of Indian honey. *Food Chemistry, 58*(1-2), 129-133.

Singh, R. P. (2011). Prospects of nanobiomaterials for biosensing. *International journal of electrochemistry, 2011*.

Sioi, M., Bolosis, A., Kostopoulou, E., & Poulios, I. (2006). Photocatalytic treatment of colored wastewater from medical laboratories: photocatalytic oxidation of hematoxylin. *Journal of Photochemistry and Photobiology A: Chemistry, 184*(1-2), 18-25.

Sohrabi, N., Valizadeh, A., Farkhani, S. M., & Akbarzadeh, A. (2016). Basics of DNA biosensors and cancer diagnosis. *Artificial cells, nanomedicine, and biotechnology, 44*(2), 654-663.

Solero, G. A. G. (2017). Synthesis of nanoparticles through flame spray pyrolysis: experimental apparatus and preliminary results.

Solomun, T., Schimanski, A., Sturm, H., & Illenberger, E. (2004). Reactions of amide group with fluorine as revealed with surface analytics. *Chemical physics letters, 387*(4-6), 312-316.

Sonker, R. K., Sabhajeet, S., Singh, S., & Yadav, B. (2015). Synthesis of ZnO nanopetals and its application as NO2 gas sensor. *Materials Letters, 152*, 189-191.

Sorgenfrei, S., Chiu, C.-y., Gonzalez Jr, R. L., Yu, Y.-J., Kim, P., Nuckolls, C., & Shepard, K. L. (2011). Label-free single-molecule detection of DNA-hybridization kinetics with a carbon nanotube field-effect transistor. *Nature nanotechnology, 6*(2), 126.

Sousa, C. P., de Oliveira, R. C., Freire, T. M., Fechine, P. B., Salvador, M. A., Homem-de-Mello, P., . . . Correia, A. N. (2017). Chlorhexidine digluconate on chitosan-magnetic iron oxide nanoparticles modified electrode: electroanalysis and mechanistic insights by computational simulations. *Sensors and Actuators B: Chemical, 240*, 417-425.

Souza, E., Nascimento, G., Santana, N., Campos-ferreira, D., Bibiano, J., & Arruda, M. (2014). Electrochemical DNA biosensor for sequences related to the human papillomavirus type 16 using methylene blue. *Biosens. J, 3*, 3-7.

Spasova, M., Salgueiriño-Maceira, V., Schlachter, A., Hilgendorff, M., Giersig, M., Liz-Marzán, L. M., & Farle, M. (2005). Magnetic and optical tunable microspheres with a magnetite/gold nanoparticle shell. *Journal of Materials Chemistry, 15*(21), 2095-2098.

Steenbergen, R. D., Snijders, P. J., Heideman, D. A., & Meijer, C. J. (2014). Clinical implications of (epi) genetic changes in HPV-induced cervical precancerous lesions. *Nature Reviews Cancer, 14*(6), 395.

Stoeva, S. I., Huo, F., Lee, J.-S., & Mirkin, C. A. (2005). Three-layer composite magnetic nanoparticle probes for DNA. *Journal of the American Chemical Society, 127*(44), 15362-15363.

Su, C. (2017). Environmental implications and applications of engineered nanoscale magnetite and its hybrid nanocomposites: A review of recent literature. *Journal of hazardous materials, 322*, 48-84.

Sun, H., Chao, J., Zuo, X., Su, S., Liu, X., Yuwen, L., . . . Wang, L. (2014). Gold nanoparticle-decorated MoS 2 nanosheets for simultaneous detection of ascorbic acid, dopamine and uric acid. *RSC Advances, 4*(52), 27625-27629.

Sun, S., Zeng, H., Robinson, D. B., Raoux, S., Rice, P. M., Wang, S. X., & Li, G. (2004). Monodisperse mfe2o4 (m= fe, co, mn) nanoparticles. *Journal of the American Chemical Society, 126*(1), 273-279.

Sun, X., Zheng, C., Zhang, F., Yang, Y., Wu, G., Yu, A., & Guan, N. (2009). Size-controlled synthesis of magnetite (Fe3O4) nanoparticles coated with glucose and gluconic acid from a single Fe (III) precursor by a sucrose bifunctional hydrothermal method. *The Journal of Physical Chemistry C, 113*(36), 16002-16008.

Suntako, R. (2015). Effect of synthesized ZnO nanograins using a precipitation method for the enhanced cushion rubber properties. *Materials Letters, 158*, 399-402.

Takahashi, S., Watahiki, R., Tomida, K., Wang, B., & Anzai, J.-i. (2013). Voltammetric Studies on Gold Electrodes Coated with Chitosan-Containing Layer-by-Layer Films. *Materials, 6*(11), 5427-5439.

Tamer, U., Gündoğdu, Y., Boyacı, İ. H., & Pekmez, K. (2010). Synthesis of magnetic core–shell Fe 3 O 4–Au nanoparticle for biomolecule immobilization and detection. *Journal of Nanoparticle Research, 12*(4), 1187-1196.

Tan, Y., Dai, X., Li, Y., & Zhu, D. (2003). Preparation of gold, platinum, palladium and silver nanoparticles by the reduction of their salts with a weak reductant–potassium bitartrate. *Journal of materials chemistry, 13*(5), 1069-1075.

Tarafdar, J., Sharma, S., & Raliya, R. (2013). Nanotechnology: interdisciplinary science of applications. *African Journal of Biotechnology, 12*(3).

Tardif, K. D., Simmon, K. E., Kommedal, Ø., Pyne, M. T., & Schlaberg, R. (2013). Sequencing-based genotyping of mixed human papillomavirus infections by use of RipSeq software. *Journal of clinical microbiology, 51*(4), 1278-1280.

Taufik, S., Yusof, N. A., Tee, T. W., & Ramli, I. (2011). Bismuth oxide nanoparticles/chitosan/modified electrode as biosensor for DNA hybridization. *Int. J. Electrochem. Sci, 6*, 1880-1891.

Teengam, P., Siangproh, W., Tuantranont, A., Henry, C. S., Vilaivan, T., & Chailapakul, O. (2017). Electrochemical paper-based peptide nucleic acid biosensor for detecting human papillomavirus. *Analytica chimica acta, 952*, 32-40.

Templeton, A. C., Wuelfing, W. P., & Murray, R. W. (2000). Monolayer-protected cluster molecules. *Accounts of chemical research, 33*(1), 27-36.

Teng, X., Black, D., Watkins, N. J., Gao, Y., & Yang, H. (2003). Platinum-maghemite core–shell nanoparticles using a sequential synthesis. *Nano letters, 3*(2), 261-264.

Teow, Y., Asharani, P., Hande, M. P., & Valiyaveettil, S. (2011). Health impact and safety of engineered nanomaterials. *Chemical communications, 47*(25), 7025-7038.

Terrab, A., Díez, M. J., & Heredia, F. J. (2002). Characterisation of Moroccan unifloral honeys by their physicochemical characteristics. *Food Chemistry, 79*(3), 373-379.

Teymourian, H., Salimi, A., & Khezrian, S. (2013). Fe3O4 magnetic nanoparticles/reduced graphene oxide nanosheets as a novel electrochemical and bioeletrochemical sensing platform. *Biosensors and Bioelectronics, 49*, 1-8.

Thakkar, K. N., Mhatre, S. S., & Parikh, R. Y. (2010). Biological synthesis of metallic nanoparticles. *Nanomedicine: Nanotechnology, Biology and Medicine, 6*(2), 257-262.

Thakur, N., Das Adhikary, S., Kumar, M., Mehta, D., Padhan, A. K., Mandal, D., & Nagaiah, T. C. (2018). Ultrasensitive and highly selective electrochemical detection of dopamine using poly (ionic liquids)–cobalt Polyoxometalate/CNT composite. *ACS omega, 3*(3), 2966-2973.

Thamilselvan, A., Manivel, P., Rajagopal, V., Nesakumar, N., & Suryanarayanan, V. (2019). Improved electrocatalytic activity of Au@ Fe3O4 magnetic nanoparticles for sensitive dopamine detection. *Colloids and Surfaces B: Biointerfaces, 180*, 1-8.

Titkov, A. I., Logutenko, O. A., Gerasimov, E. Y., Shundrina, I. K., Karpova, E. V., & Lyakhov, N. Z. (2019). Synthesis of silver nanoparticles stabilized by carboxylated methoxypolyethylene glycols: the role of carboxyl terminal groups in the particle size and morphology. *Journal of Inclusion Phenomena and Macrocyclic Chemistry, 94*(3), 287-295.

Torres-Gómez, N., Nava, O., Argueta-Figueroa, L., García-Contreras, R., Baeza-Barrera, A., & Vilchis-Nestor, A. R. (2019). Shape tuning of magnetite nanoparticles obtained by hydrothermal synthesis: effect of temperature. *Journal of Nanomaterials, 2019*.

Tran, L. T., Tran, H. V., Dang, H. T. M., Huynh, C. D., & Mai, T. A. (2020). Silver nanoparticles decorated polyaniline nanowires-based electrochemical DNA sensor: two-step electrochemical synthesis. *Journal of the Electrochemical Society, 167*(8), 087508.

Tyagi, P., Postetter, D., Saragnese, D., Randall, C., Mirski, M. A., & Gracias, D. (2009). Patternable nanowire sensors for electrochemical recording of dopamine. *Analytical chemistry, 81*(24), 9979-9984.

Vagin, M. Y., Karyakina, E. E., Hianik, T., & Karyakin, A. A. (2003). Electrochemical transducers based on surfactant bilayers for the direct detection of affinity interactions. *Biosensors and Bioelectronics, 18*(8), 1031-1037.

Vagin, M. Y., Trashin, S. A., Karyakin, A. A., & Mascini, M. (2008). Label-free detection of DNA hybridization at a liquid| liquid interface. *Analytical chemistry, 80*(4), 1336-1340.

Vallabani, N. S., & Singh, S. (2018). Recent advances and future prospects of iron oxide nanoparticles in biomedicine and diagnostics. *3 Biotech, 8*(6), 1-23.

Venu, M., Venkateswarlu, S., Reddy, Y. V. M., Seshadri Reddy, A., Gupta, V. K., Yoon, M., & Madhavi, G. (2018). Highly sensitive electrochemical sensor for anticancer drug by a zirconia nanoparticle-decorated reduced graphene oxide nanocomposite. *ACS omega, 3*(11), 14597-14605.

Vijayakumar, R., Koltypin, Y., Felner, I., & Gedanken, A. (2000). Sonochemical synthesis and characterization of pure nanometer-sized Fe3O4 particles. *Materials Science and Engineering: A, 286*(1), 101-105.

Villa, L. L., & Denny, L. (2006). CHAPTER 7 Methods for detection of HPV infection and its clinical utility. *International Journal of Gynecology & Obstetrics, 94*, S71-S80.

Vince, A., & Lepej, S. Ž. (2010). Diagnostic methods and techniques in cervical cancer prevention Part II: Molecular diagnostics of HPV infection. *Medicinski Glasnik, 7*(1).

Wallyn, J., Anton, N., & Vandamme, T. F. (2019). Synthesis, principles, and properties of magnetite nanoparticles for in vivo imaging applications—A review. *Pharmaceutics, 11*(11), 601.

Wang, A. Z., & Tepper, J. E. (2014). Nanotechnology in radiation oncology. *J Clin Oncol, 32*(26), 2879-2885. doi:10.1200/JCO.2014.55.0699

Wang, C., Du, J., Wang, H., Zou, C. e., Jiang, F., Yang, P., & Du, Y. (2014). A facile electrochemical sensor based on reduced graphene oxide and Au nanoplates modified glassy carbon electrode for simultaneous detection of ascorbic acid, dopamine and uric acid. *Sensors and Actuators B: Chemical, 204*, 302-309.

Wang, C., Li, J., Amatore, C., Chen, Y., Jiang, H., & Wang, X. M. (2011). Gold nanoclusters and graphene nanocomposites for drug delivery and imaging of cancer cells. *Angewandte Chemie International Edition, 50*(49), 11644-11648.

Wang, C., & Palefsky, J. (2016). Human papillomavirus-related oropharyngeal cancer in the HIV-infected population. *Oral diseases, 22*, 98-106.

Wang, C., Zhou, H., Zhu, W., Li, H., Jiang, J., Shen, G., & Yu, R. (2013). Ultrasensitive electrochemical DNA detection based on dual amplification of circular strand-displacement polymerase reaction and hybridization chain reaction. *Biosensors and Bioelectronics, 47*, 324-328.

Wang, H.-B., Zhang, H.-D., Xu, S.-P., Gan, T., Huang, K.-J., & Liu, Y.-M. (2014). A sensitive and label-free electrochemical impedance biosensor for protein detection based on terminal protection of small molecule-linked DNA. *Sensors and Actuators B: Chemical, 194*, 478-483.

Wang, J., Jiang, M., & Mukherjee, B. (1999). Flow detection of nucleic acids at a conducting polymer-modified electrode. *Analytical chemistry, 71*(18), 4095-4099.

Wang, M.-H., Ma, X.-Y., & Zhou, F. (2015). Synthesis and characterization of monodispersed spherical ZnO nanocrystals in an aqueous solution. *Materials Letters, 142*, 64-66.

Wang, S., Li, L., Jin, H., Yang, T., Bao, W., Huang, S., & Wang, J. (2013). Electrochemical detection of hepatitis B and papilloma virus DNAs using SWCNT array coated with gold nanoparticles. *Biosensors and Bioelectronics, 41*, 205-210.

Wang, X., Cui, Y., Yu, S., Zeng, Q., & Yang, M. (2016). Core–shell interaction and its impact on the optical absorption of pure and doped core-shell CdSe/ZnSe nanoclusters. *The Journal of chemical physics, 144*(13), 134307.

Wang, Y., Chen, M., Zhang, L., Ding, Y., Luo, Y., Xu, Q., . . . Fu, W. (2009). Rapid detection of human papilloma virus using a novel leaky surface acoustic wave peptide nucleic acid biosensor. *Biosensors and Bioelectronics, 24*(12), 3455-3460.

Wang, Y., Cheng, M., Wang, L., Zhou, D., He, S., Liang, L., . . . Yuan, J. (2021). Nanocrystalline graphite nanopores for DNA sensing. *Carbon, 176*, 271-278.

Wang, Y., Nkurikiyimfura, I., & Pan, Z. (2015). Sonochemical synthesis of magnetic nanoparticles. *Chemical Engineering Communications, 202*(5), 616-621.

Wang, Z., Fu, H., Tian, Z., Han, D., & Gu, F. (2016). Strong metal–support interaction in novel core–shell Au–CeO 2 nanostructures induced by different pretreatment atmospheres and its influence on CO oxidation. *Nanoscale, 8*(11), 5865-5872.

Wang, Z., Shen, B., Aihua, Z., & He, N. (2005). Synthesis of Pd/Fe3O4 nanoparticle-based catalyst for the cross-coupling of acrylic acid with iodobenzene. *Chemical Engineering Journal, 113*(1), 27-34.

Wei, F., Lillehoj, P. B., & Ho, C.-M. (2010). DNA diagnostics: nanotechnology-enhanced electrochemical detection of nucleic acids. *Pediatric research, 67*(5), 458-468.

Wen, T., Zhu, W., Xue, C., Wu, J., Han, Q., Wang, X., . . . Jiang, H. (2014). Novel electrochemical sensing platform based on magnetic field-induced self-assembly of Fe3O4@ Polyaniline nanoparticles for clinical detection of creatinine. *Biosensors and Bioelectronics, 56*, 180-185.

White Jr, J. W. (1978). Honey. In *Advances in food research* (Vol. 24, pp. 287-374): Elsevier.

Wipawakarn, P., Ju, H., & Wong, D. K. (2012). A label-free electrochemical DNA biosensor based on a Zr (IV)-coordinated DNA duplex immobilised on a carbon nanofibre| chitosan layer. *Analytical and bioanalytical chemistry, 402*(9), 2817-2826.

Worley, J. (2017). The role of pleasure neurobiology and dopamine in mental health disorders. *Journal of psychosocial nursing and mental health services, 55*(9), 17-21.

Wu, N.-y., Gao, W., He, X.-l., Chang, Z., & Xu, M.-t. (2013). Direct electrochemical sensor for label-free DNA detection based on zero current potentiometry. *Biosensors and Bioelectronics, 39*(1), 210-214.

Wu, Q., Zhang, Y., Yang, Q., Yuan, N., & Zhang, W. (2019). Review of electrochemical DNA biosensors for detecting food borne pathogens. *Sensors, 19*(22), 4916.

Wu, W., He, Q., Chen, H., Tang, J., & Nie, L. (2007). Sonochemical synthesis, structure and magnetic properties of air-stable Fe3O4/Au nanoparticles. *Nanotechnology, 18*(14), 145609.

Xu, Z., Hou, Y., & Sun, S. (2007). Magnetic core/shell Fe3O4/Au and Fe3O4/Au/Ag nanoparticles with tunable plasmonic properties. *Journal of the American Chemical Society, 129*(28), 8698-8699.

Xuan, S., Wang, F., Gong, X., Kong, S.-K., Jimmy, C. Y., & Leung, K. C.-F. (2011). Hierarchical core/shell Fe 3 O 4@ SiO 2@ γ-AlOOH@ Au micro/nanoflowers for protein immobilization. *Chemical communications, 47*(9), 2514-2516.

Xuan, S., Wang, Y.-X. J., Yu, J. C., & Cham-Fai Leung, K. (2009). Tuning the grain size and particle size of superparamagnetic Fe3O4 microparticles. *Chemistry of materials, 21*(21), 5079-5087.

Xuan, S., Wang, Y.-X. J., Yu, J. C., & Leung, K. C.-F. (2009). Preparation, characterization, and catalytic activity of core/shell Fe3O4@ polyaniline@ Au nanocomposites. *Langmuir, 25*(19), 11835-11843.

Xue, C., Han, Q., Wang, Y., Wu, J., Wen, T., Wang, R., . . . Jiang, H. (2013). Amperometric detection of dopamine in human serumby electrochemical sensor based on gold nanoparticles doped molecularly imprinted polymers. *Biosensors and Bioelectronics, 49*, 199-203.

Yang, Y., Li, M., & Zhu, Z. (2019). A novel electrochemical sensor based on carbon nanotubes array for selective detection of dopamine or uric acid. *Talanta, 201*, 295-300.

Yoon, J.-Y. (2016). *Introduction to biosensors: from electric circuits to immunosensors*: Springer.

Yougbaré, S., Mutalik, C., Krisnawati, D. I., Kristanto, H., Jazidie, A., Nuh, M., . . . Kuo, T.-R. (2020). Nanomaterials for the photothermal killing of bacteria. *Nanomaterials, 10*(6), 1123.

Yu, D., Zeng, Y., Qi, Y., Zhou, T., & Shi, G. (2012). A novel electrochemical sensor for determination of dopamine based on AuNPs@ SiO2 core-shell imprinted composite. *Biosensors and Bioelectronics, 38*(1), 270-277.

Yu, H., Chen, M., Rice, P. M., Wang, S. X., White, R., & Sun, S. (2005). Dumbbell-like bifunctional Au− Fe3O4 nanoparticles. *Nano letters, 5*(2), 379-382.

Yuan, M., Li, J., Yu, Y., Fu, Y., Fong, A., & Hu, J. (2016). Fabrication of a Fe2O3 Nanoparticles Implantation-modified Electrode and its Applications in Electrochemical Sensing. *Electroanalysis, 28*(5), 954-961.

Zare, H. R., & Nasirizadeh, N. (2007). Hematoxylin multi-wall carbon nanotubes modified glassy carbon electrode for electrocatalytic oxidation of hydrazine. *Electrochimica Acta, 52*(12), 4153-4160.

Zare, H. R., Nasirizadeh, N., Mazloum-Ardakani, M., & Namazian, M. (2006). Electrochemical properties and electrocatalytic activity of hematoxylin modified carbon paste electrode toward the oxidation of reduced nicotinamide adenine dinucleotide (NADH). *Sensors and Actuators B: Chemical, 120*(1), 288-294.

Zari, N., Amine, A., & Ennaji, M. (2009). Label-free DNA biosensor for electrochemical detection of short DNA sequences related to human papilloma virus. *Analytical Letters, 42*(3), 519-535.

Zhang, C., Ren, J., Zhou, J., Cui, M., Li, N., Han, B., & Chen, Q. (2018). Facile fabrication of a 3, 4, 9, 10-perylene tetracarboxylic acid functionalized graphene–multiwalled carbon nanotube–gold nanoparticle nanocomposite for highly sensitive and selective electrochemical detection of dopamine. *Analyst, 143*(13), 3075-3084.

Zhang, D.-H., Li, G.-D., Li, J.-X., & Chen, J.-S. (2008). One-pot synthesis of Ag–Fe 3 O 4 nanocomposite: a magnetically recyclable and efficient catalyst for epoxidation of styrene. *Chemical communications*(29), 3414-3416.

Zhang, H., Li, F., Wang, L., Shao, S., Chen, H., & Chen, X. (2020). Sensitive homogeneous fluorescent detection of DNA glycosylase by target-triggering ligation-dependent tricyclic cascade amplification. *Talanta, 220*, 121422.

Zhang, J., Post, M., Veres, T., Jakubek, Z. J., Guan, J., Wang, D., . . . Simard, B. (2006). Laser-assisted synthesis of superparamagnetic Fe@ Au core− shell nanoparticles. *The Journal of Physical Chemistry B, 110*(14), 7122-7128.

Zhang, J., Yang, S., Chen, Z., Yan, Y., Zhao, J., Li, J., & Jiang, Z. (2018). In Situ synthesis of SiC-graphene core-shell nanoparticles using wet ball milling. *Ceramics International, 44*(7), 8283-8289.

Zhang, M., Sheng, Q., Nie, F., & Zheng, J. (2014). Synthesis of Cu nanoparticles-loaded Fe3O4@ carbon core–shell nanocomposite and its application for electrochemical sensing of hydrogen peroxide. *Journal of Electroanalytical Chemistry, 730*, 10-15.

Zhang, W., Shen, F., & Hong, R. (2011). Solvothermal synthesis of magnetic Fe3O4 microparticles via self-assembly of Fe3O4 nanoparticles. *Particuology, 9*(2), 179-186.

Zhang, X., & Zheng, J. (2020). High-index {hk0} facets platinum concave nanocubes loaded on multiwall carbon nanotubes and graphene oxide nanocomposite for highly sensitive simultaneous detection of dopamine and uric acid. *Talanta, 207*, 120296.

Zhang, Y., Cheng, Y., Zhou, Y., Li, B., Gu, W., Shi, X., & Xian, Y. (2013). Electrochemical sensor for bisphenol A based on magnetic nanoparticles decorated reduced graphene oxide. *Talanta, 107*, 211-218.

Zhang, Z., Zhu, H., Wang, X., & Yang, X. (2011). Sensitive electrochemical sensor for hydrogen peroxide using Fe 3 O 4 magnetic nanoparticles as a mimic for peroxidase. *Microchimica Acta, 174*(1-2), 183-189.

Zhao, J., Zhang, Y., Li, H., Wen, Y., Fan, X., Lin, F., . . . Yao, S. (2011). Ultrasensitive electrochemical aptasensor for thrombin based on the amplification of aptamer–AuNPs–HRP conjugates. *Biosensors and Bioelectronics, 26*(5), 2297-2303.

Zhao, X., Cai, Y., Wang, T., Shi, Y., & Jiang, G. (2008). Preparation of alkanethiolate-functionalized core/shell Fe3O4@ Au nanoparticles and its interaction with several typical target molecules. *Analytical chemistry, 80*(23), 9091-9096.

Zheng, Y., Song, H., Chen, S., Yu, X., Zhu, J., Xu, J., . . . Liu, T. (2020). Metal-Free Multi-Heteroatom-Doped Carbon Bifunctional Electrocatalysts Derived from a Covalent Triazine Polymer. *Small, 16*(47), 2004342.

Zhou, C., Li, S., Zhu, W., Pang, H., & Ma, H. (2013). A sensor of a polyoxometalate and Au–Pd alloy for simultaneously detection of dopamine and ascorbic acid. *Electrochimica Acta, 113*, 454-463.

Zhou, H., Lee, J., Park, T. J., Lee, S. J., Park, J. Y., & Lee, J. (2012). Ultrasensitive DNA monitoring by Au–Fe3O4 nanocomplex. *Sensors and Actuators B: Chemical, 163*(1), 224-232.

Zhou, X., Guo, S., Gao, J., Zhao, J., & Xu, W. (2017). Cascade dual-signal enhancement by integrating exonuclease III-assisted target-recycling and rolling circle amplification for ultrasensitive electrochemical detection of DNA. *Journal of the Electrochemical Society, 164*(13), B603.

Zhou, X., Xu, W., Wang, Y., Kuang, Q., Shi, Y., Zhong, L., & Zhang, Q. (2010). Fabrication of cluster/shell Fe3O4/Au nanoparticles and application in protein detection via a SERS method. *The Journal of Physical Chemistry C, 114*(46), 19607-19613.

Zhu, N., Ji, H., Yu, P., Niu, J., Farooq, M., Akram, M. W., . . . Niu, X. (2018). Surface modification of magnetic iron oxide nanoparticles. *Nanomaterials, 8*(10), 810.

Zhu, W., Jiang, G., Xu, L., Li, B., Cai, Q., Jiang, H., & Zhou, X. (2015). Facile and controllable one-step fabrication of molecularly imprinted polymer membrane by magnetic field directed self-assembly for electrochemical sensing of glutathione. *Analytica chimica acta, 886*, 37-47.

Zhu, Y., & Wu, Q. (1999). Synthesis of magnetite nanoparticles by precipitation with forced mixing. *Journal of Nanoparticle Research, 1*(3), 393-396.

Zou, L., & Ling, L. (2018). Ultrasensitive detection of HIV DNA with polymerase chain reaction–dynamic light scattering. *Analytical chemistry, 90*(22), 13373-13377.